This is to certify that the

dissertation entitled

Fabrication of Functionally Gradient Materials with

Internal Channels in Ceramics and Ceramic Composites

presented by

Hyea-Weon Shin

has been accepted towards fulfillment
of the requirements for

_____Ph.D._____ degree in Materials Science
                                          and Engineering

[signature]
Major professor

Date May 22, 2002

PLACE IN RETURN BOX to remove this checkout from your record.
TO AVOID FINES return on or before date due.
MAY BE RECALLED with earlier due date if requested.

DATE DUE	DATE DUE	DATE DUE

6/01 c:/CIRC/DateDue.p65-p.15

FABRICATION OF FUNCTIONALLY GRADIENT MATERIALS WITH INTERNAL CHANNELS IN CERAMICS AND CERAMIC COMPOSITES

By

Hyea-Weon Shin

A DISSERTATION

Submitted to
Michigan State University
In partial fulfillment of the requirements
for the degree of

DOCTOR OF PHILOSOPHY

Department of Chemical Engineering and Materials Science

2002

ABSTRACT

FABRICATION OF FUNCTIONALLY GRADIENT MATERIALS WITH INTERNAL CHANNELS IN CERAMICS AND CERAMIC COMPOSITES

By

HYEA-WEON SHIN

Functionally Gradient Materials (FGMs) are inhomogeneous materials whose compositions vary from one phase to another. By tailoring the inhomogeneous properties, FGMs can be used to reduce the stresses that are caused by severe thermal gradients. Thermal gradient loading can further be compensated by heat transfer into a cooling fluid circulating in a network of channels and manifolds. In an envisioned application, heat from a localized source is transferred to the cooling fluid, easing sharp thermal loads while minimizing the unwanted spread of heat energy to the ambient surroundings.

This study reports on the fabrication of functionally gradient ceramics and the embedding of simple internal channels within these ceramics. Functional gradiency (variation of composition) is built in via the layering of different components across the thickness of a plate sample. Traditional powder processing techniques are applied to fabricate the test pieces, and recently developed methods of joining are used to build assemblies from individually sintered plate layers.

For a well-formed FGM to be made, materials parameters need to be selected based on mechanical, thermal and chemical properties. As a class, ceramics are hard, wear-resistant, refractory, electrically and thermally insulative, nonmagnetic, chemically stable, and oxidation-resistant. However, because of their brittleness, ceramics with

minute channels are difficult to machine. Instead, for this study, a graphite fugitive phase is used as a spacer to support channel volumes within a ceramic powder compact; during pre-sintering, the graphite burns out to expose a network of channels. Full sintering fixes the final shape. At the operating temperatures of the ovens used in our fabrication study, sintering of alumina, partially stabilized zirconia, fully stabilized zirconia and hydroxyapatite have been successful, and these ceramic powders form the basis of the present fabrication studies.

Inhomogeneities inherent in the composition of layered FGMs and non-uniformities introduced in the fabrication process (possibly during powder compaction) give rise to non-uniform densification behavior, which leads to warping, cracking, and the development of residual stress both within the layers and along layer boundaries. As a remedy, powders of different particle size are mixed within component layers, and the effect of particle mixture on final specimen curvature is shown. The optimal mixture ratio gives a flat layer, wherein the effects of thermal expansion and densification are balanced. Different pressing procedures and layer-stacking orders have also been used to minimize warping; these are viewed as optional, complementary steps to particle mixing.

A study of the difference between conventional and microwave heating is also presented. The main interest has been to quantify the different sintering behavior associated with conventional heating and microwave heating.

Finally, scanning electron microscopy and energy dispersive spectroscopy are used to illustrate the gradual changes in element composition across the thickness of the produced functionally gradient ceramic plates.

DEDICATION

To

MY PARENTS

WHO LOVED ME AND SUPPORTED ME DURING THE PAST

YEARS

ACKNOWLEDGEMENTS

I would like to express my deep gratitude to my advisor, Dr. Patrick Kwon, and co-advisor, Dr. Eldon Case for their instruction, guidance and encouragement to complete this research.

I also wish to thank the members of my committee, Dr. Dashin Liu, Department of mechanical Engineering, and Stanley L. Flegler for their advice, assistance and valuable comments on this research.

Special thanks are extended to my parents for their patient support and encouragement during entire graduate study.

TABLE OF CONTENTS

APPENDICES

LIST OF TABLES

LIST OF FIGURES

xiii

Chapter 1

INTRODUCTION

Recently developed techniques in ceramic joining and processing are applied to the development and fabrication of thermal management materials. The intended application is a mesoscale, ceramic heat exchanger in which coolants flow through a network of interior channels and manifolds. Although this technology can be applied in aerospace, manufacturing, and medical industries, the current discussion will focus on the issue of thermal management in microelectronics. In the past, common methods of removing heat from microelectronic devices have included the conduction of heat through highly conductive materials such as diamond, silicon nitride, and molybdenum [1,2] and cooling by air convection [3]. However, by circulating coolants through a closed system of channels, we can achieve not only better conduction by design, but we can also minimize the unwanted spread of heat to other peripheral devices.

The current research work combines existing techniques in ceramics processing and an economical technique to introduce channels within the interior of ceramics; it is viewed as a step towards the eventual implementation of mesoscale heat exchangers with an active cooling system.

As a class of materials, ceramics are wear-resistant, hard but brittle and prone to thermal shock, electrically and thermally insulative, nonmagnetic, chemically stable, and oxidation-resistant [4]. Although the hardness and fracture toughness of ceramic

composites are adequate for microstructural applications, ceramics having complex shapes are difficult to manufacture.

While the production of channels inside ceramics bodies has previously been achieved, for instance, by the etching of silicon wafers [5], the current method of creating channels uses of a graphite fugitive phase that offers more control over channel geometry at a relatively low cost. The graphite fugitive phase in the shape of the channels is embedded inside the ceramic powder before compaction. During pre-sintering, the graphite is dissolved to expose a system of internal channels. Crumm et al. [6] used the term "fugitive material" to describe a space-filling buffer that is extruded from an initial mixture of carbon black powder in a thermoplastic/mineral-oil melt. The buffer supports channel volumes in the green state, but oxidizes at high temperatures to leave the channel volumes empty. In the current work, the choice of fugitive material is readily available and does not require the pre-processing steps of thermoplastic-melt mixing and extrusion. Also, the work of Crumm [6] et al. is primarily concerned with a process of multiple-pass co-extrusion (for size reduction) of repeating units of ceramic channels separated by metal electrodes, which is a different process from the one envisioned in this dissertation.

Because ceramics are brittle, a main concern for their use in building a heat exchanger is the presence of residual stresses, warping and interface cracking caused by thermal gradients. During fabrication, thermal gradients can result from the joining of two or more simpler parts with different coefficients of thermal expansion, or different temperatures of sintering. Also, during the operation of the heat exchanger, thermal gradients can result from the circulation of coolants around the embedded channels, or from the desired removal of heat from localized, external sources.

The following technique is used to address the problems of residual stresses and warping which arise during the fabrication process. Namely, ceramic particles of different sizes are mixed in the composite layers to ensure a flat specimen surface (e.g. for joining). The optimal mixture ratio is obtained by varying powder characteristics so that compatibility between layers (i.e. flatness) is assured in the presence of thermal expansion and shrinkage from sintering. Different pressing procedures and layer stacking orders have also been used as complementary steps to minimize warping. Details of our study on warping are given in Chapter 4.

Joining techniques are applied to combine component layers. Hence, instead of sintering an entire FGM stack at one time, we join different layers that have been separately sintered to control warping and cracking. A background of joining techniques is given in Chapter 2, and an elaboration of the current results on the use of joining to control warping and residual stresses can be found in Chapter 4.

The proposed media belong to the class of functionally gradient materials (FGMs), which consist of component phases endowed with spatially varying properties, compositions, or microstructures for the purpose of achieving desired material response [7,8,9]. By tailoring their inhomogeneous properties, FGMs can be designed to minimize the stress during operation while reducing detrimental, process-induced residual stress. A background of FGM's is given in Chapter 2, fabrication procedures in Chapter 3, and results related to the control of warping, SEM examination, etc., in Chapter 4.

Two different types of sintering processing—conventional sintering and microwave sintering—were applied. Fundamentally, there are many differences between the two heating methods. Conventional electrical furnace for sintering materials is

composed of heating elements and their insulation. By contrast, the heating chamber of a microwave is composed of a port through which electromagnetic waves are guided into the cavity from a power supply. By using these two methods of heating, different sintering mechanisms can be studied. This is discussed in more detail in Chapter 4.

To check the effectiveness of the current fabrication procedure, the sintered FGM specimens are observed using scanning electron microscopy (SEM) and energy dispersive spectroscopy (EDS). This work is found towards the end of Chapter 4.

This dissertation is divided into five parts. Chapter 2 contains a background to FGM and the different types of joining techniques. The salient features of FGM and a discussion on the challenges of using ceramics as a base material are presented. This is followed by a discussion on the different types of joining techniques. Glaze bonding is chosen for this work because of its reliability in bonding materials having different coefficients of thermal expansion. The processing parameters such as fusing temperatures and hold times are also well known to us from previous work.

Chapter 3 contains general experimental procedures. The composition and properties of the ceramic powders used—alumina, partially stabilized zirconia, fully stabilized zirconia and hydroxyapatite—are given. Powder preparation and sintering procedures, including powder pressing, pre-sintering and full sintering are discussed along with data on processing temperature, pressure, and hold times. Specifics on specimen polishing, coating, and joining are also described. The final section touches briefly on the sectioning of specimens for SEM observation.

The beginning sections of Chapter 4 contain previously published results by the author on the fabrication of ceramic FGMs with internal channels, joining techniques

applied to alumina, zirconia, and bioinert ceramics, and the control of warping and residual stress. This is followed by section 4.5 on the difference between conventional and microwave sintering, section 4.6 on some updated results regarding the control of warping, cracking and residual stress, section 4.7 on SEM/EDS imaging of FGM specimens, and finally, a summary and conclusion section.

REFERNCES

1 K. J. Gray, Diamond and Related Materials, Vol. 9, No. 2, 2000, pp. 201–204. K. Jagannadham, "Model of Interfacial Thermal Resistance of Diamond Composites," Journal of Vacuum Science and Technology, Vol. A17, No. 2, 1999, pp. 373–379.

2 P. Hui, H. S. Tan, and Y. S. Lye, IEEE Transactions on Components and Packaging Technologies, Part A, Vol. 20, No. 4, 1997, pp. 452–457

3 R. Hall, Electronic Design, Vol. 47, No. 7, 1999, pp. 29–30

4 Takashi Kawai, Shun-ichi Miyazaki, Muneki Araragi, "A New method for Forming a Piezo-Electric FGM Using a Dual Dispenser System, " The first International Symposium FGM, 1990, pp191-196

5 D. B. Tuckerman and R. F. W. Pease, "High Performance Heat Sink for VLSI," IEEE Electron Devices Letters, Vol. EDL-2, May 1981, pp. 126–129

6 A. T. Crumm and J. W. Halloran, "Fabrication of Microconfigured Multicomponent Ceramics," Journal of the American Ceramic Society, Vol. 81, No. 4, 1998, pp. 1053–1056

7 D. P. H. Hasselman and G. E. Youngblood, "Enhanced Thermal Stress Resistance of Structural Ceramics with Thermal Conductivity Gradient," Journal of the American Ceramic Society, Vol. 61, No. 1–2, 1978, pp. 49–52.

8 P. Kwon, Macroscopic Design and fabrication of Functionally Gradient Materials, PhD Dissertation, U. C. Berkeley, 1994.

9 P. Kwon, C. K. H. Dharan, and M. Ferrari, Journal of Energy Resources Technology, Vol. 116, 1994, pp. 115–120

Chapter 2

BACKGROUND

2.1 FGMs

In recent years many studies have been undertaken to develop new materials. Consequently they are continually being introduced as the demand from materials became more critical. Ceramic composite material is made from ceramic matrix and a dispersion phase of either ceramics or metal and is fabricated to use excellent properties of each of these materials. Usually, the size of the dispersion phase of ceramic composites is in the order of micrometers; however, to improve the properties of composite materials, the size in the order of nanometer (ceramic nanocomposite) have been developed [1]. These nanocomposite materials have evenly spread dispersion phase thus the property can be much more homogeneous as called homogeneous functional material. Considering aerospace applications these composite materials cannot withstand the severe thermal stress condition due to severe environment, thus, the new technologies often force to have that composites perform multiple functions instead of having only single characteristic. In order to meet this demand, a new class of composite materials called Functionally Gradient Materials (FGM) have been emerged in two recent international conferences in the mid-1980s [2, 3, 4]. The term FGM, now widely used by the materials society, as a new material having spatially inhomogeneous microstructures and properties. FGM, a novel engineered composite material, was arisen to seek a high

temperature material for a recently proposed space-plane project by Nino in Japan [5]. The resistant material for use in the space plane must endure a ultrahigh temperature oxidizing environment At the same time it must be able to withstand a high degree of thermal stress related with its own ability to be a thermal barrier [6, 7]. The space technologists, estimate that nose cone of the space-plane will be heated to about 2000K and the air intake of the multi-propulsion engine up to 1900K with a temperature difference of over 1000K in a thin layer toward the inner portion of the material. Such a high temperature heating is mainly caused by the aero-dynamic friction with air during long time cruising in the atmosphere in comparison with the present vertical launching type rocket. No industrial materials could withstand such severe thermomechanical loading. Three features are important in the designing of the material used under the above mentioned environment; heat-resistant and anti-oxidation properties in the high temperature surface layer of the material, mechanical toughness in the other side and an effective thermal stress relaxation throughout the material. Also, FGMs provide low cost ceramic surfaces displaying grace failure at moderate to high temperatures and high thermal heat flux. FGM is applicable not only to space-plane thermal-protection systems but also to the electronic, chemical, nuclear power and biomedical such as dental implants fields as well as many others (Figure 2.1) [8, 9]. FGM is a novel engineered composite which is designed to optimize material properties for use in real environments by place-to-place control of composition and microstructure. In this simplest structure, it consists of one material on one side, a second material on the other, and an intermediate layer whose structure composition and morphology vary smoothly from one material to the other at the micron level. Similar to composite materials, FGM consists of at least two

distinct phases. However, the concentration level of each phase is spatially varying to attain inhomogeneous properties in macroscopic and microscopic level (Figure 2.2). Therefore, FGM is the novel material providing the innovative properties and / or functions that cannot be performed by homogeneous materials, emphasizing the following two essential features. The first essential feature includes the tailoring of chemical composition and microstructure due to the gradient change of properties. The second essential feature includes the availability of good reproducibility. Thus, FGM may undoubtedly be classified into a distinct category separated from conventional homogeneous composites. Figure 2.3 explains the differences between the homogeneous materials and FGMs.

It is now well known that sudden transitions in materials composition and properties within component can be one of reasons of sharp local concentrations of stress. In other words, if the transition in materials gradually changes from one side to the other these residual and thermal stress concentrations can be much more reduced and enhanced the bonding strength. From the view point of fracture mechanics, the distinguishing feature of FGMs is in their strength-related properties such as yield and ultimate strength, fracture toughness, and creep, fatigue, and corrosion crack growth parameters [10, 11, 12, 13 , 14 , 15]. Continuously or discontinuously varying compositions and / or microstructures over definable geometrical distances porosity ratio between the low and high – temperature can control the thermal stress. Similar to the service condition of a tool, one practical application of FGMs is to compensate for very stiff thermal gradient loadings. In many applications, FGMs may be exposed to constant or alternating thermal loading with high temperature gradient from one side to the other. Therefore, the thermal

stability of the FGM structure must be evaluated, because of microstructural change caused by Ostwald ripening and because of unstable compositional distribution due to the diffusion of structural elements [16]. Also thermal shock resistance, thermal fatigue characteristics, temperature profile and overall heat flow must be evaluated. The main problem with this kind of FGM is the development of residual thermal stresses at the interface between the different layers as a consequence of the thermal expansion mismatch.

In these works, a steep gradient temperature field was compensated by the variation of the coefficient of thermal expansion (CTE). Designing FGMs for thermal gradient loading conditions was shown by Kwon [17] and Kwon and Dharan [18,19]. In a simple elastic analysis, the thermoelastic properties (which are functions of the volume fraction of the reinforcement phase) as well as the type of applied loads, such as thermal gradients, pressure, force and moments, and the geometry of the structure have to be considered simultaneously in defining the type of gradient, and the required properties. The gradients can be continuous on a microscopic level, or they can be laminates comprised of gradients of metals, ceramics, polymers, or variations of porosity/ density. Brittle structural ceramics for high-temperature applications are highly susceptible to thermal stress fracture. The incidence of such fracture can be reduced by the selection of materials with values as low as possible of the coefficient of thermal expansion, Young's modulus of elasticity, poison's ratio, and emissivity in combination with high values of tensile strength, thermal conductivity, and thermal diffusivity. Rapid crack arrests after thermal stress fracture can be promoted by selecting materials with moderate strength, high young's modulus, and high values of fracture energy and which exhibit stable crack

propagation. From the point of view of engineering design, thermal stresses can be reduced by decreasing the structure size and developing highly compliant structures with a minimum of external mechanical constraints. Thus, the introduction of compositional gradients materials can be beneficial such as (i) the "smoothing" of the transitions in thermal with vast thermal expansion mismatch (ii) the flexibility to tailor the magnitude of thermal stresses and hence the onset and spread of plastic flow and cracking by tailoring the geometry of the graded layer as well as the gradient in composition within that layer ; (iii) the possibility to minimize or even fully eliminate the deleterious effects of stress concentrations and singularities at free edges ; and (iv) making possible the deposition of thick protective ceramic layers of 1mm thickness or higher by thermal spraying on to metallic substrates. For the design of FGMs, necessarity of material properties, such as thermal-expansion-coefficient and Young's modulus in the specific region, is optimized by controlling the distribution profiles of composition and microstructures, as well as micropores in the materials [20,21]. Various methods are used in FGM technology to control the composition and structure of a composite. The simplest one is step by step stacking of mixed powders of different compositions such as Chemical Vapor Deposition (CVD), Physical Vapor Deposition (PVD), ion plating, plasma spraying, diffusion treatment, sedimentation, sintering or self-propagating high temperature synthesis. Another methods which enable to make continuous stacking with changing composition, include wet filtration process, vibrating stacking process, centrifugal process, wet powder spray forming process, sequential slip casting and slurry dipping process [22, 23].
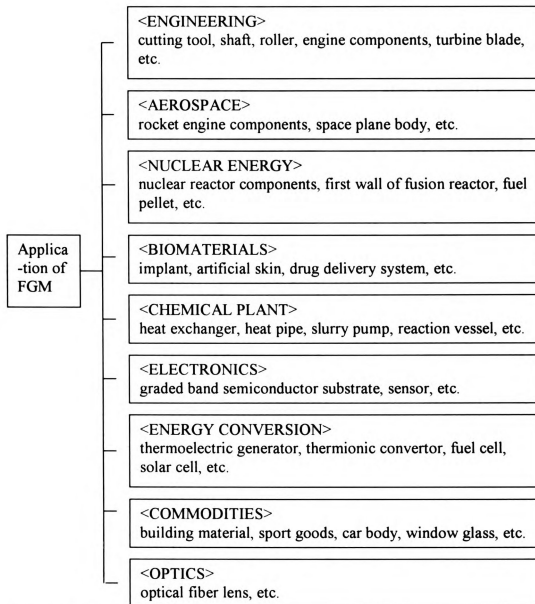
Figure 2.1. Application of FGM.
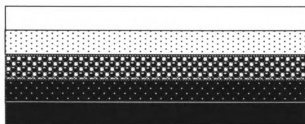
Figure 2.2. Schematic figure of Functionally Gradient Material
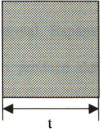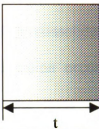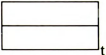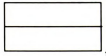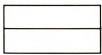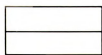
	HOMOGENEOUS MATERIAL	FUNCTIONALLY GRADIENT MATERIAL
	t	t
CTE	t	t
FRACTURE TOUGHNESS	t	t
STRESS	t	t
OXIDATION RESISTANCE	t	t
HEAT RESISTANCE	t	t

Figure 2.3. The difference between homogeneous material and functionally gradient material

This study involves sintering powder mixtures with spatially varying concentrations of two or more constituent powders. However, due to the apparent inhomogeneous nature of FGMs, residual stress occurs in the structural level. This causes non-uniform shrinkage [24,25]. Most solids shrink when the temperature decreases after the final phase of consolidation processing. This phenomenon is best described by examining the Coefficient of Thermal Expansion (CTE). During consolidation, a mechanism for shrinkage exists to produce densification. Densification occurs in a powder compact because the interstitial spaces are filled by the mass transport mechanisms of densification. While the shrinkage difference due to CTE mismatch cannot be altered for a given combination of materials, shrinkage occurring during densification can be mixing the powder and optimizing the sintering conditions (time, temperature, heating/cooling cycles, etc) [26, 27]. During cooling from the sintering temperature, thermal stress will be generated in the graded compacts, causing crack formation within the compacts. We must incorporate a composition profile into a graded compact for sufficient thermal stress reduction to avoid crack formation. The retarding influence of inclusions on matrix densification can be significant, although the spread in sintering rates with varying inclusion volume fraction in the non-percolating regime is not dramatic. Discrepancies in sintering rate are none of the less undesirable, as they cause warping and, potentially, cracking in the FGM during densification. These effects may therefore have to be taken into account in FGM densification. Thermal stress generated during fabrication shows a maximum at the ceramics rich side of the surface of the FGM sample, which contributes to crack formation. Thus to fabricate crack-free FGM it is necessary to improve the fracture strength and toughness of the material in the

composition range where maximum thermal stress arises. For the fabrication of the P/M (powder metallurgy) FGM, the thermal stress generated during cooling from the sintering temperature for the first, is to be minimized. For the actual condition, the thermal stress generated in a temperature gradient in a thermal barrier situation is to be minimized. In powder processing of homogeneous materials, the starting powder is often characterized by an average particle size and particle size distribution. As shown in Reed [28] with alumina powder, the different combinations of these characteristics result in different packing fraction. Because the packing fraction after consolidation should approach 1.0, the overall shrinkage will be different even using the same material with different powder characteristics. This study address the solution to the most difficult problems associated with PM processing of FGMs. The processing behavior of PM materials depends on the starting powder characteristics such as size, shape, particle size distribution, etc. and sintering temperature, pressure and time. Shrinkage difference between wide and narrow size distribution powders was studied by Yeh and Sacks [29]. To quantify the nonuniform deformation in the PM during sintering, the measurement of two-and three-dimensional and local sintering shrinkage is required by all means for their effective dimensional control. The powder metallurgical process is a very viable and suitable route for FGM fabrication. The key points are essentially two-fold: how to obtain the graded green compact and how to temperature without defect formation. The defects, such as large residual porosity or small cracks in the compacts, are healed, if necessary, by HIP. Powder metallurgical (P/M) processing of FGMs provides a wide range of compositional and microstructural control, along with shape-forming capability [30]. Apart from the usual advantages and disadvantages of powder metallurgy, there are several technical

15

challenges to be met for successful fabrication of FGM samples: (1) stacking powders with different mixing ratios according to the predesigned composition profile with the desired sample shape and size, and (2) compacting and sintering the stacked powder heap, which has variable compacting and sintering behaviors layer by layer. Powder compacts with different mixing ratios usually exhibit a different sintering behavior, which will cause various sintering faults in the FGM samples (such as warping, frustum formation, splitting, and crack formation) (Figure 2.4). The following figure 2.5 shows the P/M process.
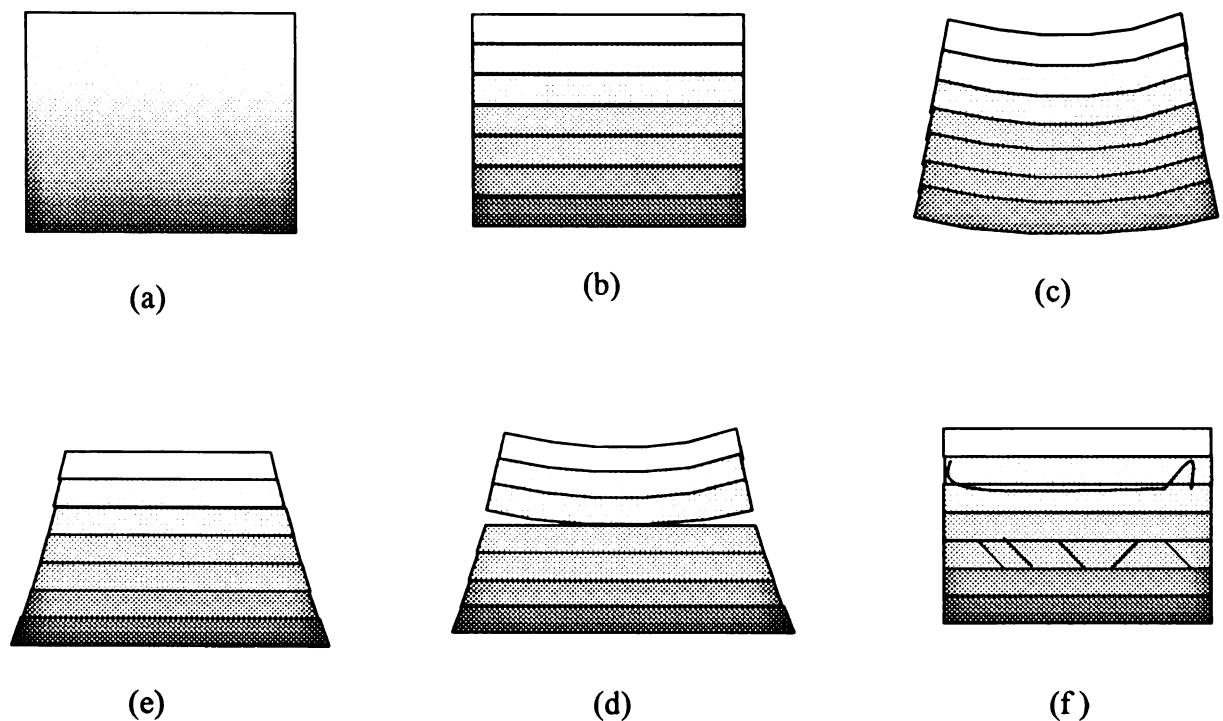
Figure 2.4. Schematic figures for sintering faults (a) ideal FGM, (b) stepwise figures of FGM, (c) warping, (d) frustum formation, (e) splitting and (f) cracking.

16
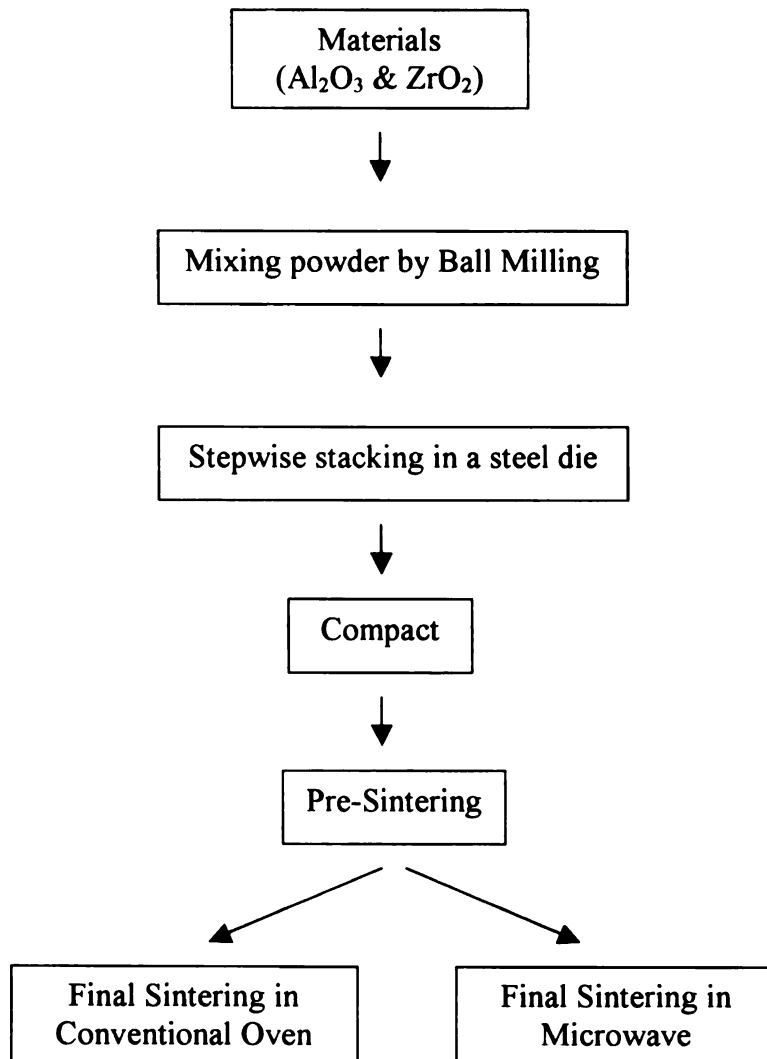
Figure 2.5. Procedure of P /M

2.2 Joining

Ceramic materials (Al_2O_3, ZrO_2, SiC, and Si_3N_4, etc.) have been used extensively due to their structural and functional properties for the last two decades. These properties make them attractive for the industrial application. Generally, ceramics are strong (particularly in compression), excellent oxidation – resistant, wear- resistant, brittle, high temperature properties, corrosion resistance, electrically and thermally insulative, nonmagnetic, chemically stable, low densities, the lack of ductility, sensitivity to defects and very difficult to fabricate. Most ceramic materials are produced in a powder form, thus, making the certain shapes as a green state and then sintering to consolidate them.. Hence, it is necessary to depend on joining techniques to fabricate the desired complex shapes from easily produced simple components. The need for joining technologies has arisen recently due to the frequent use of ceramics. Accordingly, the joining techniques must be considered in dependence on the partners to be joined.

2.2.1 Joining techniques

There are many processes to join ceramic materials [31, 32, 33, 34, 35, 36, 37, 38]. The main techniques can be divided to two categories such as mechanical attachment and direct bonding processes.

2.2.1-1 Mechanical Attachment

Mechanical attachment is widely used to join ceramics to other materials by avoiding stress concentrations due to uneven contact. Crimp, clamp, shrink fit, bolt, screw thread and other variants applications are used as this technique. The techniques, which are performed without bonding medium and creating interface can be quite simple to apply and cheap. Usually, screw thread includes expensive machining and shrink

fitting uses the difference in thermal expansion coefficient between ceramics and metals. Generally, metals contract more than ceramics on cooling and expand more on heating. The joint is performed at the temperature where the metal expanded enough to surround the ceramic, and contract and clamp it on cooling.

2.2.1-2 Direct Bonding processes

Direct bonding processes such as Glaze bonding, Metallized and Brazed joints, Diffusion bonding, Adhesive bonding, Cast around includes the formation of an intimate and continuous interface between the different materials [39, 40, 41, 42, 43, 44, 45]. The interface area describes a discontinuity. This discontinuity is a essential key to make a decision of whether the joining is successful or not.

Glaze bonding is a good process for most types of ceramic materials to join. To join, the mating surfaces should be polished to be flat then coated with a suitable glaze slip and the fired to fuse the glaze and then bonding the two pieces together. Many of the techniques used to join oxide ceramics can be used to join non-oxide ceramics. However, it is important to distinguish between the two classes of materials; due to differences in the chemical nature of non-oxide ceramics, the interfacial ceramic/metal reactions, bonding mechanisms and resulting joint properties are often significantly different. Especially, most oxide ceramics can be joined by silicate glasses or glazes. Also joints can be made with borate and phosphate based glasses or glazes. But non-oxide ceramics are more difficult to join. They tend to react with the glazes and release gas bubbles, which weaken the bond.

Brazing (liquid phase process) has been most often used for joining ceramic to ceramic and ceramic to metal due to the requirement of lower temperature than the

requirement of other techniques. There are two different ways to join by brazing [46]. First, indirect brazing, where the surface of the ceramic material has been metallized with braze filler metal before brazing second, direct brazing, where the filler alloys include active elements like titanium. One of the advantages of the brazing compared with the conventional welding is that the base materials do not melt. Brazing can be applied for dissimilar materials that are impossible to be joined by fusion process because the metallurgical properties are incompatibility. Even though, different mechanical property such as Coefficient of thermal expansion results in thermal stress between the substrate and the bond-layer generally brazing produces less thermal stress and distortion since the whole component is subjected to heat treatment, therefore the distortion can be avoided from localized heating in welding. Moreover, it is a process that can be easily adopted for mass production. The process is relatively simple but depend on complex chemistry, which is occurring at the interface to promote wettability between the substrate material and metal braze such as Ag-Cu alloy braze [47,48], aluminum [49,50] and Ti-Sn alloy braze[51] due to improving the bond strength with improving wettability. For example 72Ag-28Cu alloy is often used because its low melting temperature (780°C) makes work easy and its good ductility make to overcome the mismatches of thermal expansions. Also, CuNiTiB paste are used as the braze filler metals to join Si_3N_4 to Si_3N_4 [52]. A blaze filler metal has been melted up to the melting temperature between two ceramic substrates to perform the brazing with or without external pressure but most advanced ceramics such as alumina, zirconia, silicon carbide and silicon nitride are not wetted by silver, copper or gold that is basic constituents of many brazing alloys [31]. The steps of brazing process have been depicted in Figure 2.6 [32].

Diffusion bonding can be used to join ceramic to metal than ceramic to ceramic (Figure 2.7) [43]. Diffusion boned joints have higher strength than brazed or mechanical joints [53]. It is important than direct diffusion bonding must be used only when the thermal expansions of the two components are matched. With the materials of different thermal expansions, interlayers must be used. This is call as the indirect diffusion bonding. Interlayers are widely used in the form of foils or coatings; electroplated, evaporated or sputtered to reduce values for the bonding parameters such as temperature, pressure and time. The high strains introduced during the cooling of the bond from a relatively high temperature can be accommodated by a combination of elastic and plastic deformation within the interlayer. Thus, interlayers are sometimes used to reduce this effect. However, to avoid the changes in microstructure or composition, the interlayers must be carefully chosen. These changes can be affected in mechanical properties and corrosion behavior. Schematic examples are shown in Figure 2.8. The two components, pressure and high temperature for a certain period of time are needed to apply this method. Generally, small grain size helps for fast grain boundary diffusion, however, only time and temperature are essential factors for many metals in experiment. Even though diffusion bonding requires high temperatures to enhance diffusion but little macroscopic deformation is involved. The mechanism of diffusion bonding illustrates in Figure 2.9. As pressure were applied, plastic deformation and creep deformation have been arisen in the first step then diffusion, recrystallization and grain boundary migration have be placed as following step. Finally, the low pressure (much less than the macroscopic yield stress) and the high temperatures (> 0.5m Tm where Tm is the absolute melting point) have been used to eliminate the pore. Isothermal anneals without

pressure can be help to remove the small voids. The deformation, which has been effected in the beginning of the process involves the power law of creep:

$$\varepsilon = A\sigma^{\pi}\exp - (Qc/RT)$$

where ε = creep rate, σ = stress, Qc= activation energy for diffusion and A and n are constant with n $\approx$ 3-4 for Ti6Al-4V.

The interface consists of bonded areas separated by area containing small voids at the end of this step. Hydrostatic pressure can accelerate void closure by diffusion and plastic deformation for voids greater than 20μm, but below the size diffusion alnoe controls the elimination of voids by surface, grain boundary, and volume diffusion mechanism.

One of the most exciting examples of this process has been observed between alumina and yttria stabilized zirconia since good interface contact can be achieved under superplastic conditions. The diffusion bonding joints were produced at 1475°C under pressure of 12.5MPa to give a bonding strength of 1360MNm^{-2} [54].

Adhesive bonding such as gluing and cementing (for example, Portland cement) give stress free joint when high temperature and vacuum tightness are not presented. This process depends on temperature, the duration and the rate of stressing and may be possible to reduce the strength due to long service. Epoxide, phenolic, acrylic and polyurethane adhesive can be used up to 200°C then, the temperature above the 200°C polymides or other thermally stable polymers can be used.
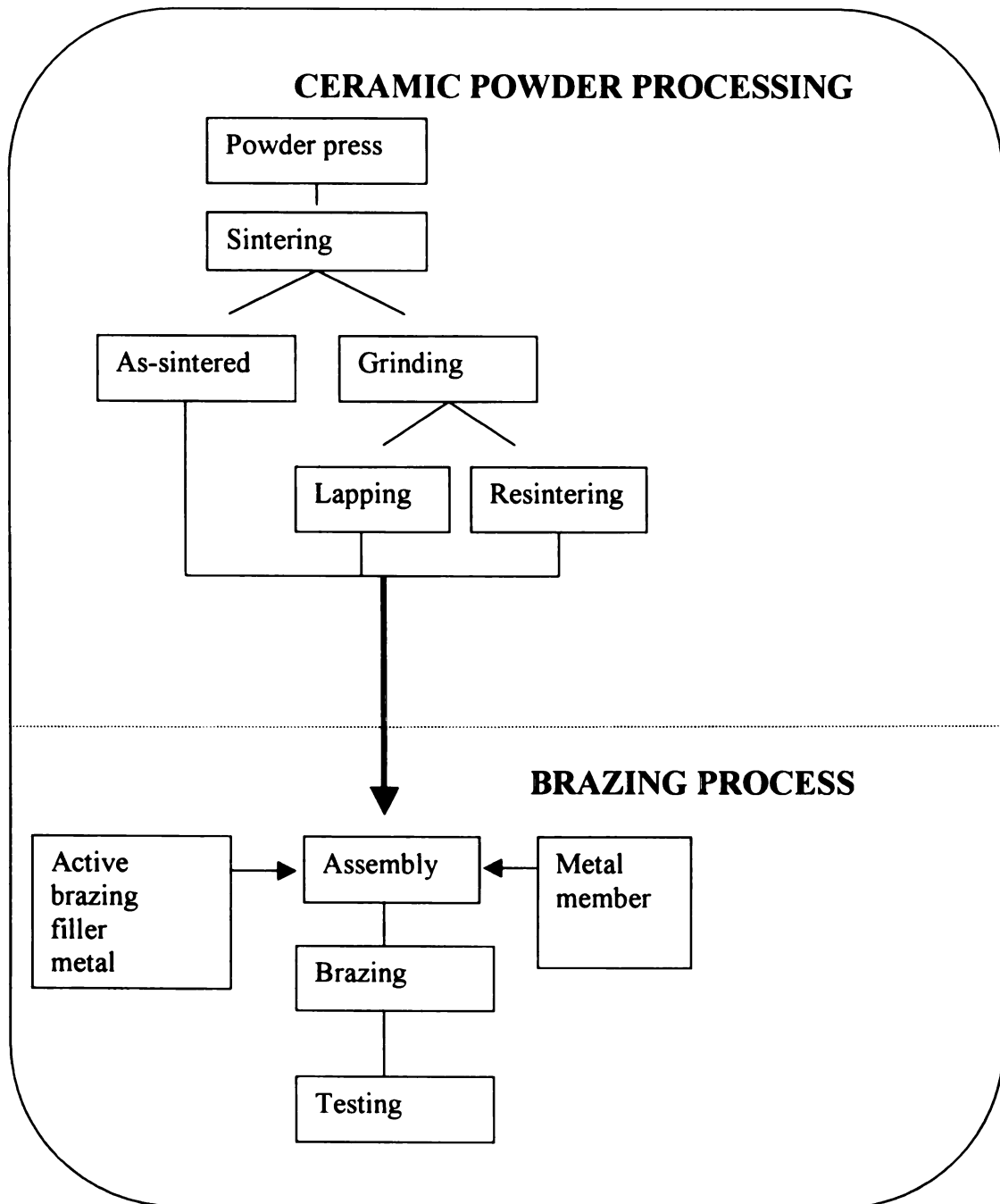
Figure 2.6. Schematic drawing for active brazing process [32]

23

DIFFUSION BONDING TECHNIQUES

PROCESS WITH THE SOLID STATE

Parent/pa rent material interface	Interf -ace foil	Interface coating

Roll Bond-ed	Electro-plated	CVD	CVD

PROCESS WITH THE LIQUID PHASE

Low melting point elements and alloy	Liquid phase Produced by diffusion

Interf-ace foil	Inter faceing coating	Inter Face foil	Inter Faceing coating
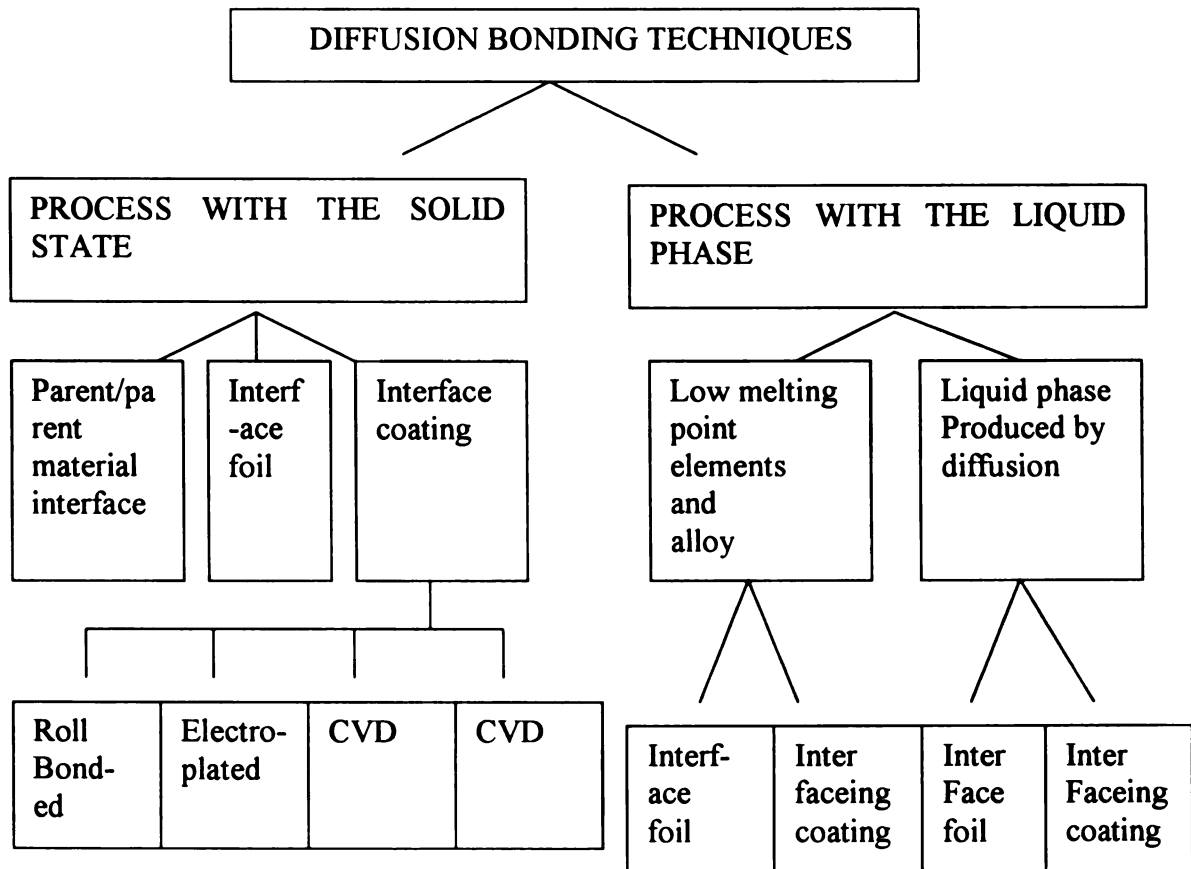
Figure 2.7. Diffusion bonding Techniques [43]

24
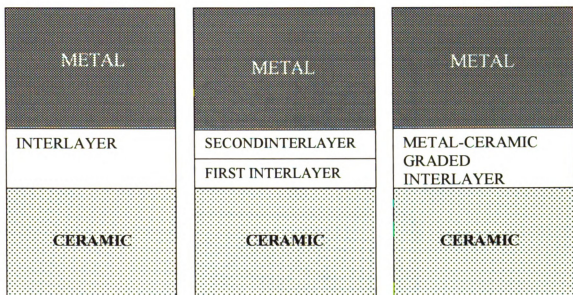
Figure 2.8. Schematic figure of illustrating the multiple interlayers to join the ceramic to metal [31]
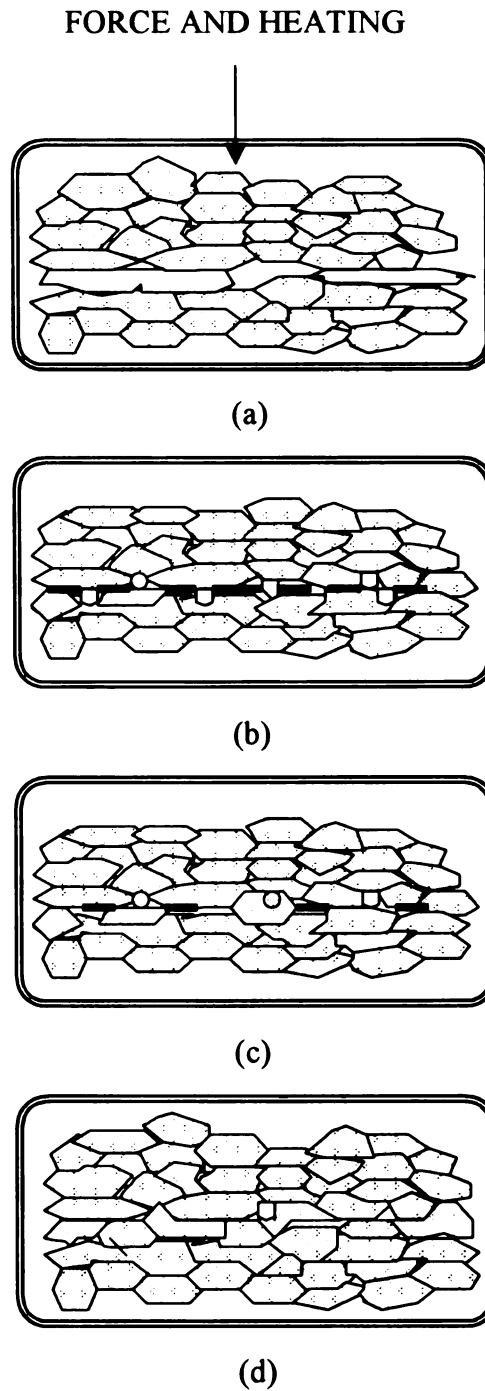
Figure 2.9. Schematic drawing of the reaction of diffusion bonding on bond interface. (a)contact, (b)deformation and interfacial boundary formation, (c)grain boundary migration and elimination and (d) volume diffusion and pore elimination.

REFERNCES

1 Makoto Sasaki and Toshio Hirai, "Fabrication and properties of Functionally Gradient Materials", The Chemical Material Issue of the Ceramic Society of Japan, 9Vol.99, No.10, 1991, pp1002-1013

2 Holt, J. B., Koizumi, M., Hirai, T. and Munir, Z., 1993, Ceramic Transactions: Functionally Gradient Materials, The American Ceramic Society, Westerville, OH.

3 Akira Kawasaki and Ryuzo watanabe, "Concept and Fabrication of Functionally Gradient Materials", Ceramics: charting the future: proceedings of the world Ceramics, 1994, pp1715-1726

4 Kawasaki, A, Watanabe, R, "Concept and P/M Fabrication of Functionally Gradient Materials", Ceram. Int., Vol. 23, No. 1, 1997, pp.73-83

5 H.J. Feng and J.J.Moore, ["The application of Combustion Synthesis in the In-Situ Production of Functionally Graded Materials (FGM)", The Minerals, Metals and materials Society, 1994, pp81-95

6 M. Koizumi and M.Niino, "Overview of FGM Research in Japan", MRS Bulletin, Jan. 1995, pp19-21

7 Shabana, Y M, Noda, N and Tohgo, K, "Combined Macroscopic and Microscopic Thermo-Elasto-Plastic Stresses of Functionally Graded Plate Considering Fabrication Process", JSME International Journal Series A: Solid Mechanics and Materials Engineering (Japan), Vol. 44, No. 3, July 2001, pp.362-369

8 Takashi Kawai, Shun-ichi Miyazaki, Muneki Araragi, "A New method for Forming a Piezo-Electric FGM Using a Dual Dispenser System", The first International Symposium FGM, 1990, pp191-196

9 Chu, C, Zhu, J, Yin, Z and Lin, P, "Structure Optimization and Properties of Hydroxyapatite-Ti Symmetrical Functionally Graded Biomaterial", materials Science and Engineering A(Switzerland), Vol.316, No. 1-2, 15 Oct. 2001, pp.205-210

10 John J. Lannutti, " FGMS in High-Heat –Flux Environments: Cost/ Performance Issues", MRS Bulletin, Jan. 1995, pp50-51.

11 Uzun, H, "Effect of Different Factors on Crack Growth Behavior of SiC(P)/Al2124 Single Core Bulk Functionally Graded Materials", Proc. Turkish Ceram. Soc. IV. Ceramic Congress Proceedings Book, Eskisehir, Turkey, 22-25 September 1998, 4, 1999, pp.481-487

12 Huang, PJ, Hubbard, C , Swab, JJ, Cole,MW, Sampath, S, Depalo,S, Gutleber, J, Kulkarni, A and Margoloes, J, "Functionally Graded Materials for Gun Barrels", Ceram. Eng. Sci. proc., Vol.20, No.4, 1999, pp.33-38

13 Lee, C S, De Jonghe, L C and Thomas, G, "Mechanical properties of polytypoidally Joined Si sub 3 N sub 4- Al sub 2 O sub 3", Acta materialia (USA), Vol. 49, NO. 18, 26 Oct. 2001, pp.3767-3773

14 Yokoyama, A, Watari, F, Miyao, R, matsuno, H, Do, M, Kawasaki, T, Kohgo, T, Omori, M and Hirai, T, "Mechanical Properties and Biocompatibility of Titanium-Hydroxyapatite Implant Material Prepared by Spark Plasma Sintering Method", Key Engineering Materils (Switzerland), Vol.192-195, 2001, pp.445-448

15 Ma, J, Tan, GEB, "Processing and Characterization of Metal-Ceramics Functionally Gradient Materials", Journal of Materials Processing Technilogy (Netherlands), Vol. 113, No. 1-3 15 June 2001, pp.446-449

16 Akira "Concept and P/M Fabrication of FGMs, p73

17 Kwon, P., 1994, Macroscopic Design and Fabrication of Functionally Gradient Materials, Ph. D. Dissertation, U.C. Berkeley

18 Kwon, P., Dharan, C.K.H. and M. Ferrari, 1994, J. Energy Res. Tech., 116, pp.115-120

19 A. J. Sanchez-Herencia, K. Morinaga & J. S. Moya, "Al2O3/Y-TZP Continuous Functionally Graded Ceramics by Filtration-Sedimentation", Journal of European Ceramic Society, 17, 1997, pp1551-1554

20 D.P.H.Hasselman and G.E.Youngblood, "Enhanced Thermal Stress Resistance of Structural Ceramics with Thermal Conductivity Gradient", Journal of The American Ceramic Society, Vol. 61, No.1-2, 1978, pp.49-52

21 Tohru Hirano and Kenji Wakashima, "Mathematical modeling and design", MRS Bulletin, Jan. 1995, pp40-42

22 Makoto Sasaki and Toshio Hirai, " Fabrication and Properties of Functionally Gradient Materials", Journal of the Ceramic society of Japan international edition, vol99, No. 10, 1991 pp970-980.

23 Biesheuvel, PM and Verweij, H, "Calculation of the Composition profile of a Functionally Graded Material Produced by Centrifugal Casting", J. Am. Ceram. Soc., Vol.83, No.4, 2000, pp.743-749

24 Zang, L.M., Yuan, R.Z., Oomori,M. and hirai, T., 1995, J.Mat.Sci.Let., 14, 22, pp1620-1623

25 Mizno, Y., Kawasaki, A., and Watanabe, R., 1995, Metall. Trans., Vol. 26B, pp75-79

26 German, R.M. 1994 Powder Metallurgy Science, metal Powder Industries Federation, Princeton, New Jersey

27 Hur, S K, Yoo, S H, Groza, J R , Doh, J M, Yamazaki, K and Shoda, K, "Graded Coatings by Gradient Temperature Densification", J. Mater. Res., Vol. 13, No. 5, 1998, pp.1255-1259

28 Reed, J., 1989, Introduction to the principles of Ceramic processing, john Wiley & Sons, New York, p99 &p191

29 Yeh, T. and Sacks. M.D., 1988, J. Am. Ceram. Soc., Vol. 71, no. 12, ppC484-487

30 Zhu, J, Lai, Z, Yin, Z, Jeon, J and Lee, S, "Fabrication of ZrO sub 2- NiCr Functionally Graded Material by Powder Metallurgy", Material Chemistry and Physics (Switzerland), Vol. 68, No. 1-3, 15 Feb. 2001, pp.130-135

31 J. Fernie, A. Sturgeon, "Joining Ceramic Materials", Ceramic Te^{c}hnology International, 1993, pp183-186

32 A.S. Bahranic, "The Bonding of Ceramic to Ceramic and Ceramic to Metal", The international journal for the joining of metals : the journal of the European Institute for the joining of materials (JOM), vol.2(4), Dec. 1990, pp.104-107

33 "Ceramics and Glasses', Engineered Materials handbook, vol4, ASM International pp.477-531, section 7 Joining

34 A.Meier, D.A. Javernick, and G.R.Edwards, "Ceramic-Metal Interfaces and the Spreading of Reactive Liquids," JOM Feb. 1999, pp.44-47

35 Servet Turan, Ian A. Bucklow, and Robert Wallach, "Capacitor-Discharge Joining of Oxide Ceramics," J. Am. Ceram. Soc., vol.82 No.5, 1999, pp.1242-1248

36 A.G.Foley, "Ceramic Joining Applications in Gas Turbines," Industrial Ceramics, vol.19 No.3, 1999, 193-195

37 A.Kara-Slimane, D.Juve, E.Leblond and D.Treheux, "Joining of AlN with Metals and Alloys," Journal of European Ceramic Society, vol.20, 2000, pp.1829-1836

38 N.D.Tinskey, J.Huddleston, and M.R.Lacey, "Reduction of Residual Stress Generated in Metal-Ceramic Joining," materials and manufacturing processes, vol.13, No. 4, 1998, pp.491-504

39 E.Butler, M.H. Lewis, A.Hey and R.V. Sharples, Ceramic Joining in Japan. Report, The welding Institute, 1986

40 R.E. Loehmanm, "Joining of Ceramics", American Ceramic Society Bulletin, 67(2), pp375-380, 1988

41M.G. Nicholas and R.J. Lee, "Joining dissimilar Materials", Metals and Materials, 5(6), 1989, pp.348-351

42 M.G. Nicholas and D.A. Mortimer, "Ceramic / Metal Joining for Structural Applications", Material Science and Technology, vol.1, pp.657-665,1985

43 P.G. Partridge and C.M. Ward-Close, "Diffusion Bonding of Advanced materials", Metals and Materials, vol.5 (6), pp334-339, 1989

44 H.E. Pattee, "Joining Ceramics to metals and other materials". Welding Research Council Bulletin 178, pp1-43, 1972

45 Lee, C S, Zhang, X F and Thomas, G, "Novel Joining of Dissimilar Ceramics in the Si sub 3 N 4 – Al sub 2 O sub 3 System Using polytypoid Functional Gradients", Acta Materialia (USA), Vol. 49, No. 18, 26 Oct. 2001, pp.3775-3780

46 O.M.Akselsen, "Review Advances in Brazing of Ceramics", Journal of Materials Science vol. 27, 1992, pp1989-2000

47 T.Kuzumaki, T. Ariga and Y.Miyamoto, "Effect of Additional Elements in Ag-Cu Based Filler Metal on Brazing of Aluminum Nitride to metal", ISIJ International, Vol. 30, No. 12, 1990, pp.1135-1141

48 D.Sherman, "The Mechanical Behavior of Layered Brazed Metal/Ceramic Composites", Materials Letteres, Vol. 33, 1998, pp.255-260

49 K.Suganuma, 'New Process for Brazing Ceramics Utilizing Squeeze Casting", Journal of Materials Science, Vol. 26, 1991, pp.6144-6150

50 K.Suganuma, T. Okamoto and M. Koizumi, "Joining of Silicon Nitride to Silicon Nitride and to invar Alloy Using An Aluminum Interlayer", Journal of Material Science, Vol. 22, 1987, pp1359-1364

51 C.G. Wang, H.P.Xiong and Z.F. Zhou, "Joining of Si3N4/Si3N4 with CuNiTiB paste Brazing Filler Mtals and Interfacial Reactions of the Joints", Journal of Materials Science, Vol. 34, No. 12, 1999, pp.3013-3019

52 Chuahgeng Wan, Huaping Xiong and Zhenfeng Zhou, "joining of Si3N4/Si3N4 with CuNiTiB paste brazing filler metals and interfacial reactions of the joints", Journal of materials science, Vol. 34, 1999, pp.3013-3019

53 Yamada T, et al, high Temp Tech, Vol. 5, 1987, pp.193

54 Nagano T, hidezumi K and Fumihiro W, MRS int. meeting on advanced materials, Tokyo,1988

Chapetr 3

EXPERIMENATAL PROCEDURE

3.1 Materials

Materials used to fabricate the specimens for this thesis are commercial powders of alumina (Table 3.1), hydroxyapatite (Table 3.2), two kinds of partially stabilized zirconia (Table 3.3, Table 3.4), fully stabilized stabilized zirconia (Table 3.3) and MaCor™ (Table 3.5) were used.

Alumina is chemically so stable, because of their strong ionic and covalent bonding between the Al and O ion, as expected from the value of heat formation (~400 Kcal / mol), Al_2O_3 has also outstanding physical stability, such as a high melting point (2050°C, or 3720°F), the highest hardness among oxides, and high mechanical strength that is high at room temperature but is lowered largely above 1100°C for wear application. The superb tribological properties (friction and wear) of Al_2O_3 occur only when the grains very small (<4 μm) and have a very narrow size distribution. If large grais are present, they can pull out and lead to very rapid wear of bearing surfaces due to local dry friction. And, high density, high purity (> 99.5%) alumina is used in load-bearing hip prostheses and dental implants because of its combination of excellent corrosion resistance, good biocompatibility, wear resistance. Moreover, Al_2O_3 is a typical electrically insulating material. The most demanding use is for Al_2O_3 as a high-voltage, high temperature insulator with thermodynamic stability in a reducing environment. In

these reasons, a 99.99% pure alumina powder (TM-DAR, Taimi chemical Co. LTD) has been successfully used.

Two kinds of partially stabilized zirconia powder and one kind of fully stabilized zirconia powder were used: (1) A 99.9% pure partially stabilized 3 mol% yttria – zirconia (PSZ) powder (TZ – 3YS, Tosoh Ceramic Division, Bound Brook, New Jersey), (2) a typically 99.95% pure stabilized 5 mol% yttria powder (ZrO_2, Cerac INC. Milwaukee, WI) and (3) a 99.9 % pure fully-stabilized 8 mol % yttria- zirconia (FSZ) powder (TZ-8YS, Tosho Ceramic Division, Bound Brook, New Jersey). In this study, two difference kind zirconia powders with almost similar chemical composition had the difference in average particle size. Yttria stabilized zirconia powder has attracted considerable attention for their superior mechanical properties such as bending strength and fracture toughness [1,2]. The high temperature stable form of zirconia has a cubic fluorite structure. Because the ionic radius of Zr^{4+} is too small (0.084nm, or 0.003μm.) to satisfy the required ratio of cation and anion radi for an 8-coordinated polyhedron of the fluorite structure, pure ZrO_2 shows a polymorphic transformation [3]:

$$Monoclinic \xleftrightarrow{\quad 1000^0 C \quad} Tetragonal \xleftrightarrow{\quad 2370^0 C \quad} Cubic \xleftrightarrow{\quad 2680^0 C \quad} Liquid$$
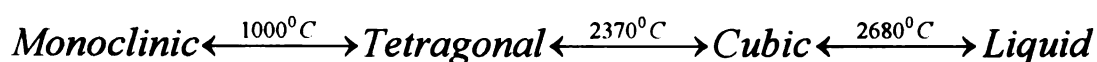
Stabilized zirconia shows high oxygen ion conductivity, because of the high concentration of oxygen vacancies. It has been widely applied as the solid electrolyte in oxygen concentration detectors or fuel cells. Generally, multiphase ceramics with tetragonal and cubic forms are called partially stabilized zirconia (PSZ), and monophase ceramics in tetragonal form are called tetragonal zirconia polycrystal (TZP). Those ceramics show very high mechanical strength and fracture toughness. Fully stabilized zirconia has flexure strength values from 360 to 660 MPa and fracture toughness values

of 2.4 MPa√m, which are much lower than those of TZP. Moreover, because stabilized ZrO_2 has a high melting point (~2680°C or 4855°F), low thermal conductivity, low vapor pressure and good corrosion resistance, it gives good performance as a refractory and a heat insulator for high temperature use.

Hydroxyapatite, known as a bio-ceramicm, is a compound that is similar to bone mineral, sharing the formula Ca_{10} $(PO_4)_6OH_2$. Crystal lattice of hydroxyapatite is hexagonal or pseudohexagonal [4]. As shown by radiographic diffraction analysis, calcium and phosphate mineralize in bone in the form of an apatite, which is similar to hydroxyapatite $[Ca_{10}(PO_4)_6(OH)]$ - other configurations may include brushite ($CaHPO_4$ $2H_2O$) or octacalcium phosphate $[Ca_8H_2(PO_4)_65H_2O]$. Crystalline structure can be changed by manipulation of the calcium-to-phosphate ratio, as well as changing the content of carbonate and fluorine. When human blood meets the hydroxyapatite, hydroxyapatite acts like human bone. Due to the chemical similarity between synthetic HAP and bone, no inflammatory reaction of tissue encapsulation is occurring during the implantation, but chemical interaction takes place. HAP with optimized microstructure supports the cell adhesion and -mineralization strongly. However, the biofunctionality of synthetic HAP is not comparable to bone. Low strength, insufficient fracture toughness and reliability exclude its application as a bone substitute material with load bearing function at the moment [5, 6,7].

MaCor™, polycrystalline alumina, is a machinable glass ceramic reinforced by a flurophlogopite mica plates (Coring code 9658) [8]. MaCor™ gives the performance of a technical ceramic with the versatility of a high performance plastic. MaCor™ glass ceramic is an outstanding engineering material and is machinable with ordinary

metalworking tools. It has a high maximum use temperature of 800°C continuously, 1000°C at peaks and low thermal conductivity and is a useful high temperature insulator. It is strong and rigid. MaCor™, unlike high temperature plastics, will not creep or deform. Moreover, it is an excellent electrical insulator and it has zero porosity. When properly baked out, it will not outgas in ultra high vacuum applications. Table 3.6 gives coefficients of thermal ecpansion used in this study.

Pencil lead was used as fugitive phase to make the internal channels and surface channels in this study. Pencil lead is made of nontoxic mineral called graphite. Graphite is one of the three forms of crystalline carbon; the other two are diamond and fullerenes. The layered crystal structure of graphite gives it some of its most important characteristics and one of the lowest coefficients of friction of any material. Over a wide temperature range, graphite is a sectile, flexible material exhibiting low coefficient of thermal expansion, high thermal and electrical conductivity, and is almost chemically inert (Table 3.7). Consequently, graphite is commonly used for the following attributes: lubrcity, electrical conductivity, refractoriness, thermal conductivity, chemical inertness, low thermal expansion, and as a carbon source.

Because of graphite's unique structure, it is highly anisotropic or directional in properties. This is due to the differences in separation distances of atoms between the layer planes (0.335mm). Hence, electrical conductivity is good along the direction of the lattice planes, and poorer perpendicular to the lattice planes. A similar result is seen with strength. The good lubricity of graphite products also results from the hexagonal arrangement of layer planes. Because each plane is weakly bonded to those above and below it, each is relatively free to slip or side past one another.

Table 3.1. Alumina (TM-DAR, Taimi Co, Japan) powder information [9].

Grade	TM-DAR
Lot No.	3116
Crystal Form	α
Surface Area (m²/g)	13.8
Average particle Size (μm)	0.20
Purity Al_2O_3 (%)	99.99
Impurity Na (ppm)	1
K (ppm)	1
Fe (ppm)	3
Ca (ppm)	1
Mg(ppm)	1
Si (ppm)	4
Green Density (g/cm³)	2.31
Fired Density (g/cm³)	3.96

Table 3.2. Hydroxyapatite powder information [10].

Description	Calcium Hydroxyapatite Ca10(OH)2(PO4)6, Powder,99%
Lot Number	X21949
Specific analysis or property	Test for Found Theoretical Ca 36.24% 39.90%
Spectrographic analysis	Element Result (%) Al <0.01 Cr <0.01 Fe <0.01 Mg 0.1 Si 0.1 Sr <0.01
X-Ray Diffraction Analysis	Chart Number: D34565 Major $Ca_5(PO_4)_3(OH)$ matches PDF 9-432 Hexagonal

Table 3.3. Tosoh zirconia powder information [11].

Materials	TZ-3YS (partially stabilized)	TZ-8YS (fully stabilized)
Y_2O_3 (mol %)	3%	8%
Y_2O_3 (wt %)	5.15±0.20	13.3±0.60
Al_2O_3 (wt %)	≤0.1	≤0.1
SiO_2 (wt %)	≤0.02	≤0.02
FeO_2 (wt %)	≤0.01	≤0.01
Na_2O (wt %)	≤0.04	0.12
Specific surface Area (m^2/g)	7±2	7±2
Density (g/cm3)	6.05	5.90
Bending Strength R.T. (MPa)	1200	300
Fracture Toughness R.T. ($Mpa\ m^{0.5}$)	5.0	1.5
Hardness (HV 10)	1250	1250
Mean particle diameter (µm)	0.59	0.54

Table 3.4. Cerac zirconia powder information [12].

Lot Number	X17183-1
Description	Zirconium Oxide-Yttria Stab. 5.2wt% Y_2O_3 100% < 3 mic. Typically 99.95% pure
Specific analysis or property	Test for Found Theoretical Y2O3 5.2% 5.2%
Spectrographic analysis	Element Result(%) Ca 0.004 Hf 1.54 Mg <0.001 Si 0.002 Ti 0.03
X-Ray Diffraction Analysis	Major $Y_{0.15}Zr_{0.85}O_{1.93}$ matches PDF30-1468 Cubic Minor ZrO_2 matches PDF37-1484 Monoclinic

Table 3.5. MaCor information [13].

Temperature Limit	1000°C
Dielectric Constant	1 Khz at 25°C 6.03
Dielectric Strength	40KV/mm
DC Volume Resistivity	At 25 °C . 1016 ohm-cm
Thermal Conductivity	At 25°C 1.46 W/m°C
Density (g/cm^3)	2.52
Modulus of Elasticity	At 25°C 64 GPa
Porosity	0

Table 3.6. Thermal expansion coefficients for the materials included in this thesis.

Materials	Temp. Interval (°C)	Thermal Expansion (10^{-6}K^{-1})	Reference
Al$_2$O$_3$	20	8	14
	25-	8.1	15
	0-1000	8.8	16
ZrO$_2$	Room temp	8.5	17
	25-	10.0	10
	1000	11	18
	Monoclinic	7	
	Tetragonal	12	
HAP	25-400	14.5	19
	400-800	17.5	
MaCor	25-300	9.3	20
	25-600	11.4	
	25-800	12.6	

Thermal conductivities, young's modulus and powder sizes which are used in this study are given in table 3.8, 3.9, and 3.10.

The Silica-Film^{TM} (Emulsitone Company, Whippany,NJ) used as an interlayer material (spin-on material) to join has impurity less than one part per million of metallic ions in alcohol based liquid material. It can be densified by annealing at 200°C for 20minutes.

Table 3.7. Graphite information.

property		Reference
Specific Gravity	2.2	
Electrical Conductivity (ohm.m) Perpendicular to c-axis Parallel to c-axis Natural	 9.8×10^{-6} 4.1×10^{-5} 1.2×10^{-6}	16
Thermal Conductivity (Watts/meter.Kelvin at 273K) Perpendicular to c-axis Parallel to c-axis Natural	 250 80 160	16
Coefficient of Thermal Expansion $(10^{-6}K^{-1})$ Overall a-axis* c-axis	 7.8(at 293K), 8.9(500K) -1.2(at293K), -0.7(at500K) 25.9(at 293K), 28.2(500K)	17
Bulk Modulus (GPa)	34 7.3-10.7(non-irradiated, uncoated) 2.5-7.3 (non-irradiated, coated) 14.0-16.9(irradiated, uncoated) 7.8-8.4(irradiated, coated)	18, 19
Mohs Hardness	1-2	
Young's Modulus (GPa) a-axis c-axis	 1060 36.5	20

*:"a" direction is parallel to the basal planes

"c" direction is perpendicular to the basal planes

Table 3.8. Thermal conductivities of the materials included in this thesis.

Materials	Thermal Conductivity (W/m°K)	Reference
Al_2O_3	21	14
	16-39	21
ZrO_2	1.9	14
	1.675 (at 100°C)	17
	2.094 (at 1300°C)	17
HAP	0.013	22
MaCor	1.46	

Table 3.9. Young's modulus for the materials included in this thesis.

Material	Young's modulus (GPa)	Reference
Al_2O_3	322	2
	366	23
	390	22
ZrO_2	131	10
	190 (partially stabilized)	24
	220 (cubic)	
HAP	80-100	22

Table 3.10. Powder size used in this thesis.

Materials	Average particle size (μm)
Alumina (TMDAR)	0.2
3 mol % Zirconia (TZ3YS)	0.59
8 mol % Zirconia (TZ8YS)	0.54
5.2 mol % Zirconia (CERAC)	90% < 1.79
	50 % < 1.23
	10 % < 0.77
Hydroxyapatite (HAP)	2~3

3.2 Powder Preparation

Monolithic ceramic specimens were prepared using the zirconia, alumina, or hydroxyapatite powders discussed above. In this study, not only each powder by itself was processed but also a variety of composite powders were processed. To fabricate the FGMs specimens, alumina and zriconia powders were balled in variety compositions. Table 3.11 presents the variety of the compositions. The mixing of powders with two or more components was performed by dry ball milling in a plastic ball mill for 24 hours with alumina grinding media at a rotation rate of 110 revolutions per minute. The ball mill charge consisted of a total of 50 grams of powder and about 250 grams of alumina media and zirconia media, which gave a volumetric ratio of roughly 1 part powder to 2 parts of the alumina media. The kind of media used was dependent on the kind of powders. For example, to mix the zirconia powders, the zirconia media was used, and to mix the two different powders together the media was dependent on the ratio of powders so the media was chosen by depending on the powder with a larger amount. The mixing was done for approximately 24 hours, with the procedure of interruptions at about 8 hour intervals to shake the ball mill. The reason for shaking is to evenly distribute the powders in order to get microscopically homogeneous materials.

Table 3.11. Summary of mixing ratios of powders.

Group	Composition
TMDAR / HAP	75% TMDAR / 25%HAP
	25% TMDAR / 75%HAP
TMDAR / TZ8YS	75% TMDAR / 25%TZ8YS
	25% TMDAR / 75%TZ8YS
TMDAR / TZ3YS	90% TMDAR / 10% TZ3YS
	80% TMDAR / 20% TZ3YS
	75% TMDAR / 25% TZ3YS
	70% TMDAR / 30% TZ3YS
	60% TMDAR / 40% TZ3YS
	50% TMDAR / 50% TZ3YS
	40% TMDAR / 60% TZ3YS
	30% TMDAR / 70% TZ3YS
	25% TMDAR / 75% TZ3YS
	20% TMDAR / 80% TZ3YS
	10% TMDAR / 90% TZ3YS
TZ3YS / CERAC	85%TZ3YS / 15% CERAC
	75%TZ3YS / 25% CERAC
	72.5%TZ3YS / 27.5% CERAC
	70%TZ3YS / 30% CERAC
	65%TZ3YS / 35% CERAC
	60%TZ3YS / 40% CERAC
	55%TZ3YS / 45% CERAC
	50%TZ3YS / 50% CERAC
	25%TZ3YS / 75% CERAC
TMDAR / TZ3YS / CERAC	70% TMDAR/30%(70%TZ3YS / 30% CERAC)
	50% TMDAR / 50%(70%TZ3YS / 30% CERAC)
	30% TMDAR / 70%(70%TZ3YS / 30% CERAC)

3.3 Specimens preparation

Thin and round shape specimens were produced by using the powders which were described above and sintered. And then, the specimens were polished, joined and sectioned to see via SEM.

3.3-1 Specimen Pressing

All specimens included in this study were pressed from commercially available powders in a uniaxial steel die at a pressure of approximately 35Mpa (Figure 3.1). From 1.8 grams to 3 grams of powders were used to form the specimens. The mass of the powders was measured with accuracy of ± 0.003 grams by using an electronic balance (Mettler Instriment Corporation). The green state specimens were about 2.2 cm in diameter after cold pressing. The fugitive phase used in this study to form channels and cavities within the specimens were incorporated during the powder compacting stage.

Two types of fugitive phase were used in this study. One type was a pencil lead, with nominal diameters of 300, 500, 700 and 900 microns. Figure 3.2 shows the microstructure of pencil lead. The pencil lead was cut into lengths approximately 0.8 cm to 1.3 cm and embedded in the ceramic powder. The second type of fugitive phase used was graphite, which was machined to a range of geometric shapes. Initially, about one-half to one-third of the powder mass to be used in pressing a given specimen was loaded into the cylindrical steel die. Then, the powder bed was smoothed and the fugitive phases were placed on the top of the smoothed powder bed. Next, the remaining powder was added to the die, and the specimen was pressed at a press of approximately 35 MPa using a hydraulic press. Several fugitive phases from one to twelve pencil leads were placed

into the powder. Two types of configurations were used for the fugitive phase placement within the powder compact. In one configuration, a single row of aligned fugitive phase rods was placed within the powder compact. In a second configuration, aligned fugitive rods were placed at two different levels within the specimen (figure 3.3 and figure3.4).

3.3-2 Presintering

After the fugitive phase rods had been incorporated into the powder compact, the presintering to burn-out the fugitive phase was done at a temperature of from 400°C to 1200°C in air for from one hour to four hours, with the average heating rate of from 5°C to 10°C per minute and cooling rate of from 5°C to 10°C. To figure out the successful holding time and the peak temperature, variety experimental conditions were done in the conventional electrical resistance furnace. During the processing the specimens were placed on a thin alumina powder bed, which was spread on an alumina setter (Figure 3.5).

3.3-3 Conventional sintering for Final Sintering

The pre-sintered specimens were subsequently fully sintered using either microwave processing or conventional processing. The conventional sintering was done with an electric resistance-heated furnace (Carbilite, Inc.) with an Eurotherm temperature controller (Figure 3.6). The heating and cooling rate was approximately 10°C per minute, with two different holding times, which are two hours and four hours at two different peak times that were1300°C and 1430°C (Table 3.12). The conventional sintering was

"Carver Laboratory Press"
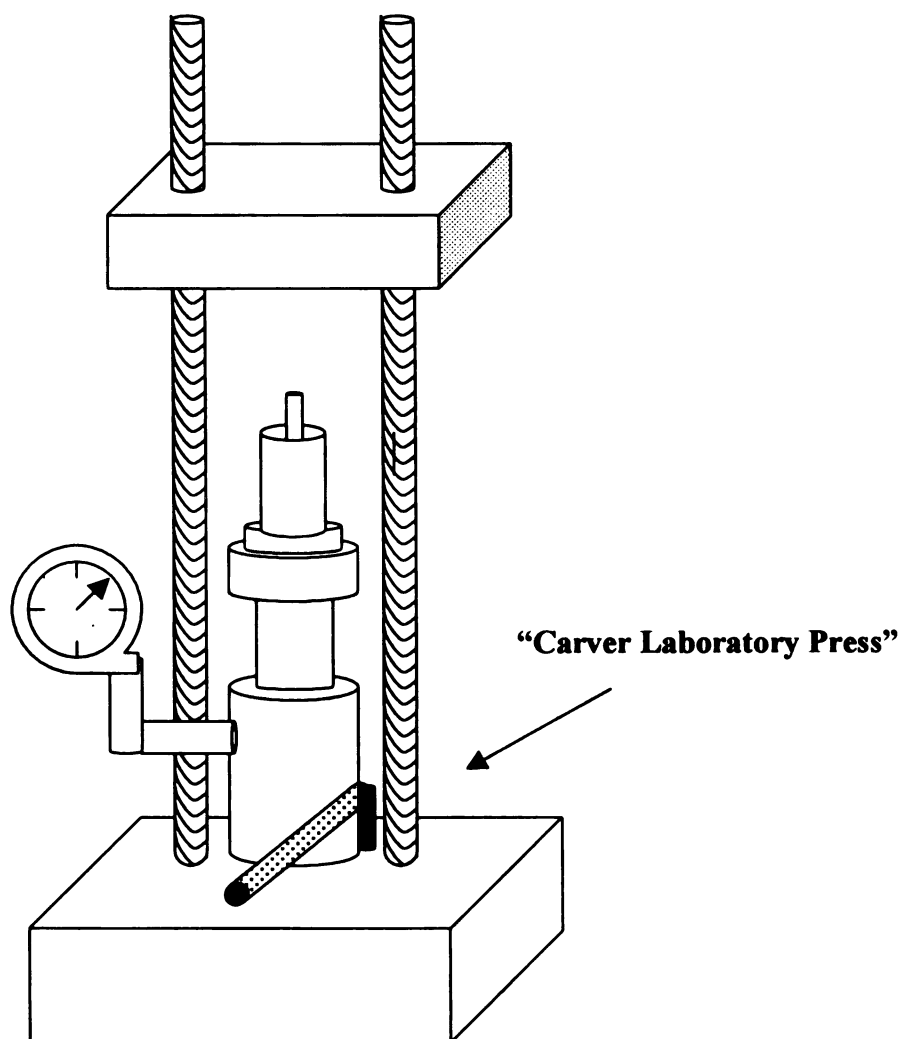
Figure 3.1. Schematic drawing of "Carver Laboratory press".
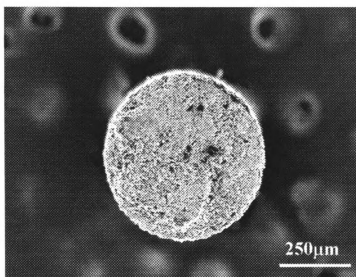
(a)
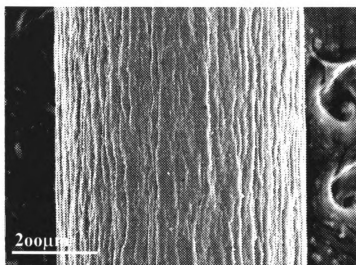
(b)

Figure 3.2. SEM picture of Pencil lead (a) one end of pencil lead, (b) the surface of pencil lead.
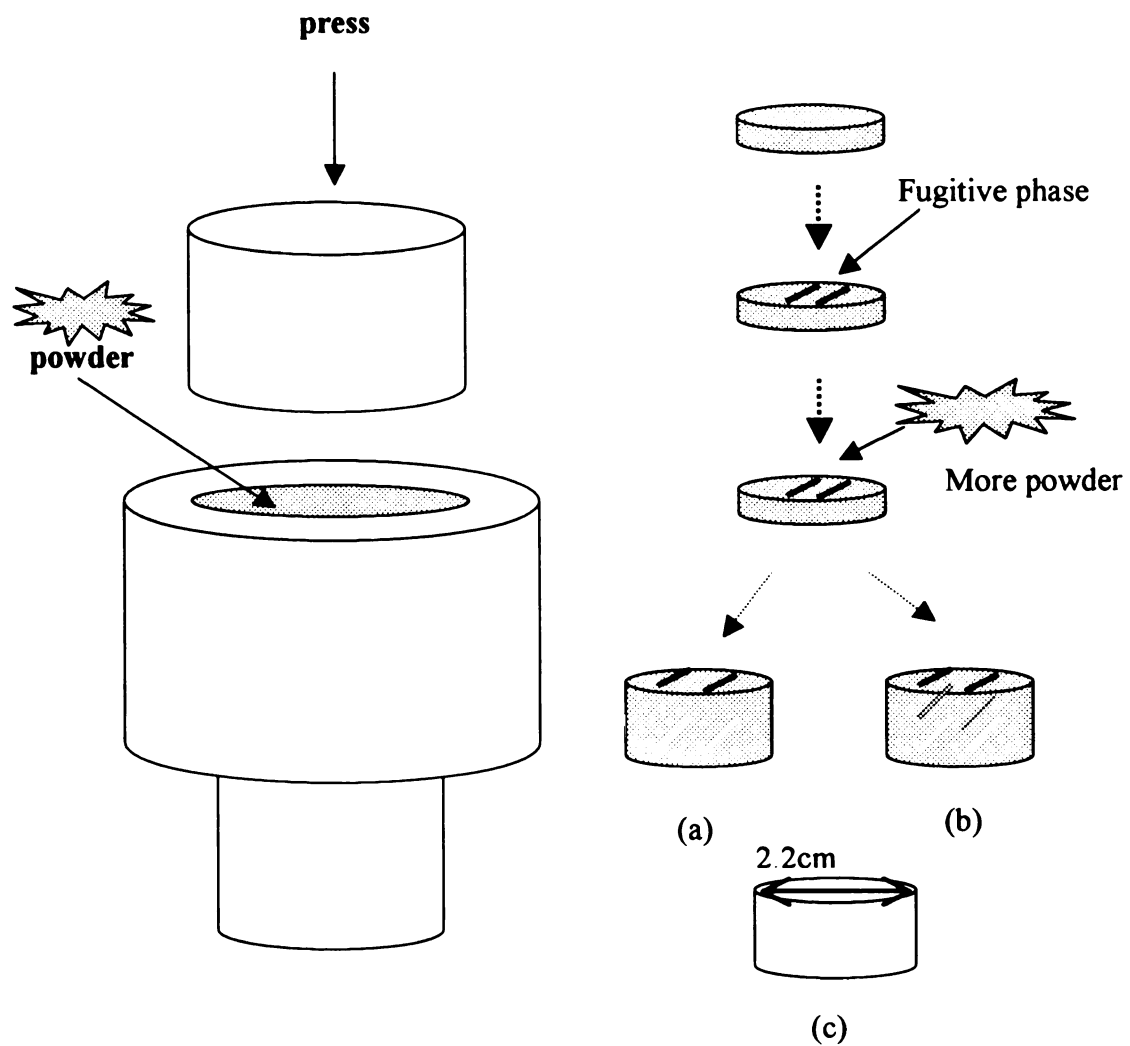
Figure 3.3. Overview of specimen processing (a) one layer embedded fugitive phases and fugitive phases on the top surface and (b) two layers embedded fugitive phases and on the top surface (c) dimension of the specimen.
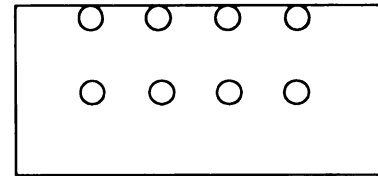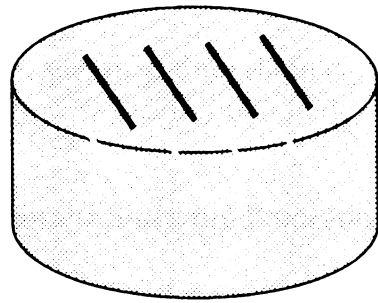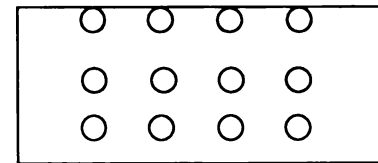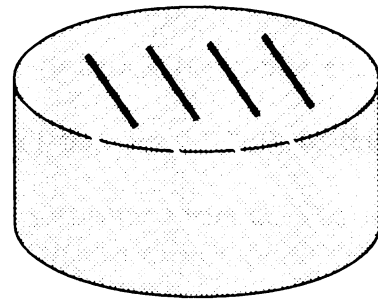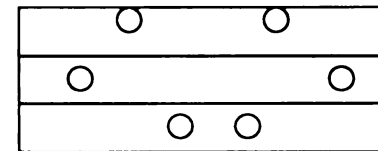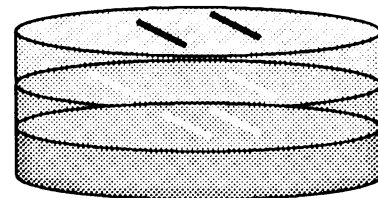
Figure 3.4. Configuration of FGMs specimens with internal channels and embedded channels (a) one internal channels and channels on surface and (b) two different levels of embedded channels and channels on surface in one homogeneous material (c) two levels of embedded channels and channels on surface in FGMs Specimens.

done at higher temperatures and longer times than the microwave sintering, since in order to get a comparable density and microstructure as obtained via microwave sintering, the conventional furnace's processing temperature and time need to be increased. During the conventional sintering, from six to eight specimens were sintered simultaneously.

3.3-4 Microwave Sintering Processing

The presintered specimens were sintered in a single mode resonant microwave cavity at a frequency of 2.45GHz using a 0-2 kW microwave power supply (Model CMPR-250, Wavemat Inc., Plymouth, MI) (Figure 3.7, 3.8). The specimens were placed in a refractory casket (specimen enclosure, Zircar Fibrous Ceramics, Zircar Products, Florida, NY) that served both to thermally insulate the specimens and to provide a microwave suspector material. The refractory casket was made from the low-density yitria stabilized zirconia (ZYC, Zircar Fibrous Ceramics). Approximately 5mm diameter view hole, which is at the 10mm above from bottom of the zirconia casket was bored through the refractory casket to measure the temperature. Then, the specimens on the aluminosilicate were placed on the bottom stage of the microwave unit. From five to six specimens were microwave sintered in a given batch (Figure 3.9).

Microwave input power was set to 100 watts and manually controlled with a ramp rate of 20 – 100 watts every 3 minutes. The temperature was measured by an optical thermometer (Accufiber Model 10 Optical Fiber Temperature Control System, Accufiber Division, Luxtron Corporation, Beaverton, OR) after starting the coupling. Before coupling, which is around 500°C, the temperature was unknown. Microwave forward power was
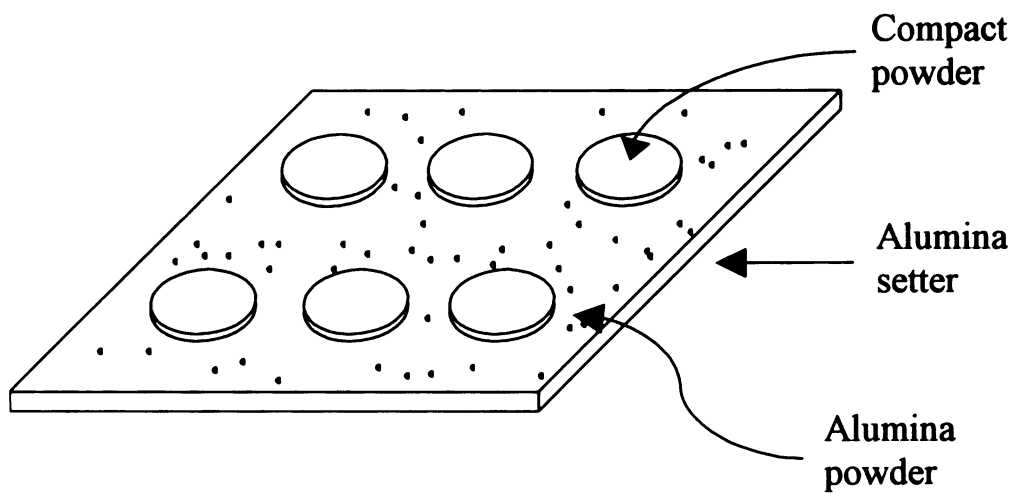
Figure 3.5. Schematic figure of specimens on the setter.
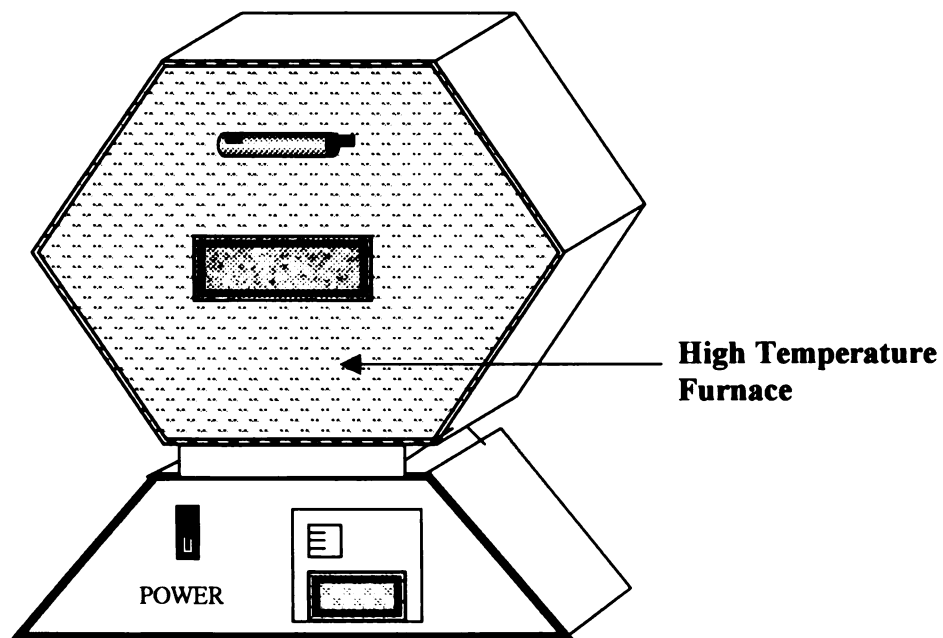
Figure 3.6. Conventional high temperature furnace.

Table 3.12. The conditions of conventional sintering

Material	Sintering Temperature (°C)	Holding Time (hour)	Heating/cooling rate (°C)
TMDAR	1430	1 or 4	10
TZ3YS	1300 or 1430	1, 2 or 4	10
TZ8YS	1300 or 1430	1,2or 4	10
HAP	1375	2	10
Alumina / Zirconia composite	1300 or 1430	1, 3 or 4	5 or 10
Alumina / HAP Composite	1300	1	10
Two kinds of zirconia mixture	1430	4	5 or 10
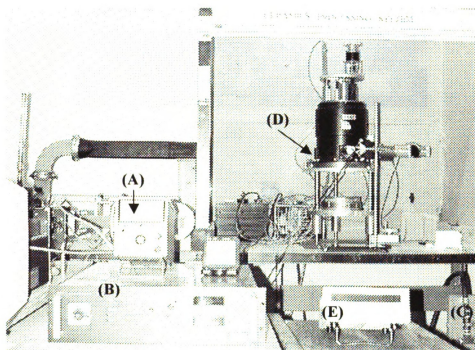
Figure 3.7. Photograph of microwave cavity and power supply used in this study. (A) reflected power detector, (B) microwave power controller, (C) water cooler, (D) microwave cavity, and (E) optical pyrometer.
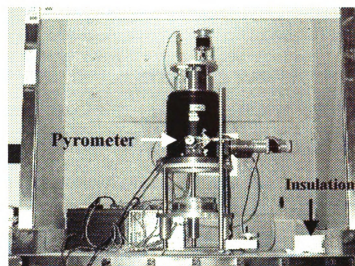
(a)
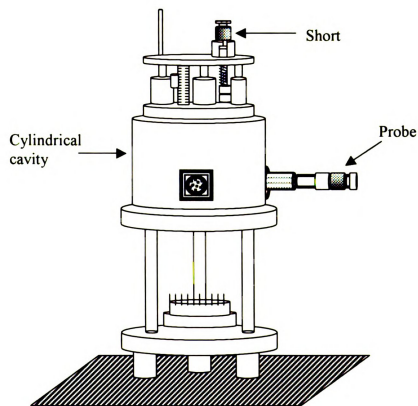
(b)

Figure 3.8. (a) Microwave cavity and (b) the schematics of microwave processing unit.
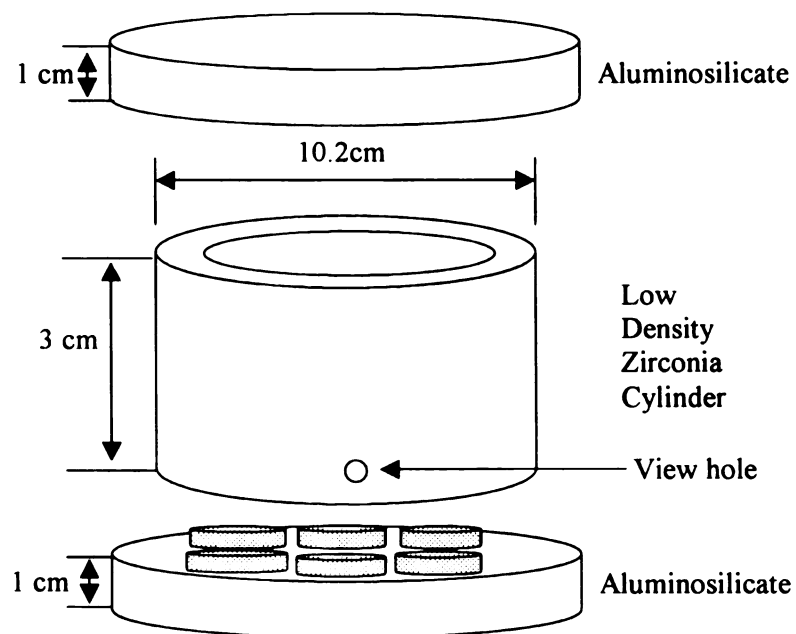
Figure 3.9. Schematic showing casket with the position of specimens.

increased to 300 watts to bring the specimens to the desired temperature. The microwave sintering was done at temperature of 1000°C to 1375°C for a time of one hour. During the process, the short and probe positions were adjusted to controlled the reflected power. After holding the desired time, the input power was decreased with the cooling rate of 10°C per minute to 500°C. Table 3.13 explained the sintering temperature and holding time which is used in this study for the microwave processing.

3.3-5 Sectioning the Sintered Specimen

The sintered specimens were cut by using the low speed saw (Leco Corporation, St. Joesph, MI) with a 10.16 cm diameter 0.3mm thick diamond saw (Superabrasive grinding wheel, Norton Company, Worcester,MA), with an oil based lubricant (VC-50, Leco Corporation).

3.3-6 Specimen Polishing

The automatic polisher (Model Vari / PoL™ VP-50, LECO Corpoeration, St. Joeph, MI) were used to polish the sintered specimens and specimens which got commercially made. The machine moved in two rotations and a swinging motion with random orbit to polish the specimens. The polishing paste (Warren Diamond Powder Co. Inc, Olyphant, PA) containing the diamond grit was graded for 35, 25, 17, 15, 10, 6, and 1 micron sizes. The specimens were first mounted to a flat 2 cm thick, 20cm diameter aluminum disk with thermoplastic (Thermoplastic cement, number 40-8100, Buehler LTD, Lake Bluff, IL) by using the hot plate (Cole Parmer Model 4658) to melt the thermoplastic up to a 1-3 mm thick layer. The specimens of almost same height are

mounted together to keep the balance during the polishing otherwise, it would take so long time to polish or it would be impossible to get the polished specimens. To densify the thermoplastic between the aluminum plate and the specimens, it should be cooled down. Size graded diamond grit was applied to grit size specific polishing cloth (LECO Co. and Buehler catalog No. 40-7122, ultra pad with adhesive backing 12", Lake Bluff, IL) affixed to a rigid metal disk. The cloth covered disk plate and the aluminum disk where the specimens are mounted were load into the polishing machine. The polishing cloth was lubricated with Ethylene Glycol solution (Polishing oil, Microid diamond compound extender, LECO Corporation). The polishing oil gave the smooth contact movement between the polishing plate and the specimens so it would be applied each time after diamond grit changed. For newly changed polishing cloth, about 10 drops (1 gram) of the diamond paste were applied otherwise several drops were used. For this study, the cloth covered metal disk rotation rate was set to 120-150 rpm. Initial polishing at grit size of 35 or 25 microns were took for 30 minutes to 1 hour after this stage, there was no change on surface of the specimens, then polishing were done in 17, 15, 10, 6 and 1 microns. After taking the 17 microns diamond grit, the specimens were shinny. Before going to next grit size and after final stage of polishing, the specimens were cleaned with liquinox soap (Liquid-Nox, Alconox, Inc, New york, NY) and soft bristle brush to remove the polishing oil and the diamond grit. Table 14 shows the approximate polishing time on each different stage.

After the polishing was done up to 1 micron grit size the specimens were demounted from the aluminum disk by heating up on the hot heater. The demounted specimens were put into acetone for 5 to 10 minutes to removed the thermoplastic from

the specimen then an ultra sonic cleaner (Ultra-Met III Sonic Cleaner, Burhler LTD, Evanston,IL) was used with de-ionized water to clean up for final stage and dried with paper towels to removed the excess water.

3.3-7 Coating Procedure

The pre-ceramic organic – based silica precursor, spin-on material, (Silica Flim^{TM}, Emulistone Co., Whippany, New Jersey) was used as an interlayer material for ceramic / ceramic joining. The specimens were coated with the silica film (Table 3.15).

To perform this procedure, the specimens were affixed to the petridish by using the double-sided adhesive tape then a few drops of the silica film to cover the whole surface were applied to the polished surfaces of the specimens that were to be joined. The specimens were then spun for 20 seconds at 3000 rpm on a commercial substrate vacuum spinner (Figure 3.10.). The coating was then cured by heating the specimens in air for twenty minutes at 200°C in conventional furnace. The resulting amorphous silica coating was a high purity silica coating approximately 200 nm thick.

3.3-8 Joining procedure

Ceramic / Ceramic joining were done in both conventional furnace (Carbilite, Inc.) and microwave cavity (2.45 GHz single mode that included a 0-2kW microwave power supply-Saiem, MWPS 2000, Wavemat Inc., Mi). The specimens were placed inside of the 7.3 cm in diameter and 1.3 cm thick cylindrical refractory casket with the 20 grams of dead

Table 3.13. The different conditions of microwave sintering.

Material	Sintering time (°C)	Holding Time(hour)	Heating/ cooling rate
Alumina (TMDAR)	1300	1	10°C/min.
3 mol% yttria stabilized ZrO₂ (TZ3YS)	1375	1	10°C/min.
8 mol% yttria stabilized ZrO₂ (TZ8YS)	1375	1	10°C/min.
Hydroxyapatite (HAP)	1100	1	10°C/min.

Table 3.14. The conditions of polishing which is done for this study (time, diamond grit size and materials used).

Material	Polishing time (minutes) on each diamond grit size						
	35μm	25μm	17μm	15μm	10μm	6μm	1μm
Alumina (TMDAR)	20	20	40	40	30	30	30
3mol%Y₂O₃ Zirconia (TZ3YS)		20	40	40	30	30	30
8mol%Y₂O₃ Zirconia (TZ8YS)		20	40	40	30	30	30
Hydroxyapatite (HAP)		20		30	30	30	30
Alumina/ Zirconia composite	20	20	30	30	30	30	30
Alumina/ Hydroxyapatite composite		20	40	30	30	30	30

Table 3.15. The condition of silicafilm coating.

Spin-on Material	Spin rate (rpm)	Spin Time (Sec)	Curing temperature (°C)	Curing holding Time (minutes)
Silica Film	3000	20	200	20

Polished
specimen

Apply silica
film on desired
surface

Spinning
control

Vacuum
pump
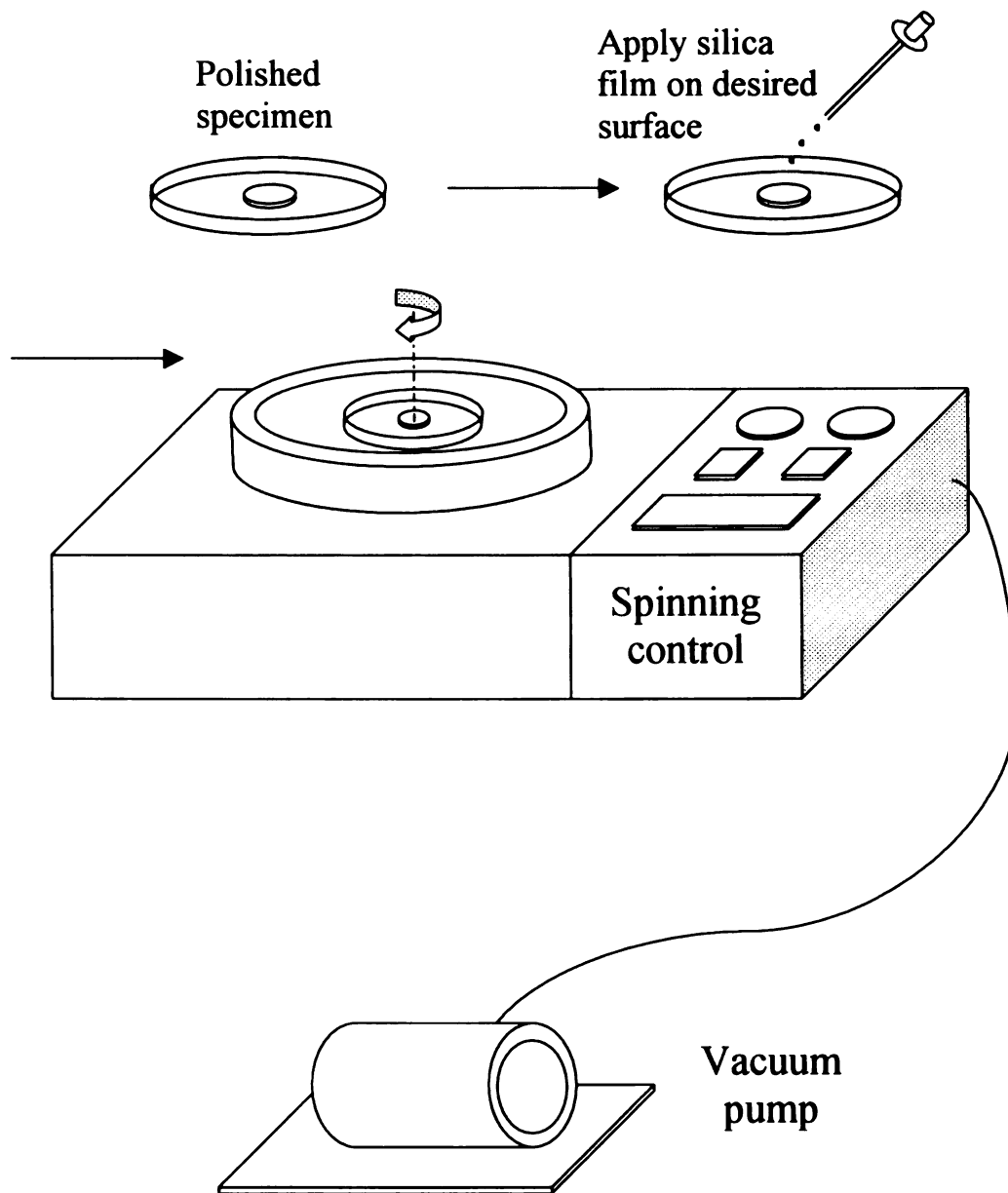
Figure 3.10 The schematic drawing for process of spin-coating.

weights (Alumina specimens) to give a low pressure for microwave joining and put into the conventional furnace with dead weight too. The heating and cooling rate was about 20°C per minute. During the microwave joining process, the reflected power was controlled by adjusting the short and probe positions. After coupling, which is occurred at input power between 200 and 250 watts the temperature quickly reached to 800°C. The comparison of joining conditions between microwave and conventional furnace are shown in Table 3.16.

Table 3.16. The comparison of joining comparison of joining conditions between microwave and conventional furnace

	Joining Temp. (°C)	Joining Time (min)	Dead Weight (gram)	Heating Rate (°C/min)
Conventional Heating	1475	240	20	10
Microwave Heating	1300	60	20	10

3.3-9 Specimen Characterization

3.3.9-1 To compare the degree of warping

To fabricate the FGMs specimens, the most difficult part is to control the residual stress to minimize the cracking or warping. In this study, two different size of zirconia powders were mixed together to reduce cracking or warping. Magnetic Base with Dial Indicator was used to measure the heights of warped the specimens to indicate the how much it was not warped (Figure 3.11.)

63

3.3.9-2 SEM Observation

The polished specimens were mounted on aluminum stub using carbon tape (Structure Probe Inc., West Chester, PA) with the specimen surface of interest facing upwards. Also, to prevent charging during SEM observation, carbon paint (Ted Pella, Inc., Redding, CA) was applied to the edges of the sample before gold coating. The specimens were coated with about 21 nm (1 minute produce approximately 7 nm gold coating) of gold by a sputter coater (Emscope SC 500). To proper coating, the timer was set for 3 minutes with a current of 20 mA.

A JEOL 6400 scanning electron microscope was used to look the around the channel of FGMs and the joined surface and fracture of materials. The accelerating voltage was 20 kV.
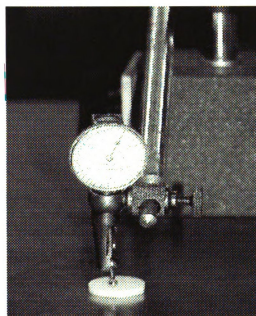
Figure 3.11. Picture of magnetic base with dial indicator.

REFERENCES

1 T. Sakuma, Y. Yoshizawa, H. Suto, "The microstructure and mechanical properties of yttria-stabilized zirconia prepared by arc-melting", Journal of Material Science 20, 1985, pp2399-2407

2 T. Tsukuma, Y. Kubota, T. Tsukitate, in: N. Claussen, M.Ruhle, A.H. Heuer (Eds.), Advances in Ceramics, Vol. 12, Science and Technology of Zirconia II, American Ceramic Society, Columbus, OH, 1984, pp.382-390

3 E.C. Subbarao, "Science and Technology of Zirconia", Vol.3, Advances in Ceramics, A.H. Heuer and L.W. Hobbs, Ed., American Ceramic Society, 1981, pp1-24

4 J.C. Elliott, Structure and Chemistry of the Apatite and Other Calcium Orthophosphates, Elsevier, 1994

5 Ralph W.G. Wyckoff: Crystal Structures Volume 3 Inorganic Compounds Rx(MX4)y, Rx(MnXp)y, hydrates and ammoniates, second edition, Interscience publisher

6 J.C. Elliot, P.E. Mackie, R.A. Young: "Monoclinic Hydroxyapatite", Acience, Vol.180, 1995, pp.1055-1057

7 Jiming Zhou, Xingdong Zhang and Jiyoung Chen, "High Temparature Characteristics of Synthetic Hydroxyapatite", Journal of Material Science: Materials in Medicine, 4, 1993, pp.83-85

8 http://www.ferroceramic.com

9 TM-DAR materal data sheet from Taimi Co

10 HAP material data sheet from Cerac INC, Milwaukee, WI.

11 Zirconia powder data sheet from Tosoh Ceramics Division, Bound Brook, NJ

12 Zirconia powder data sheet from Cerac Cerac INC, Milwaukee, WI.

13 http://www.corning.com/search_main.html

14 "Technical ceramics", Advanced materials technology international, KM Nutter and M P Davidson, 1990, p.131-133

15 O.M.Akselsen, "Review Advances in Brazing of Ceramics", Journal of Material Science, Vol. 27, 1992, pp.1989-2000

16 "Introduction to Ceramics", 2nd edition, W.D.Kingery, H.K. Bowen and D.R.Uhlmann, pp 595

17 Zirconia powder data sheet from Cerac INC, Milwaukee, WI.

18 Engineered Materials handbook Vol.4, Ceramics and Glasses, ASM international pp776

19 Joining of Ceramic Materials Using Spin-on Interlayer Master thesis of Jong-Gi Lee Michigan State University

20 E.D. Case, K.Y. Lee and J.G.Lee, "joining of Polycrystalline Ceramics and Ceramic Composites Using Microwave Heating", in proceedings of the 33rd International Microwave Power Symposium, International power Institute, Manassas, VA, pp. 17-20 (1998)

21 Engineered Materials handbook Vol.4, Ceramics and Glasses, ASM international pp974

22 Engineered Materials handbook Vol.4, Ceramics and Glasses, ASM international pp776

23 Engineered Materials handbook Vol.4, Ceramics and Glasses, ASM international pp 759

24 'Fundamentals of Ceramics', michel Barsoum, McGraw-Hill series in Materials

Science and Engineering, pp401

Chapter 4

FABRICATION OF INTERNAL CHANNELS IN CERAMICS AND CERAMIC COMPOSITES[1]

ABSTRACT

In engineering applications, ceramics possess important characteristics such as chemical inertness and high stiffness and hardness, which cannot be surpassed by most metals. However, difficulties in the processing of ceramic materials have limited the utilization of these excellent properties. In particular, it is difficult to fabricate ceramics with complex geometry, especially internal geometric features such as channels or cavities in the bulk of a ceramic component. This paper presents a unique and economical processing technique that utilizes a fugitive phase to produce cavities in the bulk of ceramics and ceramic composites. The fugitive phase in the shape of the desired channels is introduced into a die during powder compaction. During pre-sintering of the green body, the fugitive phase burns away, leaving the cavities and channels. A final sintering step via either conventional or microwave heating produces a densified ceramic component having bulk-penetrating channels or cavities. Ceramic/ceramic joining technology, developed by the authors and other researchers, together with the presented

processing technique provide the potential for fabricating very complex parts by joining subcomponents with other such subcomponents, which all have complex cavities.

4.1 INTRODUCTION

Although ceramics offer many attractive material properties, including a good resistance to chemical attack and erosion, biocompatability, and good high temperature stability, the use of ceramics has been limited, in part by the brittle nature of ceramics and in part by the difficulty in fabricating complex shapes with ceramics. The limitation of fabricating ceramics with complex shapes impacts their potential use in many engineering applications, since it is very difficult to fabricate ceramic components having internal channels. Thus, although a particular ceramic or ceramic composite may have a superior resistance to chemical attack and erosion or a remarkable biocompatability, another material will be used in place of the ceramic if the application demands internal channels that are difficult to produce in the ceramic material.

Even though the presented processing protocol can be applied in many practical engineering applications including aerospace, manufacturing and medical, we will focus this introduction with the applications to microelectronics. The development of highly efficient temperature management materials (TMMs) is becoming essential to allow the continued progresses in microelectronics such as miniaturization and multichip modules. Such devices generate higher heat output, which must be managed to avoid deleterious effects on the basic functions of the device. Advanced TMMs resolve the thermal management problem by efficiently dissipating the heat being generated. A variety of high conductivity materials such as diamond [1] and aluminum nitride have been utilized

to spread the heat generated by electronic devices. Without such materials, the generated heat locally increases the temperature, which directly affects the integrity of the devices.

In addition to spreading out the heat, TMMs can extract the heat from the site where the heat is generated by circulating cooling fluids. Internal channels, which serve as conduits for cooling fluids, can be included in the design of TMMs. The mechanical stresses and the thermal and chemical environments to which the components are subjected also help guide the selection of materials to be used in such components.

Because of the difficulties in producing ceramic components with internal channels, silicon wafer has been used in some recent work to address this challenge. For example, Tuckmerman and Pease [2] produced high flux electronic cooling channels on $1cm^2$ silicon integrated circuit chips with cooling channel widths of 57 μm and heights of 365 μm. These rectangular-cross section passages were etched onto <110> silicon wafers using KOH, where deionized water serves as the coolant through the passage. The spacing between channels was about equal to the channel width. The etched channels in the silicon wafers were converted into closed channels by anodically bonding a Pyrex plate over the channels. Tuckmerman and Pease's TMMs heat dissipation rate was 40 times higher than that for conventional IC-heat-sink cooling schemes [2].

Tuckerman and Pease's concept has extended by many researchers. For example, by adding manifolds on multiple microchannels Harpole and Eninger [3] fabricated high aspect ratio channels (25μm width, 200μm depth and 40 μm distance apart between channels) on silicon wafer diffusion bonded to diamond face sheet. Bower and Mudawar [4] fabricated mini- (2.54mm diameter) and micro- (0.51mm diameter) channeled heat sinks made of copper. The heat sink geometry such as channel spacing and overall

thickness was optimized through the experiments. By using fluorocarbon liquid as the coolant, channel length and wall thickness was thinner than when water was used as the coolant. The new design reduces the maximum component temperature and drastically reduces variation in component temperature [5].

This paper represents the part of our current study focusing on the development of powder processing protocols for highly efficient TMMs made of ceramics and ceramic composites. One of the important processing aspects related to ceramics and ceramic composites is being able to produce channels internally in the bulk of ceramic materials. Our processing protocols enable us to produce channels economically. Low temperature presintering burned out the cylindrical fugitive phases elements from ceramic powder compacts. (In this study, the fugitive phase elements consisted of pencil lead with diameters between roughly 300 and 900 microns). As a second processing step, both conventional and microwave heating were used to sinter the ceramics and ceramic composite materials, resulting in dense ceramics having circular internal channels.

The size scale of the channels included in this study is appropriate to the active cooling of electronic materials [6 - 8]. For example, some recently developed cooling systems for computer hardware include channels that are 0.78 cm across, while a variety of "microchannels" for active cooling applications range from several hundred microns across to as small as about 150 microns across.

To date, the authors and co-workers have formed internal channels in ceramics by joining specimens with "open" channels either machined into densified specimens [9 - 11] or "pressed" into the surface of powder compacts prior to sintering [12]. The internal channels formed by joining specimens with surface channels are of course constrained to

in the plane of the interface between the joined components. In contrast, in this study, we form internal channels by the burnout of fugitive phases pressed into the powder compact.

Although this study focuses on fabricating internal channels in ceramics and in particulate ceramic composites, ceramic/ceramic joining techniques are available that allow the joining of two or more subcomponents to build up increasing complex ceramic parts. For example, the authors and co-workers have successfully joined a variety of ceramics, including alumina/alumina [9], zirconia/zirconia [14], SiC/SiC, HAP/HAP [14], and MaCor™/MaCor™ [9]. (HAP is the bioceramic hydroxyapatite and MaCor™ is a machineable glass ceramic composite composed of an aluminosilicate glass matrix reinforced by mica platelets). In addition, the authors and co-workers have joined a variety of dissimilar ceramics, including alumina/zirconia [15], HAP/MaCor™ [16], MaCor™/zirconia and a variety of other ceramic/ceramic combinations. Thus, specimens with internal channels fabricated by the technique discussed in this study might be used as either stand-alone components or joined with other ceramic components to produce components with quite complicated channel or cavity structures.

4.2 EXPERIMENTAL PROCEDURE

Materials: For this study, the following commercial powders were used: (1) A 99.99% pure alumina powder (TM – DAR, Taimi chemicals Co. LTD), (2) A 99.9% pure partially-stabilized 3 mol% yttria – zirconia (PSZ) powder (TZ – 3YS, Tosoh Ceramic Division, Bound Brook, New Jersey), (3) A 99.9 % pure fully-stabilized 8 mol% yttria – zirconia (FSZ) powder (TZ – 8YS, Tosoh ceramic division, Bound Brook, New Jersey) and (4) 99% pure Hydroxyapatite (HAP: Ca_{10} $(PO_4)_6$ $(OH)_2$, Cerac Inc., Specialty

Inorganic, Milwaukee, WI). The average initial particle size of each powder is given in Table 4.1. Both single-phase specimens (alumina and FSZ) and particulate composite specimens (25% PSZ/ 75% HAP and 25% alumina/ 75% HAP) were included in this study.

The particular materials included in this study (alumina, FSZ, and the particulate composites of PSZ, alumina and HAP) were selected on the basis of their characteristics and a wide range of applications. For example, alumina is a relatively tough ceramic that is also very hard and very resistant to chemical attack. Many applications of alumina include electronic substrates and a bioinert material in implants. FSZ (fully stabilized zirconia) is an ionic conductor that is used in oxygen sensors and is a candidate material for use in fuel cells. While the coefficient of thermal expansion (CTE) of alumina (7.2-8.8x10^{-6}K^{-1}) is close to that of FSZ (7.5x10^{-6} K^{-1}), their thermal conductivities are quite different (35W/mK for alumina vs. 19W/mK for FSZ). HAP is the major mineral constituent of bones and teeth and is a bioactive material that is used in a variety of implants. However, HAP has relatively low fracture toughness and strength, thus the composites HAP with ceramics of higher fracture toughness such as alumina and PSZ, are of interest [13].

Table 4.1: List of powders used

Powder	Average particle size (μm)
Alumina (TMDAR)	0.2
3 mol % Zirconia (TZ – 3YS)	0.5
8 mol % Zirconia (TZ – 8YS)	0.54
Hydroxyapatite (HAP)	2 ~ 3

Thus, the materials included in this study represent a range of current and potential application areas of ceramics and ceramic composites.

Specimen Preparation: The composite powders included in this study were mixed using dry ball milling in a plastic ball mill with alumina media at a rotation rate of 110 revolutions per minute. The ball mill charge consisted of a total of 50 grams of powder and about 250 grams of alumina media (which gave a volumetric ratio of roughly 1 part powder to 2 parts of the alumina media). The ball milling was carried out approximately for 24 hours. All specimens included in this study were pressed in a uniaxial steel die at a pressure of approximately 35 MPa using a Carver hydraulic press. The internal diameter of the die was 22.2 mm. Between 1.5 and 3 grams of powder were used to form the specimens (Table 4.2).

During the course of our investigation, a variety of materials including cotton thread, polymer fibers, pencil lead and shrink tape has been tested as fugitive phases. Surface channels were successfully produced by each of these fugitive phase materials [12]. However, the pencil lead was the only fugitive phase medium to consistently produced internal channels without any damage in the specimen. We speculate the damage in the other samples were due to the discrepancy between the CTE of the fugitive phase and the shrinkage during consolidation and the differences between the compacting behavior of powder and the compression behavior of the fugitive phases.

For the internal channels fabricated in this study, the pencil lead was incorporated with the powder compact. About one-third to one-half of the measured powder was initially poured into the die cavity, then the pencil lead in lengths of 1.3 cm to 1.7 cm was

Table 4.2: Initial powder mass for each specimen

Powder	Mass (g)
Al_2O_3	2 g
ZrO_2-3mol%Y_2O_3	3 g
ZrO_2-8mol%Y_2O_3	3 g
HAP	1.5 g
25 % Al_2O_3 / 75 % HAP	2 g
25 % ZrO_2-3mol%Y_2O_3 / 75 % HAP	2.3 g

placed on top of the powder in the die, with a lateral spacing of roughly 1.4 mm to 1.6 mm between the lead. More powder was then added to the die cavity before pressing.

To produce two rows of internal channels, two sets of pencil leads were sandwiched between three layers of powder in the die cavity while a single row of internal channels was produced by centering a single row of pencil lead within the powder in the die cavity. Surface channels were formed by placing pencil lead on top of the powder bed immediately before pressing.

The pencil lead used had nominal diameters of 900, 700, 500, and 300 microns. Typically, four pencil leads were used in a given row of channels, with up to four surface channels per specimen. Both surface and internal channels were produced on several specimens.

After pressing, the pencil leads were burned out by a pre-sintering in air in an electrical resistance furnace at either 900°C or 1200°C for between two and four hours. Pre-sintering was done in a conventional furnace for all specimens included in this study, however the final sintering of the specimens was done either in a microwave cavity or in a conventional furnace.

The conventional sintering was done in an electrical resistance furnace in air with a heating rate of approximately 10°C per minute; with a 4-hour hold time at 1430°C. The specimens were then cooled to room temperature at a rate of roughly 10°C per minute. From six to eight specimens were sintered simultaneously.

For the microwave processing, the presintered specimens were sintered in a single-mode resonant microwave cavity at a frequency of 2.45 GHz using a 0 - 2 kW microwave power supply. The specimens were sintered in a refractory casket (specimen

enclosure) that served to thermally insulate the specimens and to provide a microwave susceptor material [17]. The microwave sintering in air was done at in the temperature range between 1300°C to 1310°C for one hour. For each sintering or joining run, the temperature was measured using an optical pyrometer. The details of the microwave apparatus and the microwave sintering procedure are given elsewhere [18]. As was the case for the conventional sintering, multiple specimens (from five to six specimens) were microwave sintered in a given batch.

Using a low-speed diamond saw, the sintered specimens were sectioned. The specimens were then mounted and polished using a series of diamond paste having grit sizes from 25 micron to 1 micron. Both the structure of the cavities and the specimen microstructure was examined using optical and scanning electron microscopy.

4.3 RESULTS AND DISCUSSION

The specimen dimensions were measured with a caliper after pressing, after pre-sintering and after final sintering. The specimen mass was measured with an electronic balance. The mass density of the specimens in the green (as pressed) state and in the sintered state was then calculated from the measured specimen mass and dimensions along with the specimens' volumetric and linear shrinkages due to sintering, which are shown in Table 4.3.

The shrinkage of the powder compacts is an important aspect of the processing. As pressed, the density of the powder compacts ranged between 40% and 62% for the powder with a narrow initial particle size distribution, where the remaining "volume" of the powder compacts consists of void spaces among the particles of the powder compact.

78

If a specimen achieved theoretical density, the specimen volume would be reduced by about 43% - 54%, which corresponds to a linear shrinkage of roughly 15% - 30%. During fabrication, one would need to take account of the volumetric and linear shrinkage values, in order to determine the final specimen dimensions and the final dimensions of the channels. However, the shrinkage of the powder compact is potentially a benefit, since one could obtain a channel diameter that is about up to 18% smaller than the diameter of the fugitive phase elements that are introduced into the powder compact. At the present time, we do not know the exact reason for a large shrinkage with 900micron fugitive phase and a small shrinkage with 700micron fugitive phase. Thus, the shrinkage provides a "reduction factor" for the final, processed channel diameters relative to the size of the fugitive phase elements themselves. For a given type of ceramic powder, if the key processing parameters (such as the heating rate, the sintering temperature and the sintering time) remain the same from run to run, then the final density of the component and the final diameter of the channels should be quite repeatable.

The channels and cavities formed by the elimination of the fugitive phases were examined by both optical microscopy and scanning electron microscopy (Figures 4.1-11).

The channels formed are generally free of cracks for both the microwave processed (Figures 4.1-3) and the conventionally processed (Figures 4.4-11) materials.

SEM micrographs showing the details of individual channels in the sinte redalumina (Figure 4.1), the 25% PSZ / 75% HAP (Figure 4.3), and the FSZ (Figures 4.5 and 4.7) reveals that the channels are quite circular.

Table 4.3: Dimension differences of the specimen (in cm)

Materials	After Pressing	After Pre-sintering	After full sintering	Linear Shrinkage	Initial Density (g/cm³)	Final Density (g/cm³)	Volumetric Shrinkage
Al₂O₃	D* = 2.19	2.16	1.85	15.5%	1.95	3.63	53.5%
	T* = 0.273	0.272	0.205	24.9%	(49.1%)	(91.9%)	
FSZ	D = 2.19	2.19	1.68	23.3%	2.413	5.64	42.9%
	T = 0.33	0.317	0.24	27.3%	(40.9%)	(95.6%)	
25 % Al₂O₃ / 75 % HAP	D = 2.19	2.215	1.749	20.1%	1.609	3.239	49.8%
	T = 0.33	0.32	0.257	22.1%	(48.5%)	(97.6%)	
25 % PSZ/ 75 % HAP	D = 2.19	2.18	1.722	21.4%	1.585	3.18	50.6%
	T = 0.335	0.325	0.27	19.4%	(44.2%)	(88.7%)	

* D = specimen diameter and T = specimen thickness (all specimens were disk-shaped).

While no obvious distortion of the channels is visible from the micrographs (Figures 4.1, 4.3, 4.5 and 4.7), repeated measurements of the channel diameter were preformed using the SEM software. For example, for 10 measurements on the diameter of the channel in FSZ material, the mean and standard deviation of the channel diameter was 729μm and 6μm, respectively. The relatively small coefficient of variation (the standard deviation divided by the mean) of 0.8% indicates the channels are indeed quite circular.

All of the specimens included in this study were fabricated with multiple internal channels (Figures 4.2, 4.4, 4.6, 4.8, 4.9 and 4.10) and most included both surface channels and internal channels (Figures 4.4, 4.6, 4.8 and 4.9). A key feature apparent in these micrographs is that no cracks are apparent between the channels and between the channels and the specimen surface. The fact that no cracks were evident on the channels near the specimen surface is significant, since in some cases the internal channels are located within approximately one channel diameter (or less) of the specimen surface (Figures 4.4, 4.6, 4.7, 4.8 and 4.9). Also, the spacing between the internal channels was as small as roughly two channel diameters or less, but despite their proximity, no cracking was apparent (Figures 4.6, 4.8, 4.9 and 4.10). The good circularity of the channels and the lack of cracks in the specimen are important in our application to TMM. The four different diameters of pencil leads used (900 microns, 700 microns, 500 microns and 300 microns, as specified by the vendor) produced four different channel sizes, from about 730 microns (from the 900 micron diameter pencil lead) down to about 280 microns (using the 300 micron pencil lead). The submillimeter size range (in this case

730 - 280 microns) includes the range of sizes that are of interest for fluid transport via microchannels, including the transport of cooling fluids in TMMs [2-6].

It is important to note that the nominal diameter of the pencil lead (900 microns, 700 microns, 500 microns and 300 microns) is not their actual diameter. SEM measurements of the pencil lead shown that in fact the diameter of individual pencil lead specimens agrees well with the diameter data provided by the suppliers. However, a careful study of the variation in diameter from one pencil lead to another in a given batch of lead has not yet been conducted, so that the shrinkage of an internal channel, from the powder compact (with the pencil lead in place) to the final sintering is probably best inferred from the overall shrinkage measurements on the specimen.

The size of the pore was measured (by using SEM at high magnification) to be much smaller than one micron. The purpose of this measurement is to find the effect of the fugitive phase in the consolidation of the powder and to confirm if the fugitive phase has any detrimental effect on the integrity of the sintered materials near the channels. Our finding shows that slightly more pores exist near the channel than away from the channel as evident in Figures 4.11a and 4.11b. However, all of the pores we observed were small, isolated pores roughly one micron or less in size. The local variations in the sintering process must be caused by the presence of the fugitive phase.
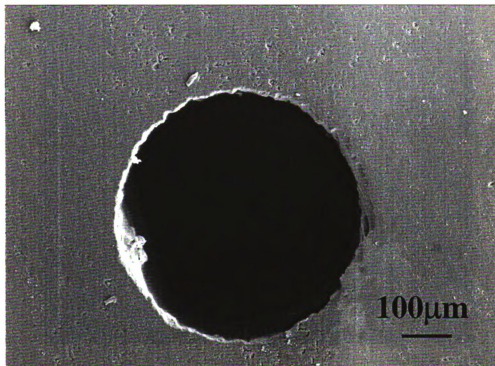
Figure 4.1. A SEM micrograph of an alumina specimen that was pre-sintered at 900°C for one hour in air in a conventional furnace, then sintered at 1300°C for 1 hour via microwave heating. The cylinder channel was formed by pressing a 500 micron pencil lead along with the alumina powder.
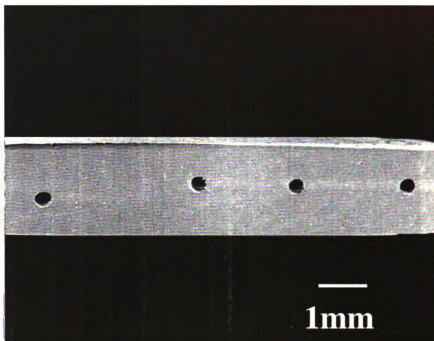
Figure 4.2. A particulate ceramic specimen (25% alumina/75% HAP) with four cylindrical channels, using 500 micron-diameter pencil lead as the fugitive elements. The specimen was pre-sintered in air at 900°C for one hour in a conventional furnace, then sintered at 1300°C for 1 hour via microwave heating.
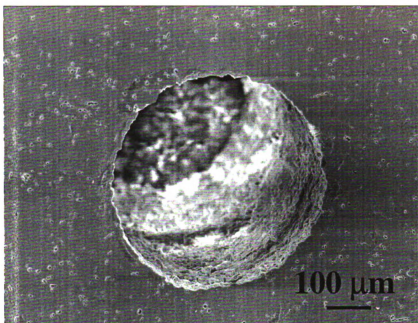
Figure 4.3. A high-magnification view of a single channel (formed from a 500 micron diameter pencil lead) in a particulate ceramic specimen (25% 3mol% Y_2O_3-partially stabilized zirconia/75% HAP). The pre-sintered in air at 900°C for one hour in a conventional furnace, then sintered at 1300°C for 1 hour via microwave heating. The specimen was cut such that the "bottom" of the channel is visible in the micrograph.
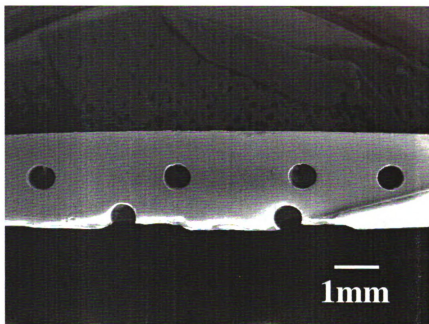
Figure 4.4. A fully-stabilized zirconia (FSZ) specimen pre-sintered conventionally at 900°C for one hour in air, then sintered for four hours at 1430°C in air in a conventional furnace. Both the four internal channels and the two surface channels were formed using 900 micron diameter pencil lead.
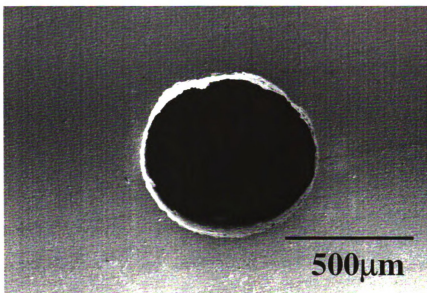
Figure 4.5. A close-up view of one of the channels in the FSZ specimen shown in Figure 4.4.
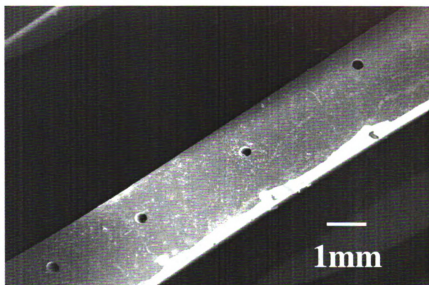
Figure 4.6. A FSZ specimen pre-sintered conventionally at 900^0C for one hour in air, then sintered for four hours at 1430^0C in air in a conventional furnace. The four internal channels were formed using 300 micron diameter pencil lead.
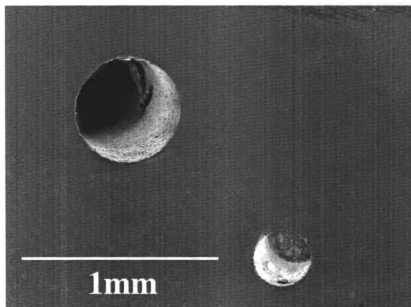
Figure 4.7. Two channels in a FSZ specimen pre-sintered conventionally at 1200°C for two hours in air, then sintered for four hours at 1430°C in air in a conventional furnace. The larger channel was formed using 700 micron diameter pencil lead, while the smaller channel was formed using a 300 micron diameter pencil lead. The cylinder axes of the two channels are oriented in different directions.
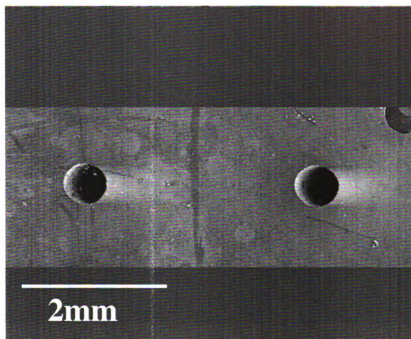
Figure 4.8. A FSZ specimen pre-sintered at 1200°C for two hours in air, then sintered for four hours at 1430°C in air in a conventional furnace. Although the specimen included four internal channels, only two internal channels (formed using 700 micron-diameter pencil lead) are in the field of view, along with one surface channel (formed using 500 micron diameter pencil lead).
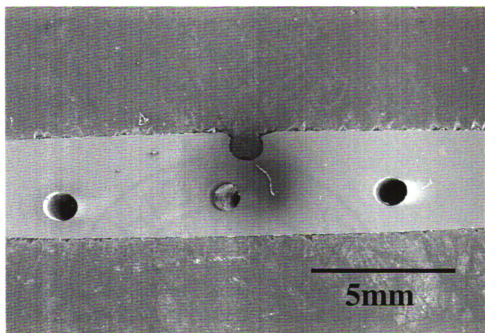
Figure 4.9. A FSZ specimen pre-sintered at 1200°C for one hour in air, then sintered for one hour at 1430°C in air in a conventional furnace. Both the surface channel and the internal channels were formed using 900 micron-diameter pencil lead. Note that two of the internal channels are within less than one channel diameter of the specimen surface.
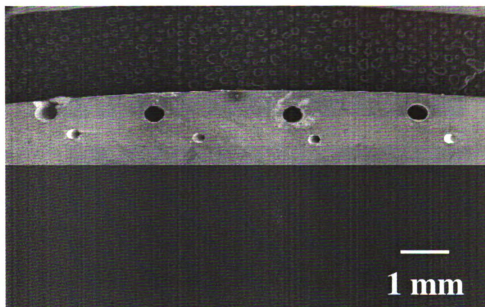
Figure 4.10. Two rows of closely spaced channels in a FSZ specimen pre-sintered at 1200°C for two hours in air, then sintered for four hours at 1430°C in air in a conventional furnace. The larger channels were formed using 700 micron diameter pencil lead, while the smaller channels were formed using 300 micron diameter pencil lead.
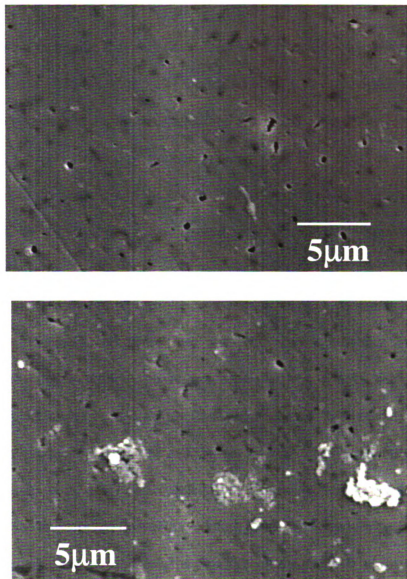
Figure 4.11. For a FSZ specimen (pre-sintered and sintered in air at 1200°C for two hours and for four hours at 1430°C, respectively), where microstructure (a) at a distance of about mm away form an internal channel is perhaps slightly less porous that the microstructure (b) at a distance of roughly 200 - 300 microns from the outer wall of an internal channel.

4.4 SUMMARY AND CONCLUSIONS

One processing technique that was developed recently enables to have the channels in a ceramic material. Crumm et al. [19] fabricated a fugitive compound formed from ethylene ethyl acrylate resin, acryloid resin, carbon black, and mineral oil. However, they used in mutliple-pass coextrusion of multicomponent ceramics. Feedstock consisting of rectangular strips of the ceramic and the fugitive phase were repeatedly co-extruded such that when firing, the fugitive phase was burned out, open channels approximately 40 microns wide were formed.

The present study does not require the co-extrusion, thus an economical method to introduce precise channels and holes into the bulk of the ceramics and ceramic composites, combining a fugitive phase procedure with a simple powder-pressing technique. Multiple circular channels with final dimensions of between about 700 and 300 microns were produced in both one and two layers with the specimens. Also, unlike the work of Crumm et al. [19], the channels will have diameters of several hundred microns to allow the unrestricted flow of the cooling fluids. A thermogravimetric analysis of the fugitive phase removal showed the burnout of the fugitive phase began at a temperature of about $300^{\circ}C$ and was nearly complete at a temperature of $800^{\circ}C$.

As shown in other ceramic processing work by the authors and co-workers [14], the most significant difference between microwave processed and conventional processed ceramics is the maximum temperature and time needed for processing. In addition, the grain size of the microwave-processed specimens tends to be somewhat lower than that for the conventionally processed ceramics/ceramic composites. However, for this study,

the circularity of the channels and the lack of cracking near the channels are very similar regardless of whether microwave or conventional processing was used.

For metal component fabrication, internal features such as channels can be either cast or compacted in a mold and then sintered. For ceramic and ceramic composites, machining and casting are not viable options. Work is presently underway to extend the techniques presented in this study to accommodate more complicated internal shapes, such as manifolds in single components. In addition, ceramic/ceramic joining techniques discussed elsewhere [9; 14-16] can potentially allow a number of individual components to be bonded into a single, much more complicated assembly.

ACKNOWLEDGMENTS

REFERENCES

1. Jagannadham, K., "Model of Interfacial Thermal Resistance of Diamond Composites," J. Vac. Sci. Technol., A17: (2), pp. 373-379, (1999).

2. D. B. Tuckerman and R. F. W. Pease, "High Performance Heat Sinking for VLSI," IEEE Electron Device Lett., 2, pp126-129, (1981).

3. G. M. Harpole and J. E. Eninger, "Micro-Channel Heat Exchanger Optimization" Proc. 7th IEEE semi-Therm. Symp., pp. 59-63, (1991).

4. M.B. Bowers and I. Mudawar, "Two-Phase Electronic Cooling using Mini-channel and Micro Channel Heat Sinks: Part 1-Design Criteria and Heat Diffusion Constraints," Journal of Electronic Packaging, 116, pp. 290-297 (1994).

5. D. Copeland, "Manifold Microchannel Heat Sink: Isothermal Analysis" IEEE Transactions on components, packaging and manufacturing technology – part A, 20, 2, pp96-102 (June 1997).

6. S. J. Kim and D. Kim, "Forced Convection in Microstructures for Electronic Equipment Cooling," J. *Heat Transfer*, 121, p. 639, (1999).

7. R. Hopkins, A. Faghri and D. Khrustalev, "Flat Miniture Heat Pipe with Micro Capillary Grooves," *Journal of Heat Transfer*, 121,1, pp. 102-109, (1999).

8. K. Take, Y. Furukawa and S. Ushioda, "Fundamental Investigation of Roll Bond Heat Pipe as Heat Spreader plate for Notebook Computers," *IEEE Trans. Components and Packaging*, 23 80 (2000).

9. K. N. Seiber, K. Y. Lee, and E. D. Case, "Microwave and Conventional Joining of Ceramics using Spin-on Materials," pp. 941-949 in Proceedings of the 12th Annual Advanced Composites Conference, Technomic Publishing Co., Lancaster, PA, 1997.

10. E. D. Case, K. Y. Lee, J. G. Lee, and T. Hoepfner, "Geometrical Stability of Holes and Channels During Joining of Ceramics and Ceramic Composites," pp. 27 - 34 in Joining of Advanced and Specialty Materials, M. Singh, J. E. Indacochea, and D. Hauser, eds., ASM International, Materials Park, OH, 1998.

11. E. D. Case and J. G. Lee, , "Joining Dissimilar Ceramics and Ceramic Composites for Biomedical and Structural Applications", pp. 318 - 324, Technology Convergence in Composites Applications, Proceedings of the ACUN-3 International Composites Conference, University of New South Wales, Sydney, Australia (2001).

12. J. G. Lee, H. W. Shin, E. D. Case, P. Kwon, "The fabrication of smooth, submilliter-diameter channels in polycrystalline ceramics without machining", J. Mater. Sci. Lett., 20[2]: 107 - 109 (2001).

13. Y. M. Kong, S. Kim, H. E. Kim, and I. S. Lee, "Reinforcement of hydorxyapatite bioceramic by addition of ZrO2 coated with Al2O3", J. Am. Cer. Soc., 82: 2963 - 2968, (1999).

14. J. G. Lee and E. D. Case, "Joining Ceramics to Produce Components with Precise Internal Channels", pp. 433 - 442 in Innovative Processing and Synthesis of Glass, Composite, and Ceramic Materials III, Volume 108, Ceramic Transactions, American Ceramic Society (2000).

15. L. Zeng, M. A. Crimp and E. D. Case, "The interfacial microstructure of Zirconia and MaCor™ joined using spin-on interlayers", accepted, Materials Science and Eng.

16. H. W. Shin, E. D. Case, and P. Kwon, "Joining bioactive and bioinert ceramics", accepted, ASM Fall 2000 Proceedings.

17. K. Y. Lee, E. D. Case, and J. Asmussen, Jr., "The Steady-State Temperature as a Function of Casket Geometry for Microwave-Heated Refractory Caskets," Materials Research Innovations, 1[2]: 101-116 (1997).

18. K. Y. Lee, L. Cropsey, B. Tyszka, and E. D. Case, "Grain size, density and Mechanical Properties of alumina batch-processed in a single mode microwave cavity," Materials Research Bulletin, 32[3]: 287-295 (1997).

19. Crumm, A. T. and Halloran, J. W., "Fabrication of Microconfigured Multicomponent Ceramics," J. Am. Ceram. Soc., 81 [4], pp. 1053 – 1056 (1998).

Chapter 5

NOVEL POWDER PROCESSING TECHNIQUES TO FABRICATE

EFFICIENT MESO-SCALE HEAT EXCHANGER[2]

ABSTRACT

This paper reports on novel ceramic processing techniques developed at Michigan

State University (MSU) during the last few years in order to fabricate an active-cooled,

efficient meso-scale heat exchanger. Its unique feature is a network of channels and

manifolds in the micro-textured medium called Functionally Gradient Material (FGM).

FGM is achieved by spatially varying the compositional ratio between two materials. The

gradiency is necessary to compensate thermal gradient loading as a result of heat transfer

into a cooling fluid circulating in the network of channels and manifolds. The gradient

medium also enhances heat transfer from a localized heat source to the cooling fluid,

minimizing the spread of heat energy to other peripheral devices. In order to reach the

goal of making such a heat exchanger, several processing challenges must be resolved.

Using conventional and/or microwave powder processing, the components needed to

achieve the proposed heat exchanger were fabricated. During this process, the residual

stresses caused by spatial gradients in thermomechanical properties are important for the

final integrity of the component. A processing technique to minimize the residual stress is

developed, which uses different powder characteristics to modulate the densification

behavior. In addition, when the powders are compacted, a fugitive phase in the shape of desired channels can be embedded. During sintering, the fugitive phase decomposes leaving cooling channels in the gradient medium. We will extend this technique to achieve a complex network of channels and manifolds. When either the CTE differentials between two materials or the difference in the sintering temperatures between two materials become too severe, the development of joining technique was necessary to join these individual components. In addition, because of the geometry complexity of the network of channels and manifolds as well as the integrity of the material after processing, the parts or components of the heat exchanger had to be made independently, which subsequently have to be joined. The incorporation of joining technology was necessary to achieve our goal.

5.1 INTRODUCTION

Many researchers have attempted to remove heat from microelectronic devices. The most common method to dissipate the heat [Gray, 2000; Jagannadham, 1999 and Hui et al., 1997] is to spread rapidly by employing highly conductive and high heat capacity materials such as diamond, silicon nitride, molybdenum, etc. Heat is dissipated to the environment either by forcing air through pin arrays or fins or by cooling naturally. Recently MEMS-sized heat exchangers [Hall, 1999] have emerged, which rely on convective heat transfer via air. In such cases, heat inevitably spreads to its surrounding and other peripheral devices.

More efficient cooling results when coolants circulated through networked channels and manifolds in a closed system. Tuckerman and Pease [1981] made a

unidirectional micro-channeled heat sink whose channels were produced by etching <110> silicon wafers using KOH on a 1cm^2 silicon wafer. The distance between the channels was the same as the width of the channels. The channels circulating deionized water were covered using a Pyrex plate by anodically bonding over the channels. These channels were slightly modified to form pins [Yin and Bau, 1997] to enhance the heat transfer into the coolants. Zhong and Bau [2001] cut low-temperature, cofired ceramic tapes into shapes to make the channels before stacking the tapes and firing. Harpole and Eninger [1991] and Copeland et al. [1997] added a simple manifold by covering only the middle section of the channel, where one side of the uncovered section is used as inlet and the other side as outlet. Bower and Mudawar [1994] and Gillot et al. [1999] developed a two-phase heat exchanger with a higher efficiency. Bower and Mudawar [1994] made mini- and microchannels with cross-sectional diameters of 2.54mm on a block of oxygen-free copper and 510□m on the block made of copper and nickel plate, respectively. Gillot et al. [1999] produced channels with a circular cross-section, a diameter of 2mm and length of 40mm. This approach is similar to a Heat Pipe [Nguyen et al., 2000], where coolants such as fluorocarbon FC72 and water undergo a cycle of evaporation and condensation to efficiently remove the heat generated by electric components.

This paper reports on the essential processing techniques for the development of an efficient, meso-scale heat exchanger. To achieve this, we propose the body of the heat exchanger to be: (1) micro-textured and (2) micro-configured. Micro-textured or FGM material can be processed by spatially modulating the compositional ratio between two powders. Micro-configured medium represents the network of micro-scale channels and

manifolds. The network will be eventually employed to transport coolants for our heat exchangers. Applications for the heat exchanger include a variety of other industrial or medical uses, such as conduits for fluids in engines or to carry medicine or biological fluids.

Achieving the aforementioned features hinges on the economical, appropriate processing technologies especially for hard-to-shape material like ceramics and small-to-make devices. The developed techniques must facilitate net-shape processing and minimal post-processing of the material. Compared to selective laser sintering process, the presented processing methods require conventional powder processing equipment such as a furnace and a press. Selective laser sintering also requires the sophisticated equipment that has laser source, computer control and several motors to control powder feeding.

5.2 BACKGROUND

In the micro-textured and micro-configured body, heat is conducted and dissipated via the coolant circulating through the holes, channels and manifolds (Figure. 5.1). We will report on the novel processing techniques that will enable us to fabricate the heat exchanger; (1) processing techniques to fabricate internal channels into an FGM in order to produce micro-configured body, (2) powder processing techniques to produce micro-textured Thermal Management Materials (TMMs) undamaged by process-induced residual stress, and (3) joining techniques to laminate the consolidated FGM layers.

A key issue in producing micro-textured medium (called FGMs) is to avoid damage due to process-induced residual stress. Residual stresses in FGM's [Zhang et al.,

102

1995 and Mizuno et al., 1995] occur due to spatial variations in Coefficient of Thermal Expansion (CTE) and densification behavior during processing. A powder processing protocol to minimize process-induced residual stress in FGMs has been developed, which can produce a mild gradiency in FGMs. For severe gradiency, two or more FGMs, each with mild gradiency, must be joined. The development of a joining protocol for two or more layers is presented. In addition to the FGM processing, another novel processing technique developed is the introduction of holes, channels and complex manifolds, without machining. Such channels can be straight or curved, with constant or variable cross section. Channels were fabricated on the specimen surface as well as in the interior of the ceramic. Two or more ceramic sub-components with the surface channels were joined subsequently to form internal channels in the final component. Ceramic/ceramic joining could be used, for example, to laminate the thin densified FGM layers.

An FGM ideally has continuous gradiency as shown in Figure 5. 2 (a). One can approximate such gradient properties by preparing subcomponents in the form of layers. Each layer is prepared by homogeneously mixing two powders in various ratios, which can be stacked to form the 'discrete' gradiency in thermomechanical properties as shown in Figure 5.2(b). However, if the process-induced residual stresses can be controlled, each layer can sustain some gradiency in properties. A smaller number of layers with some gradiency are then needed to form an FGM as depicted in Figure 5. 2 (c). The techniques presented in this paper allow us to control the residual stress and to fabricate components with less number of layers to form FGMs. This paper presents the development leading up to the arrangement similar to Figure 5. 2 (b) and the developments are currently underway leading to the arrangement similar to Figure 5. 2 (c).

As stated in the previous section, controlling residual stress is a key technological problem in making multi-layer media as well as FGM components shown in Figure 5.2 (c). Without controlling the residual stress, the processed media would be useless as shown in Figure 5.3. In order to resolve this problem, the difference in two shrinkage mechanisms existing in powder processing must be utilized; the effect of CTE and densification behavior. During densification, the interstitial spaces among the powder are filled due to mass transport mechanisms. The shrinkage differences due to CTE mismatch are intrinsic for a given combination of materials after consolidation. However, the shrinkage from the densification of powder can be altered by designing the powder characteristics and optimizing the sintering conditions such as time, temperature, heating/cooling cycles, etc. [German, 1984].
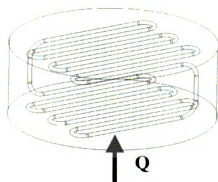
Figure 5.1: the micro-textured and configured body.

(a)Ideal FGMs   (b)Discrete FGMs   (c)FGMs
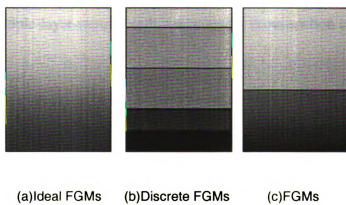
Figure 5.2: Three processing routes to attain FGMs
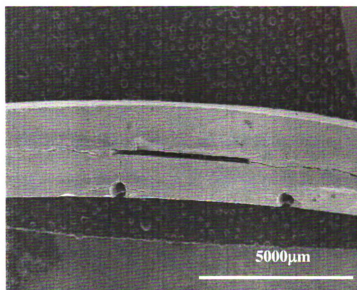
Figure 5.3: A multiple-layer sample with a rectangular cross-section channel affected by residual stress.

The starting powder characteristics and sintering conditions can compensate for the CTE difference by exploiting the differences in densification behavior among the layers. Powder shrinkage during densification must be understood as a function of various processing variables such as the powder characteristics as well as sintering conditions. The powder characteristics influence the initial powder packing density, which in turn affects the densification behavior during sintering. As shown in Reed [1989] with alumina powder, different combinations of the powder characteristics result in different packing densities.

One method to control the initial powder packing is by mixing a few batches of powders with different average particle sizes as demonstrated in Figure 5. 4. Yeh and Sacks [1988] and Ting and Lin [1994 and 1995] studied shrinkage difference between wide and narrow size distribution (WSD and NSD) powders. They show that WSD and NSD powder exhibit not only different initial packing of powder but also different densification rates. In the experiments [Kwon, 1998] conducted in our laboratory, two different powders, AA-5 and AKP-15 (manufactured by Sumitomo Chemical) were compacted with a uniaxial press. Packing density of 59.1% was attained with all AA-5 powder (an average particle size of 5.5-5.8 m). The AA-5 powder mixed in 1:3 ratio with the AKP-15 powder (whose average particle size is 0.6-0.8⊏m) yielded the packing ratio of 71.2%. McGeary's [1961] experiments with spherical particles show higher packing by mixing 'designed' size particles because smaller particles can nest interstitially among bigger particles. Irregular shaped powder can also be used to achieve low packing and different densification behavior.

Powder Preparation

Four different powders, alumina, Partially-Stabilized Zirconia (PSZ) and two kinds of Fully-Stablized Zirconia (FSZ), were used. The alumina powder designated TM-DAR is manufactured by Taimai Co., Japan, whose average size is about 0.2 micron. The PSZ powders manufactured by Tosoh designated TZ-3YS, whose average size was about 0.6 microns. Two FSZ powders were designated TZ-8YS manufactured by Tosoh Corp., Japan and 5.2 weight percentage (w/o) Y_2O_3 zirconia manufactured by CERAC, respectively. The average size of the TZ-8YS powder was about 0.58 microns. The average size of the CERAC powder was about 1.23 microns (90% <1.79 μm, 50% <1.23 μm and 10% <0.77μm). The CTEs of alumina and zirconia are close at 8.8×10^{-6} and 7.6×10^{-6}/°C, respectively. In a more practical sense, the CTE data as a function of temperature for these materials [Purdue University, 1970] must be used. The CTE-induced shrinkage can be compensated with the shrinkage due to densification in making multi-layers and FGMs. In addition, the composite layers are needed to make the discrete FGM shown in Figure 5. 2(b). The mixing of powders with two or more components was performed by dry ball milling for approximately 24 hours in a plastic ball mill with alumina media. The ball mill charge consists of approximately 50 grams of powder.

Pressing

A uniaxial steel die was used to press all specimens in this study at a pressure of approximately 35 MPa. Typically the thickness of pressed disk in a green (unfired) state ranges from 2 to 3 mm. In preparing for subcomponents of FGM, various 'composite' powder mixtures of TM-DAR and PSZ were prepared. A sub-layer of one mixture,

another sub-layer of another mixture and so on were deposited layer by layer in the die and pressed to form the discrete FGM.

Controlling Residual Stress

For a given set of two materials, the extreme condition for residual stress is expected when two powders are processed together. Initially they are processed separately to understand their shrinkage behavior individually without modulating the starting powder. Table 1 shows the dimensional changes after each processing step. TZ-3YS and TZ-8YS powders shrink substantially more than alumina TM-DAR powder after final sintering. However, after pre-sintering (an essential step to burn out fugitive phase to make channels), the dimensional differences are minute.

The sintered samples are subject to warping since the TM-DAR layer is in a state of compressive residual stress while the TZ-3YS is in a state of residual tensile stress based on the shrinkage rate reported in Table 5.1. In McGeary's [1963] experiments with spherical particles, the diameter ratio between larger and smaller particles was 6.5:1. However, the powders we used had relatively wide size distribution and were non-spherical in shape.

To understand and control the residual stress, two-layer samples, one layer with TM-DAR and the other with a various mixture of TZ-3YS and CERAC powders, are pressed together and sintered. All of the samples had some degree of warping as shown in Figure 5.5 with the mixture ratios. The minimum warpage can be observed in C (65T/35C) and D (50T/50C) showing the total height of the warped samples. Based on the observation, the ideal mixture of 45% CERAC and 55% TZ-3YZ is chosen to make an ideal two-layer (alumina and PSZ) sample.

Table 5.1: Dimensional changes during processing (Units are in cm).

Material	After Pressing	After pre sintering	After final sintering	Linear Shrinkage Rate
TMDAR	D = 2.19	D = 2.16	D = 1.85	15.5%
	T = 0.273	T = 0.272	T = 0.205	24.9%
TZ-3YS (PSZ)	D = 2.19	D = 2.19	D = 1.685	23.0%
	T = 0.33	T = 0.318	T = 0.244	26%
TZ-8YS by Tosoh (FSZ)	D = 2.19	D = 2.19	D = 1.68	23.3%
	T = 0.33	T = 0.317	T = 0.24	27.3%
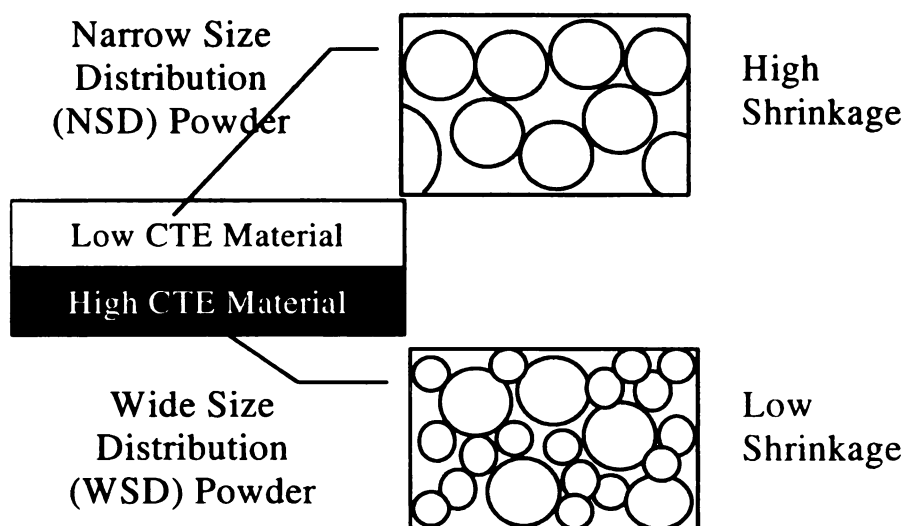
Figure 5.4: Shrinkage control using different powder size distribution.

110

Figure 5.5: Five samples with two layers (alumina and zirconia mixed in five different ratios) showing varying degrees of warpage.

Table 5.2: Height difference of the five samples on figure 5.5

	A	B	C	D	E
Height (cm)	0.05	0.03	0.03	0.025*	0.09

*Specimen destroyed in a fracture test and value extrapolated from Figure 8.2

Channels and Manifolds

Channels that penetrate the bulk of the specimen were formed using a "fugitive compound" added to the ceramic powders before firing. Among many fugitive phases used, polymers, papers and graphite work well. For circular channels, pencil leads with nominal diameters of 700, 500 and 300 microns were sectioned into 1 cm to 1.5 cm lengths prior to embedding them in the ceramic power. Prior to pressing, placing the fugitive phase on top of the ceramic powder produces surface or external channels while embedding them in the ceramic powder produces internal channels. To make internal channels, part of the powder was placed in the die before placing the fugitive phase and then the rest of the powder is placed into the die. The same process was used for other fugitive phases. The presintering was conducted in air for three hours in an electric furnace to burn out the fugitive phase, with an average heating rate of roughly $5^{\circ}C$ per minute to $900^{\circ}C$, and then a cooling rate of $10^{\circ}C$ per minute. During heating, the specimens were placed on a thin powder bed of the same material as the specimen being sintered.

We have fabricated internal channels in a variety of ceramics and ceramic composites, including alumina, zirconia, and hydroxyapatite [Shin et al. 2000 and Lee et al., 2000]. The alumina/zirconia composite samples with internal channels are shown in Figure 5.6, 5.7 and 5.8. These channels are completely internal, not exposed to any surfaces. The samples shown in Figure 5.6, 5.7 and 5.8 were cut after processing using low-speed diamond. Closed internal channels were formed when two specimens with surface channels were joined [Lee and Case, 1999b]. Virtually all the samples with the surface channels made to date were successful without any process-induced defects even

very complex shapes as shown in Figure 5.9 and 5.10. However, only pencil leads show consistent success as a fugitive phase for all the samples with internal channels. These samples can be joined to form the channels penetrating the bulk of ceramic.

Interesting points can be made with Figure 5.7 and 5.8. Figure 5.7 shows the ridges along the channel, which are the exact ridges on pencil lead like a tree trunk. The surface texture of the fugitive phase is exactly reprinted on the channel. On Figure 5.8, two channels at the top right hand corner are half of the diameter apart. The manifold-shaped channel shown in Figure 5.9 was achieved by cutting a paper into the shape of manifold and embedding on the powder before pressing. The spoke-shape manifold was achieved by making the spoke-shaped fugitive phase using rapid prototyping machine.

Sintering

Both microwave processing and conventional sintering were used to fabricate our specimens. For microwave processing, a refractory casket (specimen enclosure) serves both to thermally insulate the specimens and to provide a microwave susceptor material.

Microwave processing

The specimens that were sintered using microwave energy were processed at temperatures between 1300^0C and 1450^0C for up to one hour. The specimen temperature was measured by an optical pyrometer that was sighted on the specimen being sintered. The microwave power supply generated up to 2 kW of power at a frequency of 2.45 GHz. The specimens were heated in a single-mode microwave resonant cavity having both an adjustable short and an adjustable launch probe position. Details of the sintering procedure are given elsewhere [Lee et al., 1997, Lee and Case, 1999a].
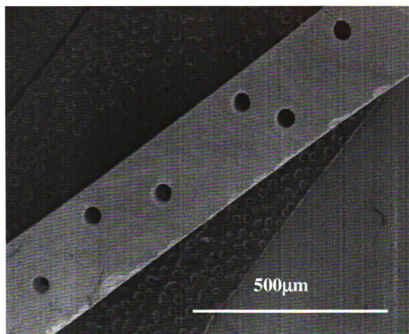
Figure 5.6: Multiple channels on a composite of 75%TMDAR and 25%TZ-8YS.
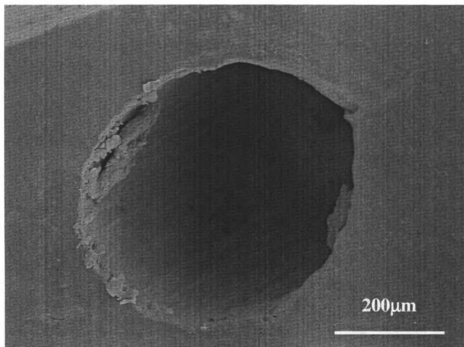
Figure 5.7: A channel showing the micro-ridges (the surface feature of a pencil lead) on alumina sample.
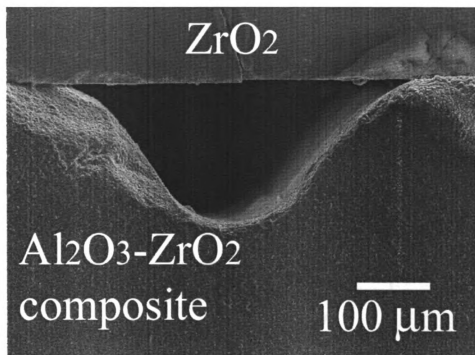
Figure 5.8: Channel formed by joining an alumina-zirconia composite specimen to a partially stabilized zirconia specimen [Lee, 2001].
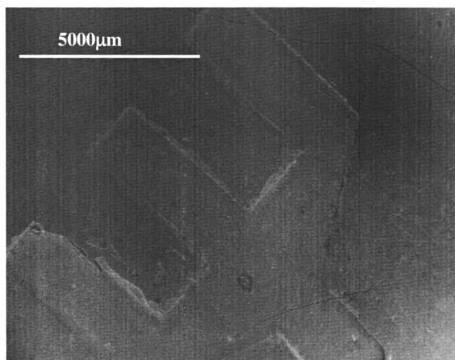
Figure 5.9: Manifold-shaped surface channel created by the graphite sheet cut out with a wire edm.
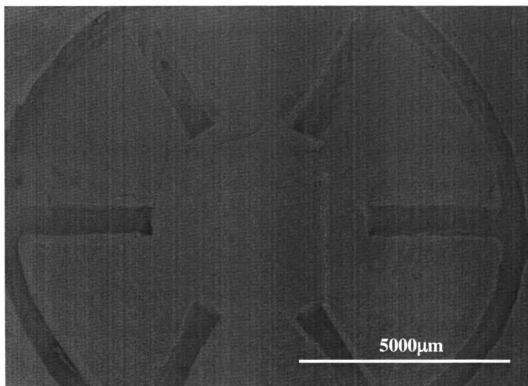
Figure 5.10: A spoke-shaped surface manifold created by rapid prototyping unit.

Conventional sintering

An electrical furnace with SiC heating elements (Carbolite, Corporation) was used to conventionally process the specimens. A furnace with a controlled atmosphere was used to sinter some of the oxide materials, while in a future controlled atmosphere furnaces will be used for the nitride materials. A number of researchers have observed that the temperatures required for "equivalent sintering" via microwave and conventional heating can be substantially different [Lee et al., 1999a]. TM-DAR powders were fired conventionally at a heating rate of approximately $5^{\circ}C$ per minute and a 3-hour hold time at $1430^{\circ}C$. As with the microwave sintering, during conventional sintering multiple-specimen batches can be sintered, with from at least six to eight specimens in a given batch.

Joining

The authors and co-workers have joined like ceramics such as alumina/alumina [Lee et al., 1997], zirconia/zirconia [Lee and Case, 2000], SiC/SiC, HAP/HAP [Lee and Case, 2000], and MaCor™/MaCor™ [Lee et al., 1997] as well as dissimilar ceramics such as alumina/zirconia [Zeng et al., 2001], HAP/MaCor™[Shin et al., 2000], MaCor™/zirconia and a variety of other ceramic/ceramic combinations. Here HAP is a bioceramic hydroxyapatite and MaCor™ is a machineable glass ceramic composite composed of an aluminosilicate glass matrix reinforced by mica platelets.

In order to prepare the sintered specimen surfaces for joining, the surfaces to be joined were first polished and cleaned. Then a coating of amorphous silica was applied to the polished surfaces. The polishing was done with diamond paste having an abrasive size as small as one micron. The polished specimens were then ultrasonicated in a

deionized water bath to help remove debris that accumulated during polishing. A coating of an organically-based silica precursor liquid was then spun onto the surfaces that were to be joined. The coatings were then converted into a thin (roughly 200 nm thick) layer of amorphous silica by heating the coated specimen in air for approximately 20 minutes at 200°C. Joining was done at temperatures of roughly 1300°C - 1450°C using the same microwave cavity and power supply that had been used to sinter the powder compacts. Sintered disks with surface channels can be joined with other disks to produce channels at the interface between the two disks.

5.3 CONCLUSIONS

Being able to micro-configure a ceramic material will impact the way we design and manufacture ceramic components. In addition, with the current research emphasis on micro-devices, we recognize that the immediate applications of the proposed processing techniques are in micro-heat exchangers for microelectronics and cryogenic surgery. Because of the inherent size of such a device, the effective use of materials is necessary. Texturing a material optimally based on a loading condition is the key element that triggered the development of FGMs. The most difficult problem with FGM is to control process-induced residual stress such that residual stresses would not damage the details (like channels) as well as the material itself.

This work is applicable to high temperature applications where the cooling is essential such as advanced semiconductor device and cutting tools. The coolant circulating through the channels and manifolds creates thermal gradient in the medium. And thermal gradient can be compensated by the micro-textured medium such as FGMs.

ACKNOLWDGEMENTS

REFERENCES

Bower, M. B. and Mudwar, I., 1994, *J. Electron Package*, **116**, pp. 290-297.

Copeland, D., 1997, *IEEE Trans. Comp. Pack. Manuf. Tech. – part A*, 20, 2, pp96-102.

Gillot, C., Meysenc L., Schaeffer, C. and Bricard, A., 1999, *IEEE Trans. Comp. Pack. Tech.*, 22: (3), pp. 384-389.

Gray, K. J., 2000, *Diamond and Related Materials*, 9: (2), pp. 201-204

German, R. M., 1984, Powder Metallurgy Science, Metal Powder Industries Federation, Princeton, New Jersey.

Hall, R., 1999, *Electronic Design*, 47: (7), pp. 29-30.

Harpole, G. M. and Eniger, J. E., 1991, Proc. 7th IEEE Semi-Therm. Symp., pp. 59-63.

Hui, P., Tan, H. S. and Lye, Y. S., 1997, *IEEE Tran. Comp. Pack. & Manuf. Tech. Part A*, 20: (4); pp. 452-457.

Jagannadham, K., 1999, *J. Vac. Sci. Technol.*, A17: (2), pp. 373-379

Kwon, P., 1996, Unpublished Results.

Lee, K. Y. and Case, E. D., 1999a, *Materials Science and Engineering*, A269: 8 - 20.

Lee, J. G. and Case, E. D., 1999b, Ceramic Transactions, American Ceramic Society, 103: 571-581.

Lee, J. G., Case, E. D., Shin, H. and Kwon, P., 2000, Ceramic Engineering and Science Proceedings, 21[4]: 103 - 110, American Ceramic Society.

Lee, J. G., Shin, H. W., Case, E. D., Kwon, P., 2001, *Journal of Materials Science Letters*, 20, 2, pp. 107-109.

Lee, K. Y., Case, E. D., and Reinhard, D., 1997, *Ceramic Eng. and Sci. Proc.*, 18: 543-550.

McGeary, R. K., 1961, *J. Am. Ceram. Soc.*, **44**, 10, pp. 613-522.

Mizuno, Y., Kawasaki, A., and Watanabe, R., 1995, *Metall. Mater. Trans.*, **26B**, p. 75.

Nguyen T, Mochizuki M, Mashiko K, et al., 2000, *IEEE Tran. Compon. Pact. T.*, 23: (1), pp. 86-90.

Purdue University, Thermophysical Properties of Matter, V.13, Ed. Y.S. Touloukian, R.K. Kirby, R.E. Taylor and T.Y.R. Lee, IFI/Plenum, New York, 1970.

Reed, J. S., 1989, Introduction to the Principles of Ceramic Processing, Wiley & Sons, New York, NY.

Shin, H. W., Kwon, P. and Case, E. D., ASM Fall 2000 Proceedings.

Ting, T. -M. and Lin, R. Y., 1994, *J. Mat. Sci.*, pp. 1867-1872.

Ting, T. -M., and Lin, R. Y., 1995, *J. Mat. Sci.*, pp. 2382-2389.

Tuckerman, D. B. and Pease, R. F. W., 1981 *IEEE Electron. Devices Lett.*, vol. EDL-2, pp. 126-129.

Yeh, T. and Sacks, M. D., 1988, *J. Am. Ceram. Soc.*, **71**, 12, pp. C484-V487.

Yin, X. and Bau, H. H., 1997, Journal of Electronic Packaging, **119**, pp. 51-57.

Zhang, L. M., Yuan, R. Z., Oomori, M. and Hirai, T., 1995, *J. Mat. Sci. Let.*, **14**, 22, p. 1620.

Zeng, L., Crimp, M. A. and Case, E. D., 2001, *Materials Science and Engineering*, A307: 74 - 79.

Zhong, J. and Bau, H. H., 2001, *American Ceramic Society Bulletin*, **80**, 10, pp. 39-42.

Chapter 6

JOINING OF BIOACTIVE AND BIOINERT CERAMICS[3]

For a number of years, ceramic materials have been of interest as permanent hard

tissue implant materials [1] such as bone screws, dental implants [2], bone replacement

[3], and as coatings on metallic implant devices [4]. For example, a number of

commercial orthopedic manufacturers produce implant materials that include plasma-

sprayed hydroxyapatite (HA, $Ca_{10}(PO_4)_6(OH)_2$) coatings. Typically these ceramic

coatings have been placed on metallic alloys, such as surgical grade Ti-6Al-4V [4–6].

Hip replacement operations are a relatively frequent procedure, with more than

200,000 Total Hip Arthroplasties (THA) performed annually in the United States.

Ceramic-coated implants have the prospect of improving the long-term outcomes of the

hip replacement surgeries [4]. For example, bone ingrowth that occurs in the presence of

bioactive ceramics such as hydroxyapatite can overcome the fixation problems that are

associated with the cracking of cemented implants [7] (implants that are cemented into

place). However, bioceramics are now being used in medical applications that go far

beyond their service as a coating material for metals such as Ti-6Al-4V.

A bioinert ceramic does not induce HA to grow on its surface when it is exposed to

blood or to a simulated biological fluid. In addition, a bioinert ceramic does not generate

[3] Summarized from H. W. Shin, E. D. Case and P. Kwon, "Joining of Bioactive and Bioinert Ceramics", Proceedings from Joining of Advanced and Specialty Materials, ASM International 2000, pp.15-22, and H. W. Shin, P. Kwon, and E. D. Case, "Fabrication of Internal Channels without Machining in Joined Alumina and Zirconia Ceramics", Proceedings from Joining of Advanced and Specialty Materials, ASM International 2000, pp.23-30.

124

corrosion products when exposed to blood or to a simulated biological fluid (although for the typical surgical alloys such as Ti-6Al-4V, corrosion products can accumulate in the tissues near the implant site).

Alumina and zirconia are two bioinert, polycrystalline oxide ceramics included as materials that go into hip replacement units, for example. Either alumina or zirconia is used in the joint region of the hip replacement, where the good wear properties and chemical inertness of these ceramics are very beneficial. In fact, bioactivity would be counterproductive for implant materials that are included in joints. Because of their superior hardness and fracture toughness, alumina and zirconia also find use in engineering applications, e.g., thermal management materials.

In addition to implant materials, bioinert ceramics are being examined as potential materials for dental restorations and tooth implants [8–10]. Glass ceramics are one particular class of ceramics that is being considered for the exterior portions of dental restorations [8]. Glass ceramics are formed by the controlled nucleation and growth of crystalline phases from a glass melt [11, 12]. If the crystalline phase that precipitates in the glass ceramic is a micaceous phase, then the mica can promote the formation of small, localized microcracks during machining, rather than forming large, catastrophic cracks. MaCor™ and other glass ceramics that contain randomly oriented mica platelets may be machined using metal-working tools, thus making such micaceous glass ceramics a potentially versatile element in the fabrication of biomedical materials.

In this chapter, we present our results on the joining of the bioactive ceramic hydroxyapatite and the bioinert ceramics alumina, zirconia, and MaCor™. The challenge is to join two or more layers of materials with distinct coefficient of thermal expansion

(CTE). Joining techniques are necessary when an assembly from simpler components is necessary and when severe warping and cracks are developed in simultaneously sintered composite layers.

6.1 Materials and Preparation

With the exception of the MaCor™, all specimens included in this section were sintered using commercial hydroxyapatite, zirconia, and alumina powders. The alumina (Al_2O_3) powder, designated by TM-DAR, is from Taimei Chemicals Co. The two types of zirconia powders used in this study include a partially stabilized zirconia (PSZ, zirconia powder with 3 mol % yttria), designated by TZ-3YS, from the Ceramic Division of Tosoh Corp., Japan, and a fully stabilized zirconia (FSZ, zirconia powder with 8 mol% yttria), designated by TZ-8YS, also from Tosoh's Ceramic Division. The specific surface areas of both the PSZ and the FSZ were approximately 7 m^2/g. The chemical purity was about 99.9 percent for both the partially-stabilized zirconia (three mol % yttria-zirconia) powder and for the fully-stabilized zirconia (eight mol % yttria-zirconia powder). The hydroxyapatite (Cerac Inc., Specialty Inorganic, Milwaukee, WI) was nominally 99% pure. The average particle size for each of the powders and its abbreviated name used in this paper are listed in Table 6.1.

In addition to the specimens that were sintered from the commercial powders, specimens were cut from billets of the machineable glass ceramic, MaCor™ (Corning Code 9658, Corning NY). MaCor™ consists of a borosilicate glass matrix phase with a reinforcing phase of fluorophlogopite mica, where the mica is in the form of randomly oriented platelets. By volume, the mica platelets make up about 55 volume percent of MaCor™, with the borosilicate glass comprising the remaining 45 volume percent.

126

In this set of experiments (prior to October, 2000), the disc-shaped powder specimens are pressure-compacted to approximately 2.2 cm in diameter in the green (unfired) state (as compared to 2.25 cm diameter in tests conducted after October, 2000).

The powder compacts were then sintered using either a 2.45 GHz single-mode microwave cavity or a conventional, electrically-heated furnace (see Chapter 3). During microwave heating, the specimens were placed in a refractory specimen enclosure (a refractory casket) and then sintered in air for the temperatures and times given in Table 6.2.

During processing, the specimen temperature was monitored by an optical pyrometer. The conventional furnace (Carbolite Inc., with a Eurotherm temperature controller) needed longer sintering temperatures and times to accomplish the same degree of sintering as obtained with the microwave furnace (Table 6.2). This difference in sintering behavior is typical for microwave and conventionally sintered ceramics [13–14].

After sintering, specimens were polished using diamond paste, with the series of grit sizes 35, 25, 17, 10, 6, and 1 microns. In order to inspect the channels, the specimens were cut with a low speed diamond saw. The channels and the specimen microstructure were then examined using optical and scanning electron microscopy.

The reader is referred to Chapter 3 for the types and composition of ceramic powders used, mixture ratios used for composite specimens, procedures for powder mixing of composites, specimen pressing, pencil lead as the choice of fugitive phase and

Table 6.1: Summary of powder average size

Powder	Material	Average Particle size (μm)
TMDAR	Al_2O_3	0.2
TZ-3YS	3 mol% PSZ	0.5
TZ-8YS	8 mol% PSZ	0.54
HAP	Hydroxyapatite	2-3

Table 6.2. For the specimens included in this study, the furnace type, sintering temperatures, sintering times and channel descriptions for channels fabricated without machining.

Material	Furnace Type	Sintering Temperature ($^\circ$C)	Sintering Time (Hours)	Channels
100% HAP	Microwave	1300	1	4 Internal
75%Alumina+ 25%HAP	Microwave	1300	1	4 Internal
25%Alumina+ 75%HAP	Microwave	1300	1	4 Internal
75% Zirconia+ 25%HAP	Microwave	1300	1	4 Internal
25%Zirconia+ 75%HAP	Microwave	1300	1	4 Internal
100%HAP	Microwave	1300	1	4 Internal + 4 External
100%HAP	Conventional	1375	4	3 Internal

its embedding configurations, temperatures and hold times for pre-sintering and full sintering, method used for polishing and joining, as well as information on the pressing and sintering equipment. It is worth noting that a polymer line (fishing thread) has also been tried as a fugitive phase. However, under the high heat of pre-sintering, the polymer phase melts before it evaporates, causing the channel shape to lose its circular cross-sectional shape. In addition, the difference in elastic rebound properties between polymers and ceramics leads to internal fractures in the both the pre-sintered and fully sintered specimens. Even shrinkage tapes used in electric work have been considered as a fugitive phase at one point. However, they exhibit anisotropy in shrinkage; e.g. one of the dimensions shrinks while another expands, which leads to fracture. Graphite/pencil lead was finally chosen as the fugitive phase.

The overview of the process route associated with the joining of ceramic layers with internal channels is depicted in Figure 6.1.
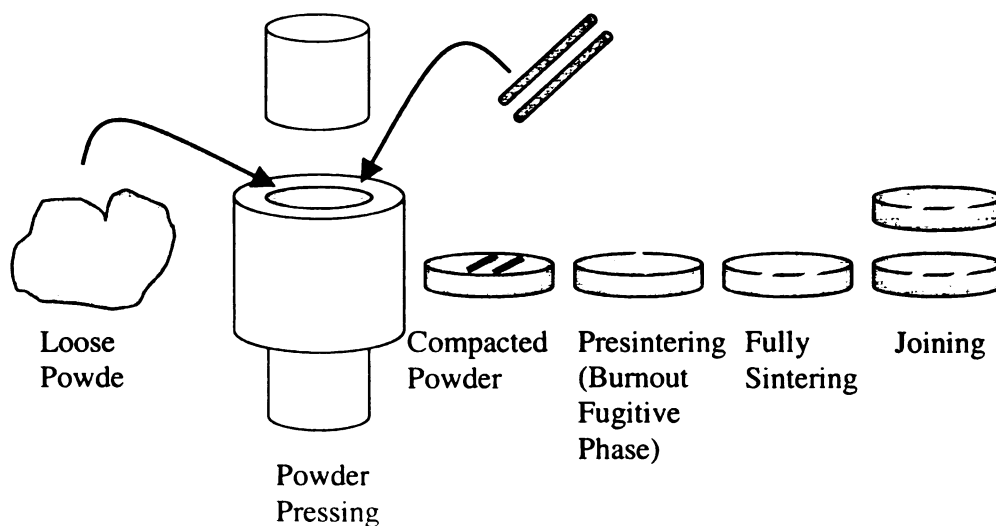

Figure 6.1: Overview of processing route

6.2 Results and Discussion

The average grain size of the sintered specimens was determined using the linear intercept method on SEM micrographs of fracture sections of the sintered specimens (Figure 6.2). The mean grain size of the alumina and zirconia specimens ranged approximately from one to two microns.

The 0.5-mm diameter and the 0.3-mm diameter fugitive-phase rods produced cylindrical channels with a circular cross section (Figure 6.3). Using a low speed diamond saw, the sintered specimens were sectioned along planes perpendicular to the cylinder axes of the internal channels (Figure 6.3). Following sectioning, selected specimens were mounted and polished with diamond paste with grit sizes down to 100 microns.

For the 0.5-mm diameter fugitive-phase rods, the final, as sintered channels were 425 microns in diameter. Using these fugitive-phase rods, internal channels were successfully formed in pure alumina, 3 mol% yttria-zirconia, and 8 mol% zirconia, using both conventional and microwave heating. In addition, pure hydroxyapatite specimens were fabricated, along with various hydroxyapatite/alumina and hydroxyapatite/zirconia particulate composites. The sintering temperature, sintering time, and chemical composition of each of the hydroxyapatite-containing specimens is listed in Table 6.2. It should be noted that hydroxyapatite/alumina and hydroxyapatite/zirconia particulate composites could be bioactive while having superior mechanical properties compared to single-phase hydroxyapatite materials [15–17]. Low magnification SEM and optical microscope examination of the sectioned specimens (Figure 6.4) showed the relative

130

placement of the multiple internal channels. Figures 6.5 and 6.6 are SEM micrographs of two different regions of a joined hydroxyapatite/MaCor™ specimen.

Fig. 6.7 shows the joined interface between a homogeneous layer of zirconia (TZ-8YS) and a composite layer made of alumina and zirconia (25% TMDAR/75% TZ-3YS). Prior to joining, one side of each specimen was polished using diamond paste of gradually reducing, mean abrasive size from 35 to 1μm. These specimens were spin-coated with silica film at a rotational speed of 3000 rpm for 20 seconds. Then, they were cured in a furnace at 200°C for 20 min. Finally, they were joined in our microwave unit at 1475°C for 20 minutes with a heating and cooling rate 10°C/min. A dead weight of 11.75 g was used to press the two specimens together. After they were joined, the specimen was cut at a low speed using diamond saw.

For the sectioned specimens containing the multiple internal channels, no cracking around or near the channels was noted upon either optical or electron microscopic examination of the sectioned surfaces, for both surface preparations (namely, the as-diamond saw cut specimen surfaces or the sectioned and then diamond-polished specimen surfaces).

Thus, pressing the fugitive-phase rods into the powder compacts, and then burning out the fugitive elements prior to sintering was a successful method of fabricating internal circular channels in both bioactive and bioinert ceramics.

To extend the potential for the use of these techniques, one can envision uses in which bioactive materials and bioinert materials would be joined to form a single structural elements. In this study, we successfully joined MaCor™ specimens with pure hydroxyapatite specimens having three internal channels.
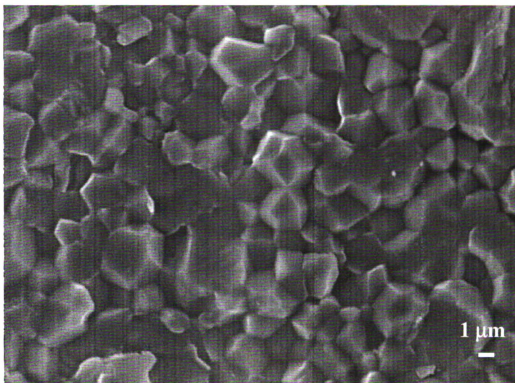
131

Figure 6.2. A SEM micrograph of the fracture of an alumina specimen sintered from commercial powders (TM-DAR, Tamaii Corp., Japan). The specimen was pre-sintered for one hour at 900ºC in a conventional furnace in order to burn out the fugitive phase. Then, the specimen was sintered at 1300°C in a microwave cavity
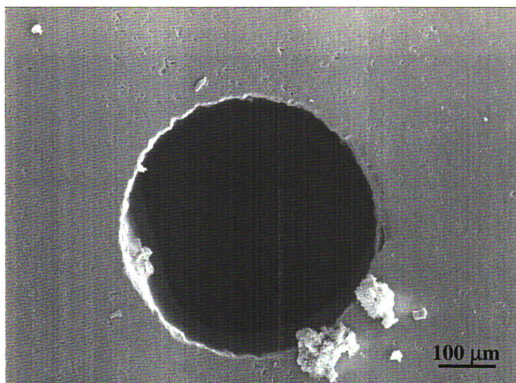
Figure 6.3. An SEM micrograph of a internal channel in a microwave sintered alumina specimen. A fugitive-phase rod 0.5 millimeters in diameter was used to initially form the channel in the powder compact.
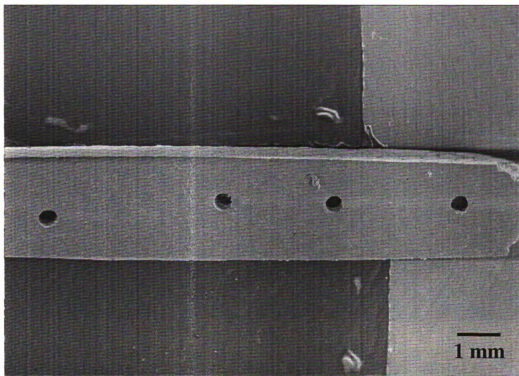
Figure 6.4. For a alumina/hydroxyapatite particulate composite (25 weight percent alumina, 75 weight percent hydroxyapatite), a low speed diamond saw cut reveals the four cylindrical channels formed internally in the specimen.
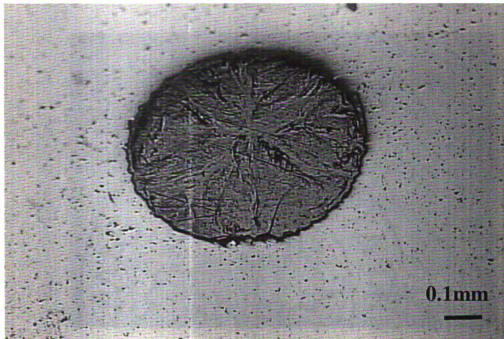
0.1mm

Figure 6.5. An SEM micrograph of a sectioned hydroxyapatite specimen showing one of the internal channels formed without machining using the fugitive-phase rod elements. After sectioning on the low speed diamond saw, the specimen surface was polished using diamond paste.
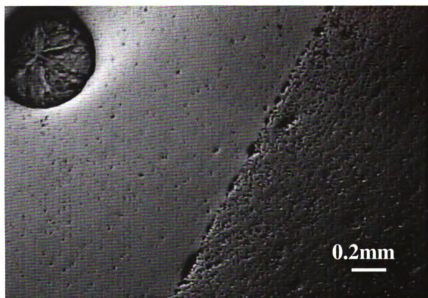
Figure 6.6. For the joined hydroxyapatite/MaCor™ specimen, the region near the interface between the two materials. Note that a portion of one of the channels is also included in the micrograph.
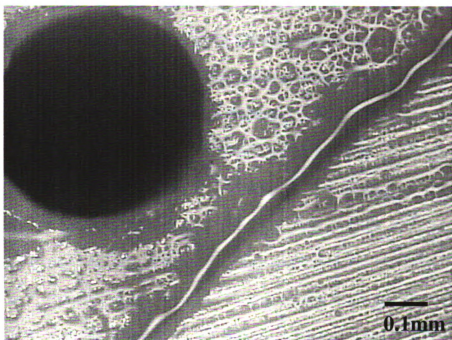
Figure 6.7: The Interface of the Joined Sample made of TZ-8YS and 25% TMDAR / 75% TZ-3YS Joined at 1475°C for 20 min. in our microwave unit.

ACKNOWLEDGMENTS

REFERENCES

1. T. L. Seitz, K. Noonan, L. L. Hench, N. E. Noonan, "Effect of Fibronectin on the Adhesion of an Established Cell Line to a Surface Reactive Biomaterial," Journal of Biomedical Materials Research, 1982, 16: 195-207

2. H. Kawahara and M. Hirabayashi, "Single Crystal Alumina for Dental Implants and Bone Screws", Journal of Biomedical Materials Research, 1980, 14: 597-605

3. A. Uchida, S. M. L. Nade, E. R. McCartney, and W. Ching, "The use of ceramics for bone replacement", Journal of Bone and Joint Surgery, 1984, 66-B: 269-275

4. S. H. Maxian, J. P. Zawadsky, and M. G. Dunn, "*In Vitro* Evaluation of Amorphous Calcium Phosphate and Poorly Crystallized Hydroxyapatite Coatings on Titanium Implants," Journal of Biomedical Materials Research, 1993, 27: 111-117

5. Y. Fujita, T. Yamamuro, T. Nakamura, T. Kitsugi, and S. Kotani, "Mechanism and Strength of Bonding Between Two Bioactive Ceramics *in Vivo*," Journal of Biomedical Materials Research, 1992, 26: 1311-1324

6. E. P. Paschalis, Q. Zhao, B. E. Tucker, S. Mukhopadhayay, J. A. Bearcroft, N. B. Beals, M. Spector, and G. H. Nancollas, "Degradation Potential of Plasma-sprayed Hydroxyapatite-coated Titanium Implants," Journal of Biomedical Materials Research, 1995, 29:1499-1505

7. N. C. Blumenthal and V. Cosma, "Inhibition of Apatite Formation by Titanium and Vanadium Ions," Journal of Biomedical Materials Research: Applied Biomaterials, 1989, 24, A1: 13-22

8. Y. G. Jung, I. M. Peterson, D. K. Kim and B. R. Lawn, "Lifetime-limiting strength

degradation from contact fatigue in dental ceramics," J. Dent. Research, 2000, 79: 722-731

9. G. J. P. Fleming, R. M. Shelton, P. M. Marquis, "The influence of clinically induced variability on the bi-axial fracture strength of cemented aluminous core porcelain discs", Dent. Materials, 1999, 15: 62-70

10. P. Magne, K. R. Kwon, U. C. Belser, J. S. Hodges and W. H. Douglas, "Crack propensity of porcelain laminate veneers: A simulated operatory evaluation, J. Prosthet. Dentistry, 1999, 81: 327-334

11. W. D. Kingery, H. K. Bowen and D. R. Uhlmann, Introduction to ceramics, Second Edition, John Wiley and Sons, New York, 1976, pp. 368-375

12. Y. M. Chiang, D. P. Birnie, III, and W. D. Kingery, Physical Ceramics: Principles for Ceramic Science and Engineering, John Wiley and Sons, New York, 1997, pp. 446-464

13. K. Y. Lee and E. D. Case, "Microwave Sintering of Alumina Matrix Zirconia Composites Using a Single-Mode Microwave Cavity," Journal Materials Science Letters, 1999, 18[3]: 201-203

14. K. Y. Lee, P. H. Dearhouse, and E. D. Case, "Microwave Sintering of Alumina Using Four Different Single-Cavity Modes," Journal of Materials Synthesis and Processing, 1999, 7[3]: 159-166

15. J. A. Delgado, L. Morejon, S. Martinez, M. P. Ginebra, N. Carlsson, E. Fernandez, J. A. planell, M. T. Clavaguera-Mora, and J. Rodriguez-Viejo, "Zirconia-toughened hydroxyapatite obtained by wet sintering", J. Materials Sci. – Materials in Medicine, 1999, 10: 715-719

16. Y. M. Kong, S. Kim, H. E. Kim and I. S. Lee, "Reinforcement of hydroxyapatite bioceramic by addition of ZrO_2 coated with Al_2O_3", J. Amer. Ceram. Soc., 1999, 82: 2963-2968

17. L. Fu, K. A. Khor and J. P. Lim, "Yttria-stabilized zirconia reinforced hydroxyapatite coatings", Surf. Coating Tech., 2000, 127: 66-75

Chapter 7

COMPARISON OF MICROWAVE SINTERING AND CONVENTIONAL

SINTERING

The principle of microwave heating is fundamentally different compared to conventional heating (Figure 7.1) [1]. In the microwave processing, heat is generated within the material; meanwhile, the heat is created by an external heating source in the conventional processing. Because of the result of this internal and volumetric heating, the thermal gradients and the flow of heat in microwave processed materials are opposite of those in materials processed by conventional heating (Figure 7.2) [2]. Due to these reasons many advantages in microwave processing over conventional processing includes (1) reduction in manufacturing costs because of saving of energy and processing time. For example, Sheppard [3] showed microwave drying and sintering require less energy than conventional processing by a factor of about two and ten respectively and lower sintering temperatures and decreasing in processing time [4,5]. Temperature differentials as high as 400°C between microwave and conventional processing have been reported [6]; (2) improved product uniformity and yields; and (3) improved microstructure and properties [7,8,9].

Janny and Kimrey [4] sintered Al_2O_3 doped with 0.1 wt% MgO under vacuum by using a 28-GHz microwave [10]. For a given temperature, a much higher degree of densification can be achieved with the use of microwave as compared to conventional heating (Figure 7.3).

Using 3.96 g/cm^3 for the theoretical density of alumina, 6.05 g/cm^3 for partially stabilized zirconia (TZ3YS), 5.90 g/cm^3 for fully stabilized zirconia and 1.64~7.44 g/cm^3 for hydroxyapatite (HAP), relative densities over 90% of theoretical were calculated for specimens which were made by using each powder. Relative mass densities of each specimen are given in Table 6.1. To get the similar densification of specimen sintered in the microwave and the specimen sintered by conventional means, the sintering temperature was increased from 1300°C to 1430 °C for alumina and zirconia specimens and increased from 1100 °C to 1300 °C for HAP. Also, the sintering time is 1 hour for the microwave as opposed to 4 hours for conventional processing.

Microwave sintering can yield smaller grain size than sintering with conventional furnaces due to fast heating and enhanced densification at lower temperature which is so called the 'microwave effect"[11,12,13]. The microwave effect results from the direct interaction of the processed material with the microwave field, resulting in internal volumetric heating. The microstructures for specimens of alumina were shown in figure4. Figure 7.4a indicates that the fracture of alumina that sintered at 1430°C for 4 hours in conventional furnace and figure 7.4b shows that the fracture mainly occurred by intergranular fracture.
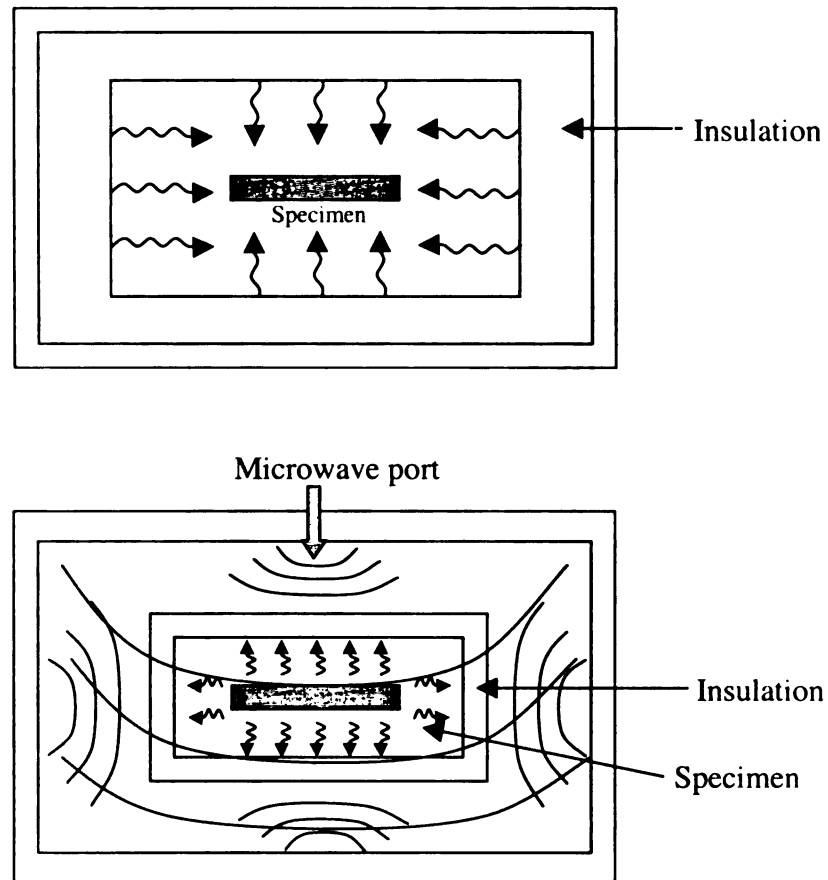
Figure 7.1. Heating patterns in (a) conventional and (b) microwave furnaces [1]
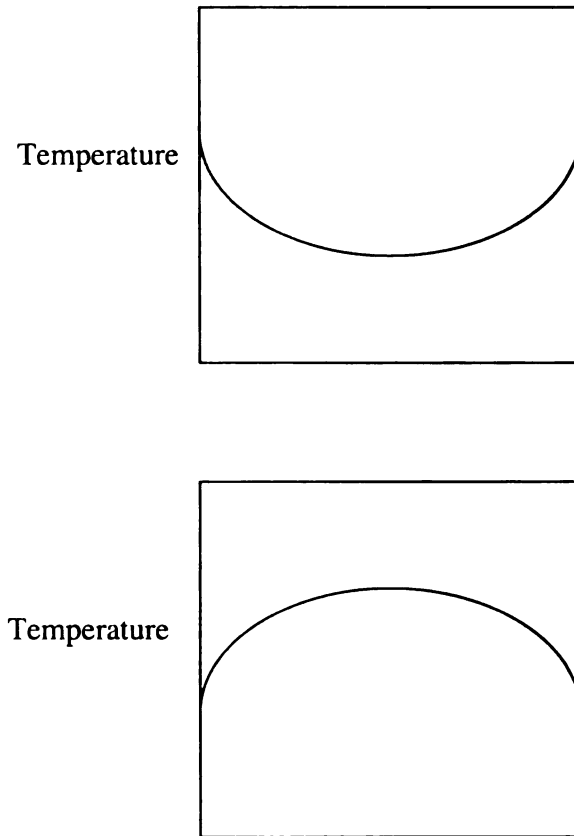
Temperature

Temperature

Figure 7.2. Temperature gradients generated during (a) conventional and (b) microwave heating of materials [2]
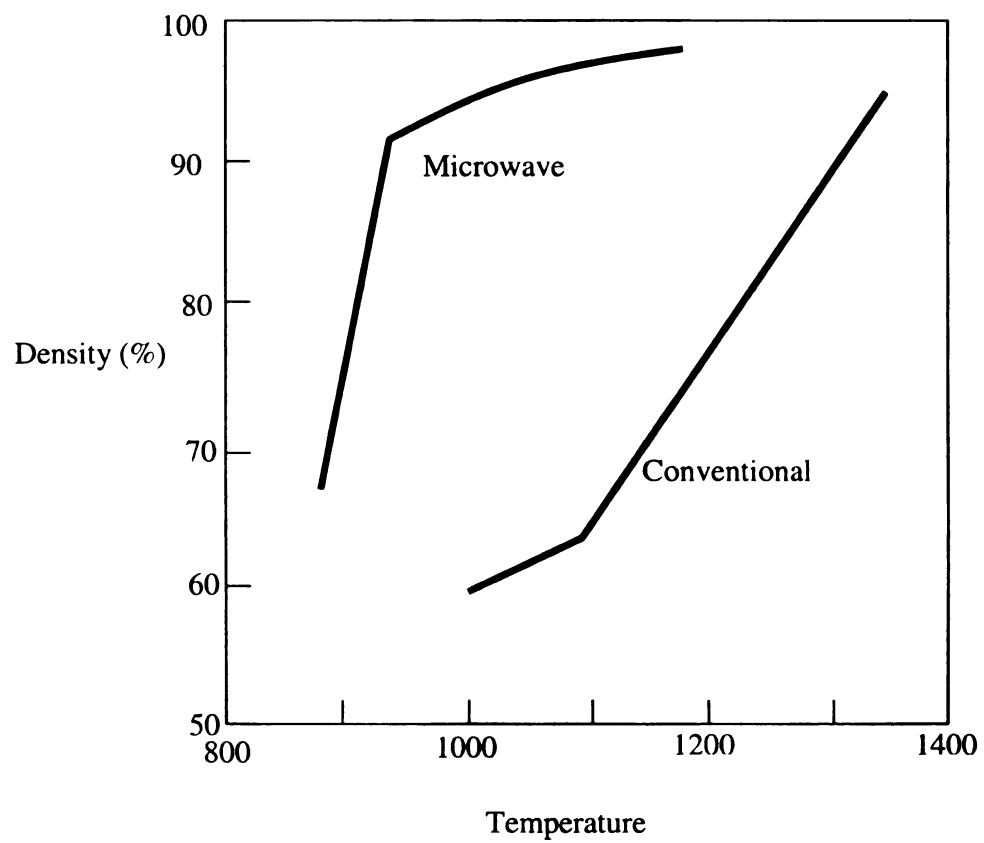
Figure 7.3. Schematic figure of density versus temperature of microwave (28GHz) and conventionally sintered Al_2O_3 [4]

Material	Average Particle Size (μm)	Theoretical Density (g/cm^3)	Conventional sintering			Microwave Sintering		
			Time (hour)	Temp. (°C)	% Densification	Time (hour)	Temp. (°C)	% Densification
TMDAR	0.2	3.96	4	1430	96.8	1	1300	97.2
TZ3YS	0.59	6.05	4	1430	95.6	1	1300	96.0
TZ8YS	0.54	5.90	4	1430	96.7	1	1300	96.8
HAP	2~3	3.156	1	1300	93.4	1	1100	94.9

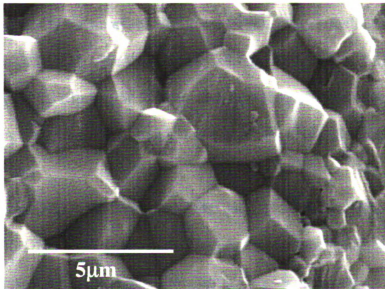Table 7.1. Summary of comparison of sintering using conventional and microwave means.
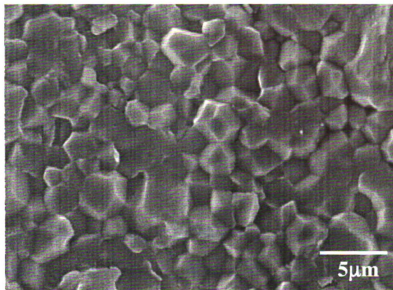
Figure 7.4. Fracture surface of alumina (a) sintered by conventional at 1430 °C for 4 hours, (b) by microwave at 1300 °C for 1 hour.

REFERENCES

1 W.H.Sutton, "Microwave Processing of Ceramic Materials", Am.Ceram.Soc.Bull.68[2], 1989, pp376-386

2 M.A. Janney, H.D. Kimrey, and J.O.Kiggans, "Microwave Processing of Ceramics: Guidelines used at the Oak Ridge National Laboratory", in Microwave Processing of Materials, III, R.L. Beatty, W.H.Sutton, and M.F. Iskander, eds., MRS Symp. Proc., Vol.269, 1992, 173-185

3 L.M. Sheppard, "Manufacturing Ceramics with Microwaves: The Potential for Economical Production", Am Ceram. Soc. Bull., 67[10], 1988, pp.1656-1661

4 M.A. Janney and H.D. Kimrey, "Microwave Sintering of Alumina at 28GHz", Ceramic Powder Science, II, B, Ceramic Transactions, vol.1, 1988, pp.919-924

5 M.A. Janney and H.D. Kimrey, "Diffusion-Controlled Processes in Microwave-Fired Oxide Ceramics", Mater.Res.Soc.Symp. Proc., vol.189, 1991, pp215-227

6 M.A. Janney, H.D. Kimrey, W.R.Allen and J.O. Kiggans, "Enhanced Diffusion in Sapphire during Microwave Heating," Journal of Materials Science vol.32, No.5, 1997,pp.1347-1355

7 A. De, I.Ahmad, E.D. Whitney, and D.E.Clark, "Microwave (Hybrid) heating of Alumina at 2.45 GHz: I. Microstructural Uniformity and Homogeneity," Microwaves: Theory and Application in Materials Processing, Ceramic Transactions, vol. 21, 1991, pp.319-328

8 C.E. Holcombe, T.T.Meek, and N.L. Dykes, "Enhanced Thermal Shock Properties of $Y_2O_3-2wt.\%ZrO_2$ heated Using 2.45 GHz Radiation," Mat.Res.Soc.symp. proc.vol. 124, 1988, pp.227-234

9 M.C.L.Patterson, P.S.Apte, R.M. Kimber, and R.Roy, "Mechanical and Physical Properties of Microwave Sintered Si3N4," Mat. Res. Soc. Symp. Proc.vol269 1992, pp.301-310

10 Yang Bin, Li Jun, Wang Jinxiang, and Zhong Xiangchong, "Influence of ZrO_2 on the Sintering Microstructure and Properties of MgO Materials," proceedings of the International Symposium on the Science and Technology of Sintering, Intering and Materials, Proc., 6th, vol. 6, 1995, pp.197-202

11 M.A. Janney and H.D. Kimrey, in Mat.Res. Soc. Symp. Proc., ed. W.B. Snyder, Jr., W.H. Sutton, M.F. Iskander and D.L.Johnson, vol.189, Materials Research Society, Pittsburgh, Pensnsylvania, 1990, pp.215-227

12 K.Y.Lee, E.D.Case, J.Asmussen, Jr., and M.Siegel, in Proceedings of the 11th Annual ESD Advanced Composites Conference, Ann Arbor, Michigan, 1995, pp.491-503

13 K.Y.Lee, E.D.Case, J.Asmussen, Jr., and M.Siegel, in Cer. Trans., vol.59, The American Ceramic Society Inc., Westerville, Ohio, 1995, pp.473-480

Chapter 8

MINIMIZING WARPING, CRACKING, AND RESIDUAL STRESS

8.1 Warping and Cracking

8.1.1 Initial Observations

Pre-sintering refers to partially sintering of the powder compact during which the graphite fugitive phase from the ceramic substrate evaporates. Heated in an oven by itself, the graphite fugitive phase evaporated near 700°C after 2 hours. However, when the same temperature and heating time were used to pre-sinter a ceramic substrate having graphite rods embedded on its surface, un-evaporated graphite residue remained. As a remedy, pre-sintering e was performed at 900°C. In a homogeneous specimen this high-temperature process presented no problem. However, warping and cracking were evident after both pre-sintering and final sintering of layered zirconia/alumina samples (viz., layers were compacted together and sintered without any joining of layers). The cause of warping and cracks was identified by visual inspection to be the difference in shrinkage behavior of the individual layers. In separate tests, the amount of shrinkage of homogeneous samples of zirconia and alumina specimens after pre-sintering and full sintering have been measured and are given in Figure 8.1 ; an interpretation of the results will be given shortly.

Few ideas are available for minimizing warping in the finally sintered specimens. Among these are (1) finding the total shrinkage (after final sintering) of different layers as a function of the pre-sintering temperature, in hopes that a range of optimal pre-

sintering temperatures can be found that would ensure shrinkage of the different layers to the same structural dimensions; (2) varying the composition of the individual layers to achieve flat, sintered composites, which can then be joined to other layers, and (3) adjusting the initial sizes of the green specimens to ensure a compatible fit between different layers after sintering.

8.1.2   Variation of Pre-sintering Temperatures to Minimize Cracking

In Figure 8.1, the presintering temperature was varied to study its effect on shrinkage. The initial, green-state geometries of the specimens are nearly the same: their diameters are controlled by the inside diameter of the die (2.25 cm), while their thickness are controlled by making sure that equal amounts of powder (3 grams) are compacted. In both plots (a) and (b), the fine lines indicate the amount of shrinkage after a set of specimens have been pre-sintered at different temperatures. The heavier lines indicate the final specimen dimensions after final sintering at 1430°C; the seeming variation with temperature is merely a reference to the respective temperatures to which the specimens have been exposed in the pre-sintering step.

Two observations can be inferred from Figure 8.1. First, the amount of total shrinkage after final sintering is independent of the choice of pre-sintering temperature. Hence, in making a two-layered, alumina/zirconia composite, we can expect the final, sintered specimen to warp regardless of the choice of pre-sintering temperature.

The second observation is with regards to cracking. It is based on the variation in the amount of shrinkage in the diameters of the alumina and zirconia specimens with respect to pre-sintering temperature. In the extreme case presented in Figure 8.1 (a), it is seen that at a processing temperature of 1200°C, there is a flip in shrinkage behavior

between alumina and zirconia in going from pre-sintering to full sintering. In particular, after 4 hours of pre-sintering at 1200°C, alumina (TMDAR) shrinks more than zirconia (TZ3YS); however, after an additional 4 hours at 1430°C to achieve final sintering, the situation is reversed—the diameters of the zirconia specimens end up smaller than those of the alumina specimens. We conclude that during the processing of two-layered, alumina/zirconia composites, a concavity will first develop along the alumina side after pre-sintering, but after final sintering, the curvature is flipped to surround the zirconia side instead. This reversal in curvature imposes cyclic loading that is the suspected cause of macroscopic cracking and layer separation along the interface, as well as spalling on the exposed concave face undergoing compression. By contrast, while the warping of a two-layered, alumina/zirconia specimen is observed even for pre-sintering temperatures of less than 900°C, there is no reversal in curvature in the sintering process (Figure 8.1(a)). Correspondingly, the severity of cracking is not nearly as severe; in fact, only hairline cracks parallel to the interface and wrinkle cracks on the compressed face are evident.

In summary, unlike the case of warping, the amount of interfacial cracking found in the alumina/zirconia composite depends greatly on the pre-sintering temperature. Based on the results in Figure 8.1, pre-sintering temperature of 900°C is chosen not only for the full evaporation of the graphite phase embedded in ceramic powders, but also for the minimization of cracking.

8.1.3 Use of FGM/Variation of Layer Composition to Minimize Warping

The most severe cracks found in the alumina/zirconia specimens are caused by warping; in turn, warping is caused by a mismatch in the densification behavior of the

different layers. The coefficient of thermal expansion of alumina and zirconia are similar. While pre-sintering temperature of 900°C minimizes cracking, it did not eliminate cracking, nor did it control warping. To control warping and cracking, we introduce an independent physical mechanism to counteract mismatches in densification. The idea is to use differences in particle-mixing ratios to control densification.

When the composition of a material is varied spatially in order to achieve a desired effect, we speak of it as a functionally gradient material (FGM). In the current application, the desired effect is the flatness of the composite layers after sintering. After sintering, such layers can be joined to other layers to produce more complex assemblies.

In what follows, the proper mixture of powders must be chosen to give the desired densification behavior. The goal is to produce a warp-free composite layer. A composite layer of mixed zirconia and alumina is being considered (see the 'Configuration' figure of Table 8.1). Mixing zirconia particles of different sizes allows us to vary the densification behavior.

Tables 8.1 (a) and (b) show the results of a preliminary study on the shrinkage of zirconia layers of different mixtures (average particle sizes are listed under the tables). Being an initial control step, this study does not include alumina. As mentioned before, the diameters of all specimens in the green state are the same, whereas the initial thickness is constant within each composition. Due to the different sizes of particles used, two powder piles of equal mass are compacted to different sizes in general; this gives rise to different, initial specimen thickness across different mixture ratios. .

It can be inferred from Table 8.1 (b) that the total shrinkage after final sintering is independent of the choice of pre-sintering temperature, and this is true for all mixtures of

zirconia considered. Also, the two compositions labeled '60T/40C' and '55T/45C' shrink differently from specimens of other compositions, in an unexpected way. Namely, after pre-sintering (Table 8.1 (a)), the specimens labeled 60T/40C and 55T/45C shrink to diameters that are smaller than those of the other mixtures, while after final sintering (Table 8.1 (b)), these specimens have diameters that are bigger than those of other mixtures. While no physical mechanisms are available to explain this shrinkage behavior across different compositions, the effect does highlight the 60T/40C and 55T/45C compositions as possible candidates for further study.

Since the publication of chapter 5. we have added more samples to refine the exact compostion where the residual stress be minimized. The results were represented in figure 8.2. and the composition is 55%T/45%C. Having conducted experiments to isolate the shrinkage behavior of zirconia mixtures, we moved on to study the warping behavior of the zirconia mixture/alumina composite layer. A schematic of the composite layer is given as part of Table 8.2. Densification behavior is controlled by varying the mixture of zirconia (ZrO_2) powders in the zirconia component layer. This mixture is composed of zirconia powder from Tosoh Corp., designated TZ-3YS, with an average particle size of 0.6 microns (histogram: 92%<2 microns, 50%<0.59 microns and 10.12%<0.3 microns), and zirconia powder from CERAC, Inc., with an average particle size of 1.23 microns (histogram: 90%<1.79 microns, 50%<1.23 microns, and 10%<0.77 microns).

The amount of warping after final sintering of different zirconia mixture/alumina composite layers is given in Table 8.2. Warping is quantified by the amount of the displacement of the specimen's center away from true flatness, as shown in the last figure of Table 8.2. A plot of this center displacement versus composition is given in Figure 8.2,

where it is seen that a composition of 55% TZ-3YS and 45% CERAC in the zirconia

component can be used to minimize the warping in the zirconia/alumina composite layer.

Diameter Shrinkage after Pre-Sintering

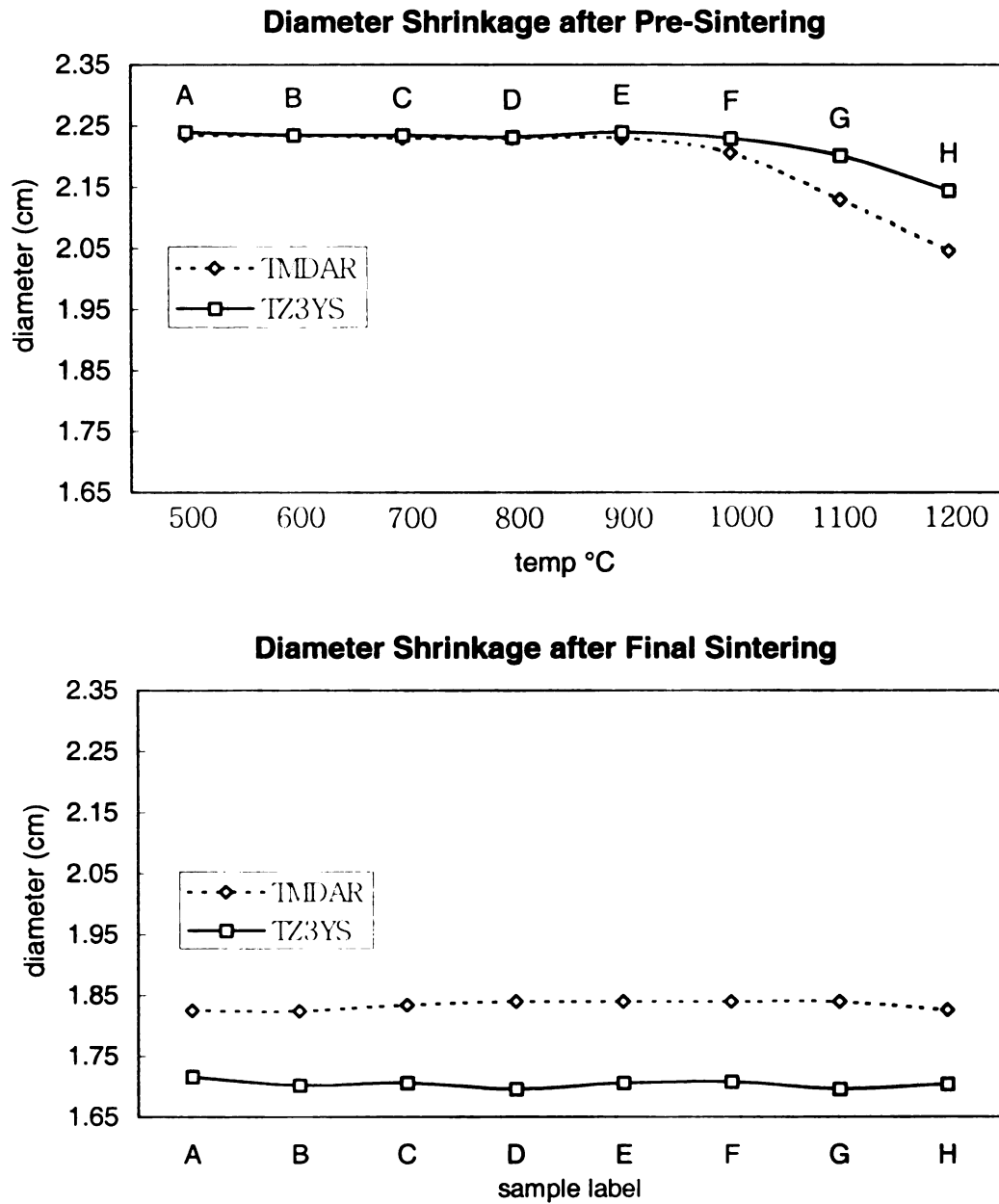**Diameter Shrinkage after Final Sintering**

Figure 8.1a. Shrinkage difference in the diameter of zirconia and alumina specimens after pre-sintering at different temperatures, and their corresponding diameter after final-sintering at 1430°C.
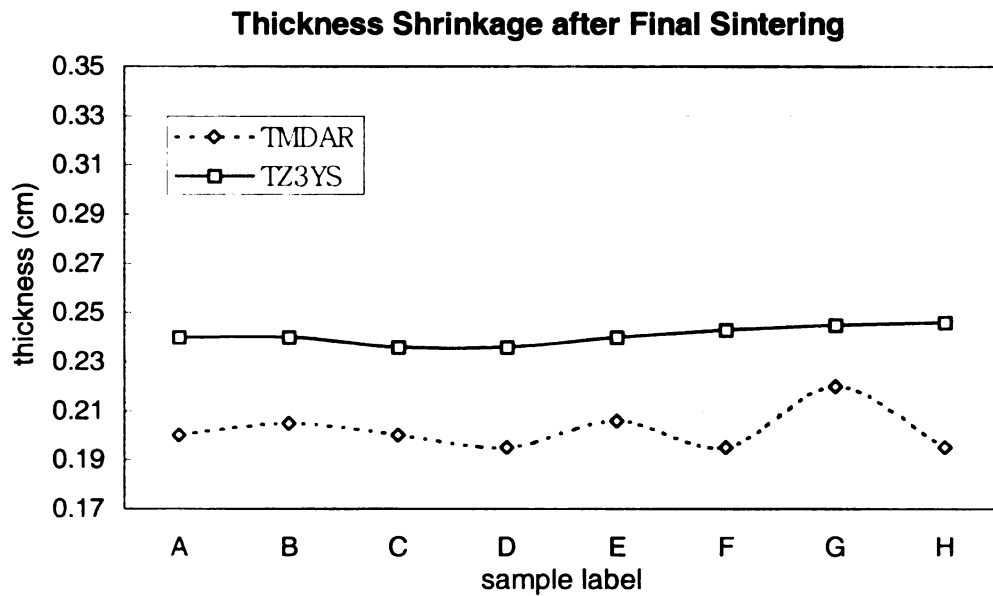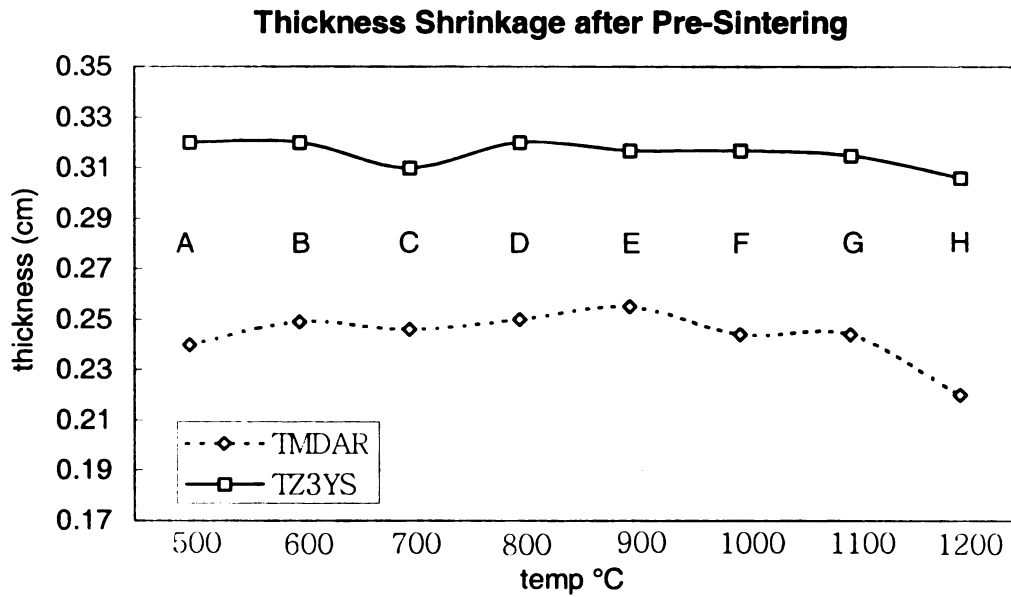
Thickness Shrinkage after Pre-Sintering

Thickness Shrinkage after Final Sintering

Figure 8.1b. Shrinkage difference in the thickness of zirconia and alumina specimens after pre-sintering at different temperatures, and their corresponding thickness after final-sintering at 1430°C.

Table 8.1(a). Size comparison of Zirconia layers of different mixtures after pre-sintering at 900°C for 4 hours (cm)

Composition / Pre-Sintering Temp.		85T /15C①	75T /15C	72.5T /27.5C	70T /30C	60T /40C	55T /45C	25T /75C
600°C	D ②	2.235	2.235	2.24	2.24	2.235	2.235	2.23
	T ③	0.25	0.26	0.26	0.26	0.24	0.235	0.26
700°C	D	2.23	2.23	2.235	2.235	2.23	2.235	2.24
	T	0.255	0.255	0.255	0.26	0.24	0.24	0.255
800°C	D	2.225	2.225	2.23	2.225	2.215	2.22	2.216
	T	0.255	0.265	0.26	0.26	0.23	0.24	0.255
900°C	D	2.215	2.225	2.22	2.22	2.21	2.22	2.21
	T	0.25	0.265	0.255	0.27	0.24	0.24	0.25
1000°C	D	2.21	2.215	2.215	2.215	2.195	2.195	2.195
	T	0.25	0.255	0.26	0.26	0.225	0.24	0.265
1100°C	D	2.165	2.17	2.17	2.165	2.11	2.125	2.14
	T	0.24	0.248	0.246	0.25	0.22	0.225	0.245
1200°C	D	2.055	2.03	2.045	2.02	1.92	1.975	1.985
	T	0.235	0.24	0.24	0.235	0.22	0.21	0.23

① T: Zirconia from Tosoh Company (TZ-3YS; average powder particle size = 0.6 μm)
C: Zirconia from Cerac Company (5 wt% Y_2O_3; average powder particle size = 1.23 μm)
② D: Diameter of the specimen
③ T: Thickness of the specimen

Table 8.1(b). Size Comparison of Zirconia Layers of Different Mixtures after final sintering at 1430°C for 4 hours (left column lists temperatures at which the specimens were pre-sintered) (cm)

Composition Sintering Temp.		85T /15C①	75T /15C	72.5T /27.5C	70T /30C	60T /40C	55T /45C	25T /75C
600°C	D ②	1.77	1.755	1.755	1.755	1.805	1.8	1.75
	T ③	0.2	0.2	0.205	0.2	0.19	0.2	0.2
700°C	D	1.77	1.755	1.755	1.74	1.8	1.805	1.755
	T	0.2	0.2	0.2	0.205	0.195	0.195	0.2
800°C	D	1.77	1.76	1.775	1.745	1.815	1.81	1.75
	T	0.2	0.2	0.2	0.2	0.19	0.195	0.2
900°C	D	1.77	1.755	1.755	1.75	1.81	1.81	1.76
	T	0.195	0.2	0.2	0.2	0.19	0.19	0.2
1000°C	D	1.77	1.775	1.75	1.75	1.815	1.8	1.76
	T	0.2	0.2	0.2	0.205	0.195	0.195	0.2
1100°C	D	1.775	1.76	1.755	1.755	1.815	1.81	1.76
	T	0.2	0.205	0.21	0.205	0.195	0.195	0.2
1200°C	D	1.775	1.75	1.76	1.75	1.8	1.805	1.765
	T	0.195	0.205	0.205	0.21	0.2	0.2	0.2

① T: Zirconia from Tosoh Company (TZ-3YS; average powder particle size = 0.6 μm)
  C: Zirconia from Cerac Company (5 wt% Y_2O_3; average powder particle size = 1.23 μm)
② D: Diameter of the specimen
③ T: Thickness of the specimen

Table 8.2. Minimizing warping by mixing two ZrO_2 powders in a top layer

1. Initial configuration of powder compact

ZrO_2 Mixture (Tosoh/Cerac)
Al_2O_3 (TMDAR)

2. Height Difference as Measured by Dial Indicator for sintered specimens (Cm)

Material	Height at Edge (HE)*	Height at center (HC)*	Height differece (HC)-(HE)	$\dfrac{(HC-HE)}{HC}$
85%(T) / 15%(C)	0.4	0.45	0.05	0.111
75%(T) / 25%(C)	0.4	0.43	0.03	0.0698
72.5%(T) / 17.5%(C)	0.4	0.435	0.035	0.0804
70%(T) / 30%(C)	0.405	0.44	0.035	0.0795
65%(T) / 35%(C)	0.4	0.43	0.03	0.0698
60%(T) / 40%(C)	0.4	0.425	0.025	0.0588
55%(T) / 45%(C)	0.405	0.425	0.02	0.047
50%(T) / 50%(C)	0.405	0.44	0.035	0.08
40%(T) / 60%(C)	0.405	0.459	0.054	0.118
30%(T) / 70%(C)	0.41	0.495	0.085	0.172
25%(T) / 75%(C)	0.41	0.5	0.09	0.18

*Position for height measurement
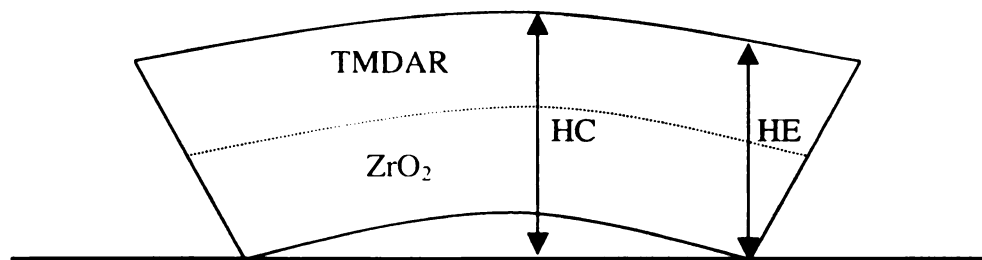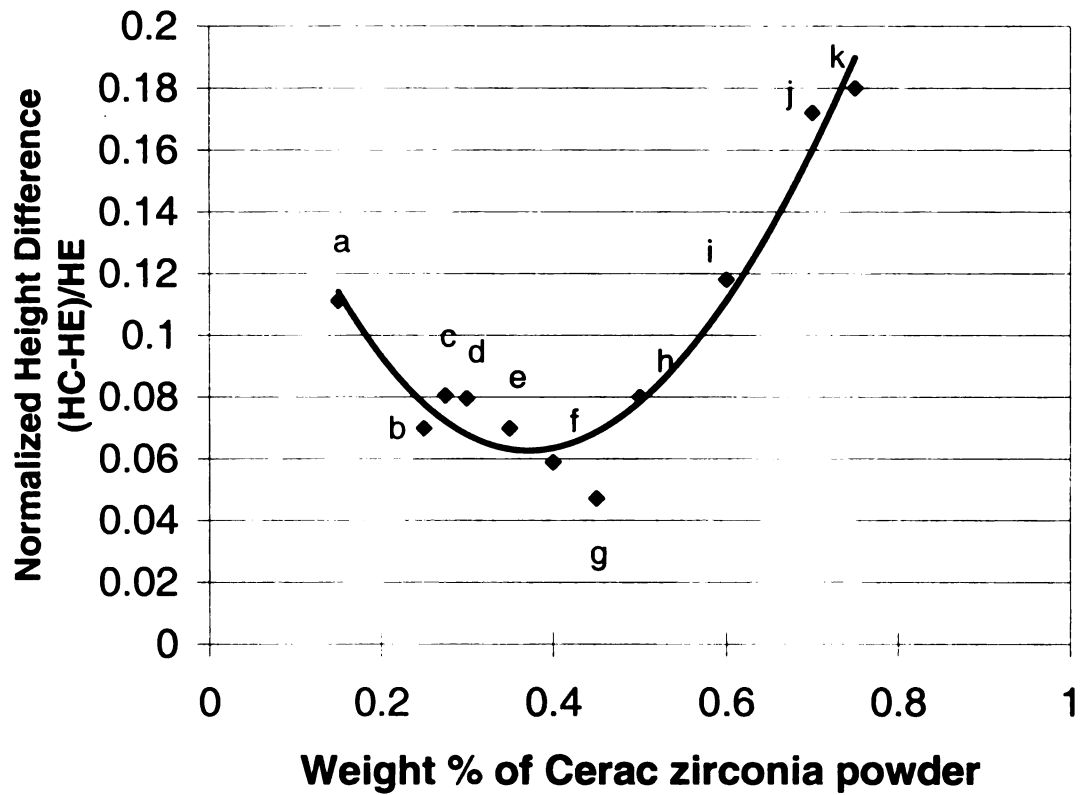
Figure 8.2. Comparison of the out-of-plane height at the center of zirconia/alumina specimens, based on a variation of particle-size mixture in the zirconia component.

8.2   Residual Stress

When a multi-layer specimen is warped due to a mismatch in thermal expansion and/or densification of the different layers, residual stresses are stored inside. Assuming spherical symmetry in the warping and small deformations, and taking into account that zirconia densifies more than alumina after full sintering, a formula for the final curvature can be derived:
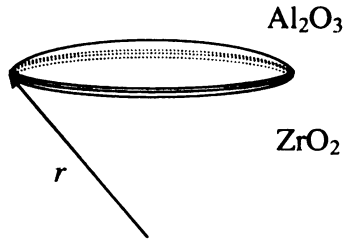
$$\kappa = \frac{1}{r} = \frac{[(\alpha_A - \alpha_Z)\Delta T - (\delta_A - \delta_Z)]}{d(1 + 1/2(\alpha_A + \alpha_Z)\Delta T - 1/2(\delta_A + \delta_Z))} \approx \frac{[(\alpha_A - \alpha_Z)\Delta T - (\delta_A - \delta_Z)]}{d},$$

where κ is the mean curvature, r is the radius of curvature, α is the coefficient of thermal expansion (subscript A for alumina, and subscript Z for zirconia), ΔT is the change in temperature in going from pre-sintering to final sintering (assuming zero curvature after pre-sintering), δ is the densification per unit original length (defined positive for shrinkage), and d is the distance between the center planes of the two layers. In the above formula; the curvature is positive when the concavity points downward towards the zirconia side. A higher thermal expansion on the alumina side ($\alpha_A > \alpha_Z$) or a higher shrinkage on the zirconia side ($\delta_Z > \delta_A$) will both lead to a positive curvature. In this case, a stress distribution is set up in the composite layer that varies linearly from maximum tension on the alumina top surface to maximum compression on the zirconia bottom face.

For convenience, this stress distribution will be referred to as the curvature stress. Also, it is noted that $\alpha_A \approx \alpha_Z$, so thermal effects do not act to increase the curvature.

Because of the difference in shrinkage behavior of the two layers, axial stresses are also present across the specimen. In particular, the alumina layer, which does not shrink as much as the zirconia layer, is under compression, while the zirconia layer is under tension. The total residual stress that is felt by the composite layer is the sum of the axial and curvature stresses. The presence of such a sum of stresses account for the experimental observation that vertical cracks can develop in various positions along the thickness.

Residual stresses are minimized by choosing two materials of similar thermal expansion and densification behavior. In the case of the alumina/zirconia composite, since $\alpha_A \approx \alpha_Z$, our approach has been to match the densification behavior by varying the particle-size mixture within the zirconia layer. Within the limits of what we can achieve in the experiments, a composition of 55% TZ-3YS and 45% CERAC in the zirconia component has been found to minimize the residual stresses.

Chapter 9

SCANNING ELECTRON MICROSCOPY (SEM)

The functionally gradient ceramic being proposed in this work is composed of a spatially varying distribution of different constituent materials. To verify its successful fabrication, topographical and compositional images of the ceramic samples have been taken using a JEOL (Japan Electron Optics Laboratory) 6400 scanning electron microscope, located at the Center for Electron Optics at Michigan State University. At working distances of 15–25 mm (depending on specimen size), the microscope has an approximate range of 5–7 nm resolution for secondary electron images; this is based on an interpolation of the following two given points: {working distance = 8 mm, attainable resolution = 3.5 nm} and {working distance = 39 mm, attainable resolution = 10 nm}. The magnification range is 10×–300,000×. In addition, an energy dispersive spectroscopy (EDS) system is attached to the SEM. An energy range of 0–20 KeV enables the EDS module to detect the presence of all elements from boron to uranium.

Details of SEM/EDS imaging can be found in [S. L. Flegler, J. W. Heckman, Jr., and K. L. Klomparens, *Scanning and Transmission Electron Microscopy, An Introduction*, Oxford University Press, 1993].

9.1 SEM Images of Topography Based on Secondary Electrons

When the electron beam (imaging beam) generated the SEM machine is directed at the specimen surface, many electrons within the specimen's atoms are given enough energy to escape their orbitals. These escaped electrons, called *secondary electrons*, have

low kinetic energy. An electron detector having positive potential collects these easily picked electrons, and the signal is amplified as an image. Cavities on the specimen surface tend to trap secondary electrons and appear as dark regions on the image, while convex bumps expose greater amounts of secondary electrons for picking and hence appear bright. SEM images based on secondary electrons primarily show the topography of specimens rather than composition. This is so because of two reasons: (1) the secondary electrons are formed closed to the specimen surface, and (2) the availability of secondary electrons does not depend significantly on the atomic number of the specimen's constituent atoms.

Another mechanism for image generation is based on the reflection of the imaging, electron beam from the nuclei of the target. These reflected electrons are called *primary*, or *back-scattered, electrons*, and they have high kinetic energy. Because the quantity of back-scattered electrons depends on the size of the nuclei within the specimen's constituent atoms, SEM images based on back-scattered electrons not only measure the surface topography of the specimen, but also its weight density. Back-scattered electron images have not been used in this work.

On the JEOL 6400 microscope, we have chosen a pixel resolution of 512×512 for secondary electron images, with an acquisition dwell time of 1e-5 seconds per pixel. From the point of view of element mapping, secondary electron images of specimen samples are merely used as reference images of the mapped regions, and examples will be included in the next subsection.

9.2   EDS Images of Element Composition Based on Released X-Rays

If the escaped electrons being forced out by the imaging beam come from the inner shells of the target atoms, electrons from the outer shells move to fill the vacancies. In the process, x-rays characteristic of the target atoms are dispersed. An energy detector can be used to generate a spectral energy plot indicating the presence of different elements in the target sample. The detector range in the EDS system on the JEOL 6400 allows all elements from boron to uranium to be detected.

In the x-ray, mapping mode of the EDS system, a detection window is chosen around a particular element's signature, x-ray peak(s). Under a two-dimensional scan of the target surface using the JEOL microscope, dots on the observation screen are generated in proportion to the x-ray count of that element (Figure 9.1). The same spectral detection window around an element's x-ray peak(s) can be retained for an element x-ray line-scan. This time an x-ray count of element composition can be plotted along the chosen line (Figure 9.2, 9.3, 9.4).

In Figure 9.2, which shows the x-ray line-scan, errors in the element count are noted in the depleted regions corresponding to the dark regions in the 2-D, x-ray map. A possible explanation is system noise. Here, we suggest a relationship between noise and the size of the imaging beam. When the resolution of the image is high, the diameter of the imaging beam should be low; this means that the resultant signal (and output) is weak, leading to a higher sensitivity to noise. Hence, to test the nature of the error in element count, one option may be to lower the resolution in the x-ray line-scan to see if the noise is reduced. If not, the observed noise may well be a characteristic system noise that needs to be reported.

To generate the element x-ray map on the JEOL microscope, a 2-D resolution of 128×128 pixels was used with an acquisition dwell time of 100 milliseconds per pixel. For the x-ray line-scan, a linear resolution of 128 pixels was used with an acquisition dwell time of 100 milliseconds per pixel.
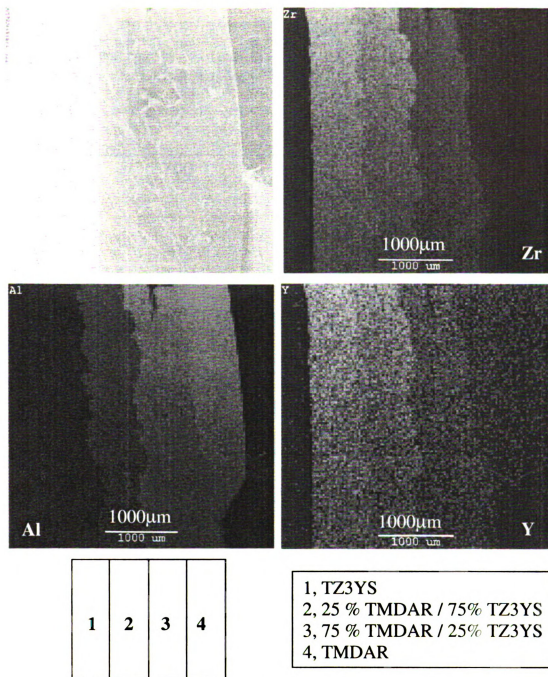
Figure 9.1. Element mapping based on energy dispersive spectroscopy (EDS) of the SEM sample. X-ray beams characteristic of aluminum, yttrium and zirconium are collected from the sample surface and the signal is magnified proportionally as brightness. The different colors are arbitrarily chosen. Line Scan of the x-ray and EDS element scan shown in figure 9.2, 9.3.
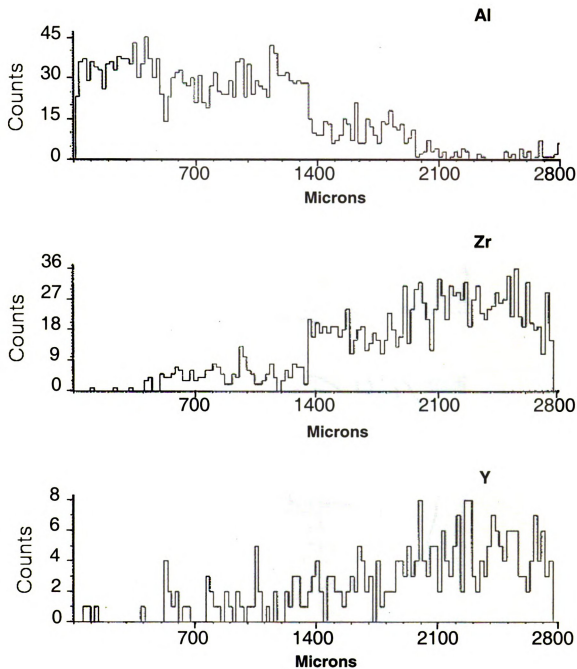
Figure 9.2. Line scan of the x-ray count based on energy dispersive spectroscopy. The amount of an element (Al, Zr, or Y) along the line(figure 9.3a) is shown by the number of x-ray particles detected over a dwell time of 100 milliseconds. Element mapping and EDS element scan shown in figure 9.1, 9.4.

(a)
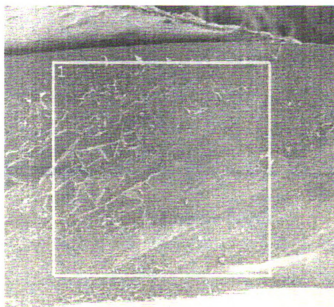
(b)

Figure 9.3. (a) Line across the samples for line scan of the x-ray count based on energy dispersive spectroscopy(Figure 9.2.), (b) square region (For figure 9.4) of the sample surface
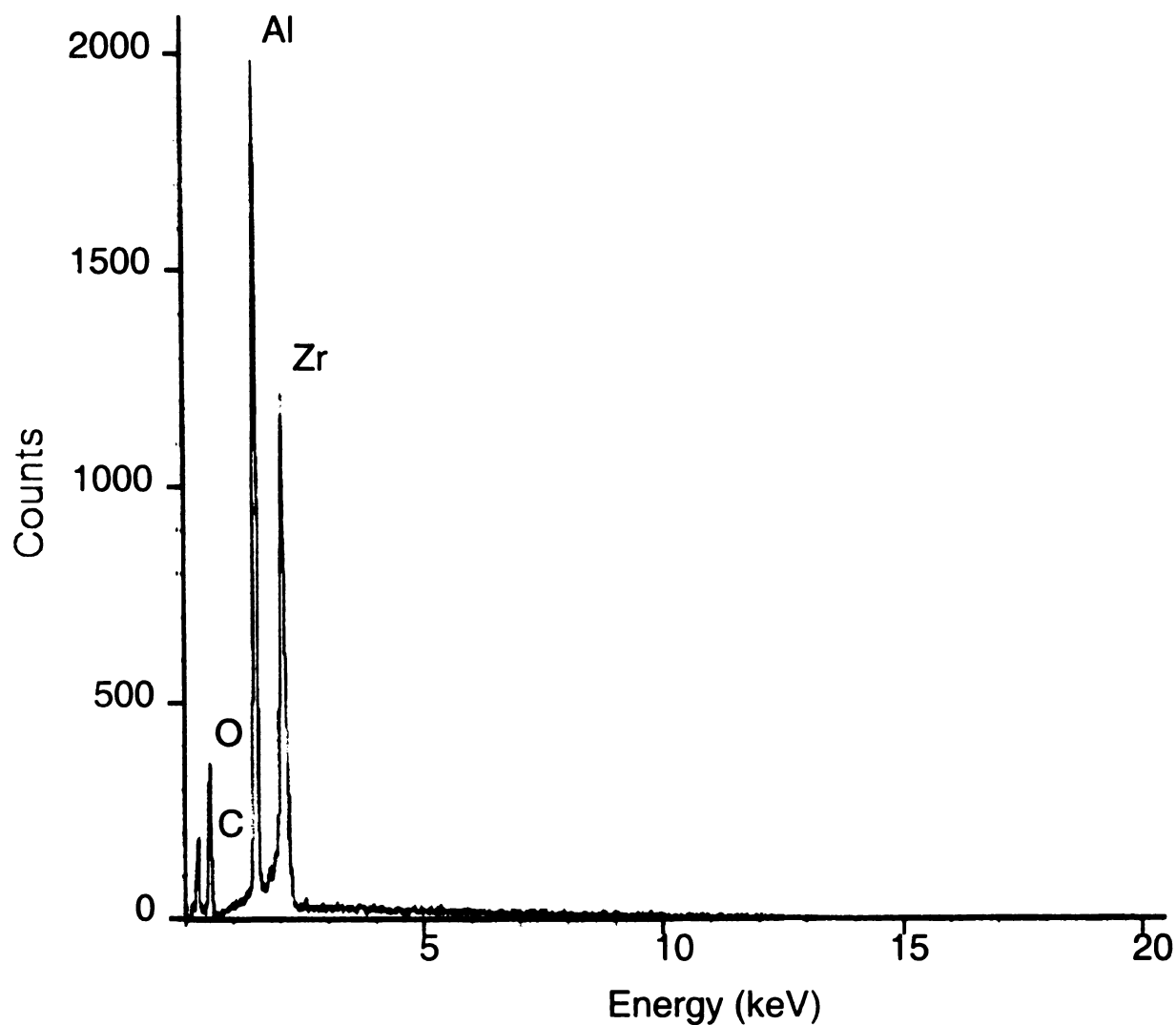
Figure 9.4. EDS elemental scan over the indicated, square region (figure 9.3b) of the sample surface. X-ray beams (created by shining an imaging, electron beam on the target) of different energies are detected are correlated to x-ray signatures of different elements. The JEOL 6400 microscope is capable of detecting all elements from boron to uranium. Element mapping and line scan of the x-ray shown in figure 9.1, 9.2.

REFERENCES

1 W.H.Sutton, "Microwave Processing of Ceramic Materials", Am.Ceram.Soc.Bull.68[2], 1989, pp376-386

2 M.A. Janney, H.D. Kimrey, and J.O.Kiggans, "Microwave Processing of Ceramics: Guidelines used at the Oak Ridge National Laboratory", in Microwave Processing of Materials, III, R.L. Beatty, W.H.Sutton, and M.F. Iskander, eds., MRS Symp. Proc., Vol.269, 1992, 173-185

3 L.M. Sheppard, "Manufacturing Ceramics with Microwaves: The Potential for Economical Production", Am Ceram. Soc. Bull., 67[10], 1988, pp.1656-1661

4 M.A. Janney and H.D. Kimrey, "Microwave Sintering of Alumina at 28GHz", Ceramic Powder Science, II, B, Ceramic Transactions, vol.1, 1988, pp.919-924

5 M.A. Janney and H.D. Kimrey, "Diffusion-Controlled Processes in Microwave-Fired Oxide Ceramics", Mater.Res.Soc.Symp. Proc., vol.189, 1991, pp215-227

6 M.A. Janney, H.D. Kimrey, W.R.Allen and J.O. Kiggans, "Enhanced Diffusion in Sapphire during Microwave Heating," Journal of Materials Science vol.32, No.5, 1997,pp.1347-1355

7 A. De, I.Ahmad, E.D. Whitney, and D.E.Clark, "Microwave (Hybrid) heating of Alumina at 2.45 GHz: I. Microstructural Uniformity and Homogeneity," Microwaves: Theory and Application in Materials Processing, Ceramic Transactions, vol. 21, 1991, pp.319-328

8 C.E. Holcombe, T.T.Meek, and N.L. Dykes, "Enhanced Thermal Shock Properties of $Y_2O_3-2wt.\%ZrO_2$ heated Using 2.45 GHz Radiation," Mat.Res.Soc.symp. proc.vol. 124, 1988, pp.227-234

9 M.C.L.Patterson, P.S.Apte, R.M. Kimber, and R.Roy, "Mechanical and Physical Properties of Microwave Sintered Si3N4," Mat. Res. Soc. Symp. Proc.vol269 1992, pp.301-310

10 Yang Bin, Li Jun, Wang Jinxiang, and Zhong Xiangchong, "Influence of ZrO_2 on the Sintering Microstructure and Properties of MgO Materials," proceedings of the International Symposium on the Science and Technology of Sintering, Intering and Materials, Proc., 6th, vol. 6, 1995, pp.197-202

11 M.A. Janney and H.D. Kimrey, in Mat.Res. Soc. Symp. Proc., ed. W.B. Snyder, Jr., W.H. Sutton, M.F. Iskander and D.L.Johnson, vol.189, Materials Research Society, Pittsburgh, Pensnsylvania, 1990, pp.215-227

12 K.Y.Lee, E.D.Case, J.Asmussen, Jr., and M.Siegel, in Proceedings of the 11th Annual ESD Advanced Composites Conference, Ann Arbor, Michigan, 1995, pp.491-503

13 K.Y.Lee, E.D.Case, J.Asmussen, Jr., and M.Siegel, in Cer. Trans., vol.59, The American Ceramic Society Inc., Westerville, Ohio, 1995, pp.473-480

Chapter 10

CONCLUSION

In this study, to fabricate the functionally gradient materials, commercially available alumina, zirconia and hydroxyapatite powders were sintered. The specimens were densified to over about 90% of theoretical density.

To densify the specimens, two different heating systems—a conventional furnace and a cylindrical single-mode microwave cavity unit—were used to compare each behavior. Microwave-sintered alumina specimens reached about 97% theoretical density at a sintering temperature of 1300°C after 1 hour, while a specimen that is sintered in conventional heating process reached about 97% at 1430°C after 4 hours. This verified that by increasing the sintering temperature and time in conventional sintering process, similar densifications comparing to microwave heating were achieved. In addition, the fracture toughness of alumina between microwave and conventional heating was examined and gave the same result. This sintering study revealed that the microwave sintering could be done rapidly and uniformly comparing conventional sintering.

For a given set of materials, the extreme condition for residual stress is expected when two or more powders having significantly different thermal expansion and/or densification behavior are processed together. The sintered samples are subject to warping since the alumina layer is in a state of compressive residual stress while the zirconia layer is in a state of tensile residual stress based on shrinkage differences.

Initially, homogeneous powder layers are processed separately to expose their individual shrinkage behavior. Then, to understand and control the residual stress, two-layered samples, one layer with alumina the other with various mixtures of two different kinds of zirconia powders, are pressed sintered. While all of the samples had some degree of warping, the mixture ratio 55% TZ3YS (from Tosoh) / 45 % zirconia (from Cerac) yields the minimum amount of warping observed.

Among the many fugitive phases used to make channels (polymer, paper, pure graphite and pencil lead), pencil lead worked well. For making circular channels, pencil leads varying in lengths from 1 to 1.5 cm with nominal diameters of 300, 500, 700 and 900 microns were sintered. To make internal channels, part of the powder was placed in the die before placement of the fugitive phase, followed by the rest of the powder.

Samples with various internal channels such as manifold-shaped surface channels and spoke-shaped surface channels were fabricated in ceramics and ceramic composites including alumina, zirconia and hydroxyapatite. In addition, the FGMs specimens were fabricated. FGMs with variable composition were characterized by a process called element mapping. The basic idea is the detection of characteristic x-rays emanating from the surface of the target material due to impact from an imaging, electron beam. This element mapping showed well the composition of each layer of FGMs.

From the past experiments and results, one of the difficult problems in fabricating FGMs is the determination of process variables so that the residual stresses would not damage the details (like channels) as well as materials themselves. Because of the presence of warping and cracks, instead of sintering an entire FGM stack at one time, specimen layers are sintered separately and then joined. With 20-gram dead weights,

HAP and Macor layers have been successfully joined at a temperature of 1475°C with 4 hours of holding time. SEM examination of the joined region showed no evidence of cracking or microcracking around channels or across the interlayer boundaries. Also, the grain structure near the joint does not differ from the grain structure in the bulk of the specimen, indicating that the process of generating the joint does not greatly perturb the specimen's microstructure, at least on a size scale of a few microns.

APPENDICES

APPENDIX I

Micrographs of Fracture Surface of Materials Used in This Study
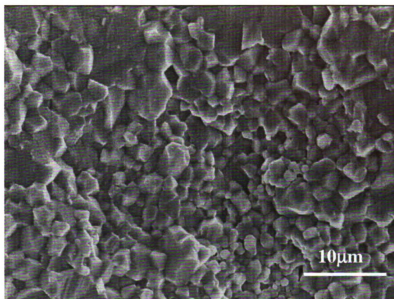
(a)
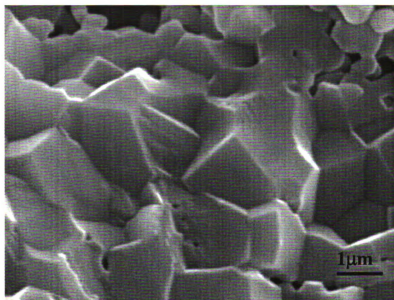
(b)

Figure I-1. SEM image of fracture surface of alumina (a) Sintered at 1430°C for 4 hours in conventional furnace, (b) Sintered at 1300°C for 1 hour in microwave.
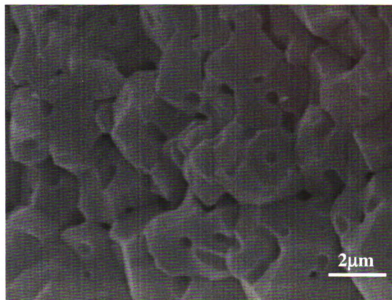
(a)
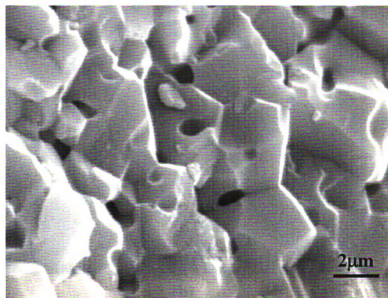
(b)

Figure I-2. SEM image of fracture surface of TZ8YS (fully stabilized 8 mol% Yttria-Zirconia) (a) sintered at 1430°C for 4 hours in conventional furnace (b) sintered at 1300°C for 1 hours in microwave
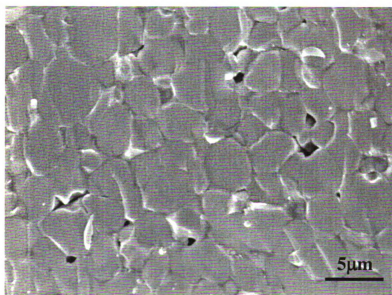
(a)
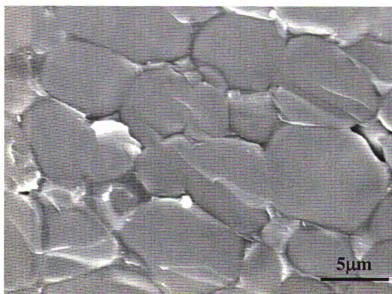
(b)

Figure I-3. SEM image of fracture surface of TZ3YS (partially stabilized 3mol% Yttria-Zirconia) sintered at 1430°C for 4 hours in conventional furnace ((a) and (b) represent images taken at different locations)
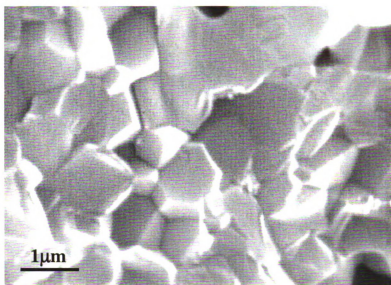
(a)
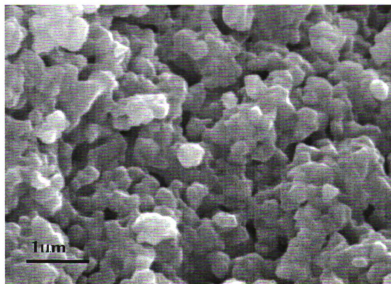
(b)

Figure I-4. SEM image of fracture surface of HAP (Hydroxyapatite) (a) sintered at 1300°C for 4 hours in conventional furenace, (b) sintered at 1100°C for 1 hour in microwave.
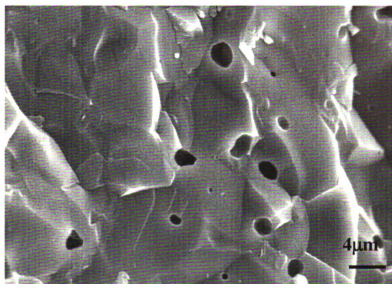
(a)
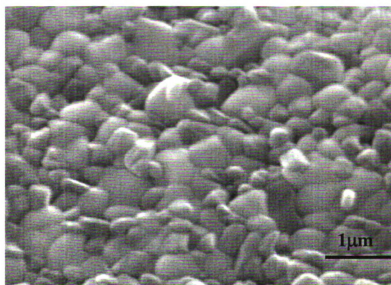
(b)

Figure I-5. SEM image of fracture surface of (a) 25% TMDAR / 75%HAP   sintered at 1300°C for 1 hour in microwave and (b) 50% TMDAR / 50% TZ3YS sintered at 1430°C for 4 hours in conventional furnace.

APPENDIX II

Micrographs of Various Shapes of Manifold Channels
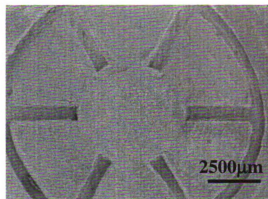
(a)
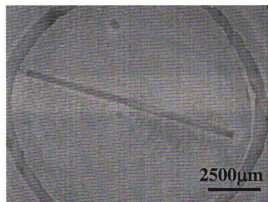
(b)
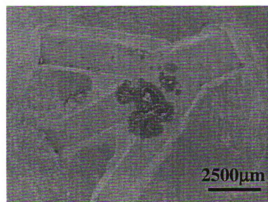
(c)

Figure II-1 TZ8YS specimens pre sintered at 900°C for 2 hours and sintered 1430°C for 4 hours in conventional furnace with various shapes of manifold channels of (a) ABS which is a thermoplastic (b) ABS and pencil lead in center and (c) paper
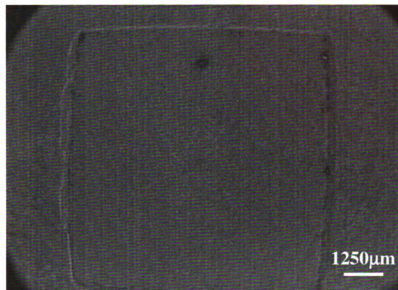
(a)
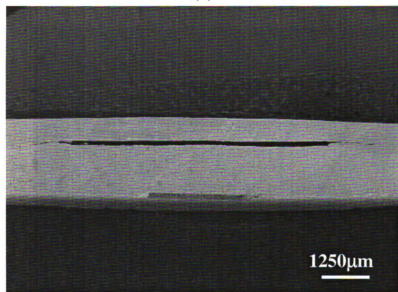
(b)

Figure II-2 TZ8YS specimens pre sintered at 900°C for 2 hours and sintered 1430°C for 4 hours in conventional furnace (a) surface channels created by paper as fugitive phase, (b) embed channel
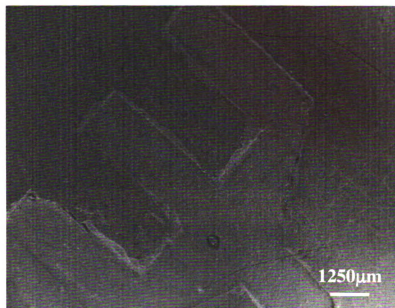
(a)
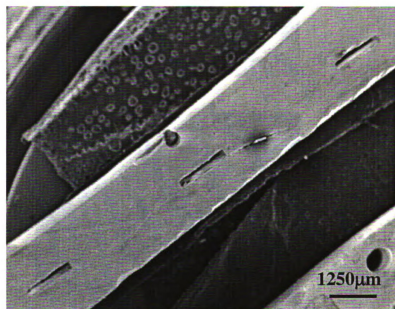
(b)

Figure II-3 TZ8YS specimens pre sintered at 900°C for 2 hours and sintered 1430°C for 4 hours in conventional furnace channels created by paper as fugitive phase (a) surface channel, (b) embed channel
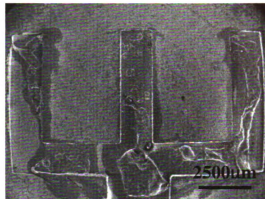
(a)
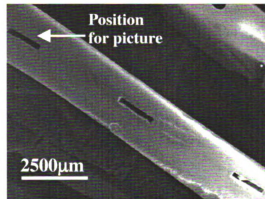
(b)
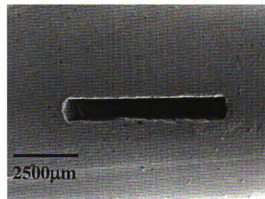
(c)

Figure II-4 TZ8YSspecimen pre sintered at 900°C for 2 hours and sintered 1430°C for 4 hours in conventional furnace with manifold shaped channels created by pure graphite as fugitive phase, (a) Surface channel, (b) Embed channel (c) Embed channel in position marked in (b)

APPENDIX III

Micrographs of Various Channels in Homogeneous Materials and Composite Materials
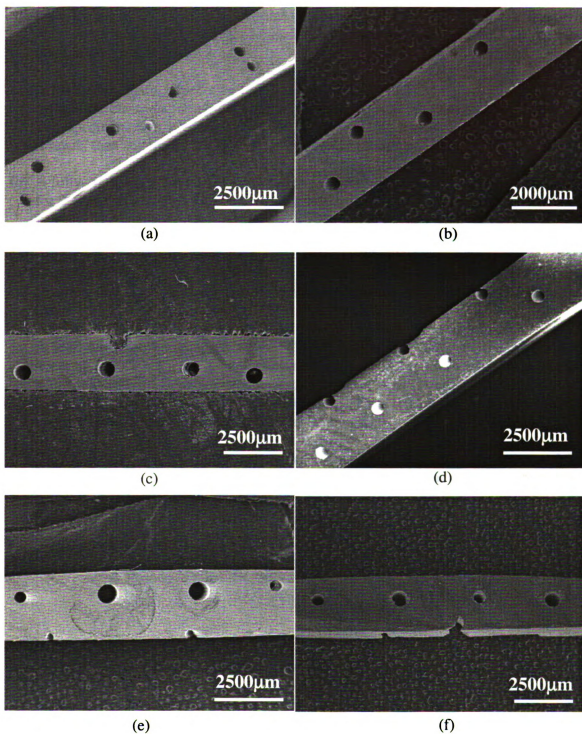
Figure III-1 Various channels in homogeneous materials and composite materials

Figure III-1.

(a) A SEM micrograph of an alumina specimen that was pre-sintered at 900°C for one hour in air in a conventional furnace, then sintered at 1300 °C for 1 hour via microwave heating. Two rows of closely spaced channels were formed by pressing 500microns pencil leads.

(b) A particular ceramic specimen (25% alumina / 75% TZ3YS) with with two layered cylindrical channels, using 500 micron-diameter pencil leads as fugitive elements. The specimen was pre-sintered in air at 900 °C for one hour in a conventional furnace, then sintered at 1300°C for one hour via microwave heating.

(c) A fully- stabilized sirconia (TZ8YS) specimen pre-sintered conventionally at 900°C for 2 hours in air, then sintered for four hours at 1430°C in air in a conventional furnace. The channels were formed using 900 microns pencil lead.

(d) A FSZ specimen pre-sintered conventionally at 950 °C for two hours in air, then sintered for four hours at 1430°C in air in a conventional furnace. Both four internal channels and three surface channels were formed using 500 micron diameter pencil leads.

(e) A FSZ specimen pre-sintered at 900 °C for two hours in air, then sintered for four hours at 1430°C in air in a conventional furnace. The larger channels were formed using 900 micron diameter pencil lead, while the smaller channels were formed using 500 micron diameter pencil lead for internal channels. And, 300 micron diameter pencil lead were used for surface channels.

(f) A FSZ speciemn (pre-sinterd and sintered in air at 1200 °C for two hours and for four hours at 1430°C, respectively) was shown with 900 micron and 700 micron pencil lead as fugitive phase.
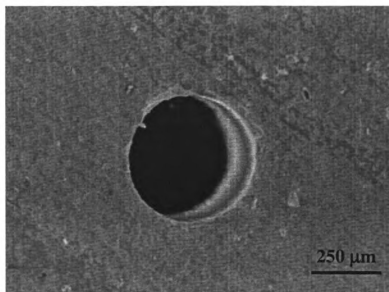
(a)
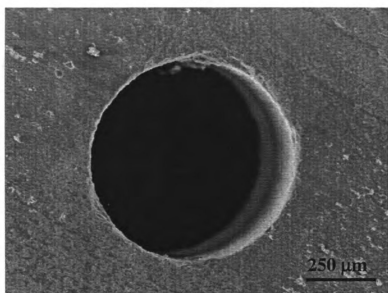
(b)

Figure III-2 A high-magnification view of a single channel formed (a) from a 500 micron diameter pencil lead (b) from 900 micron diameter pencil lead in a FSZ specimen. The specimen was pre-sintered in air at 900 °C for two hours and sintered at 1430 °C for four hours in a conventional furnace.
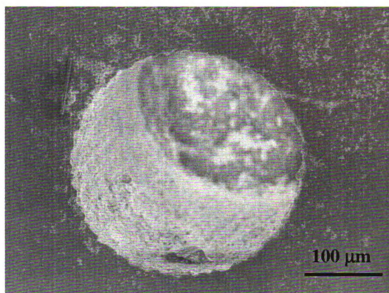
(a)
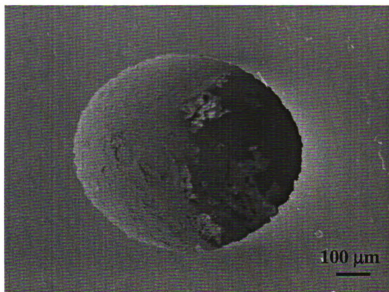
(b)

Figure III-3 A high-magnification view of a single channel (a)formed from a 300 micron diameter pencil lead (b) from 700 micron diameter pencil lead in a FSZ specimen. The specimen was pre-sintered in air at 950 °C for two hours and sintered at 1430 °C for four hours in a conventional furnace.

APPENDIX IV

Micrographs of Various Functionally Gradient Materials

TWO LAYERED SPECIMENS

(a)

(b)
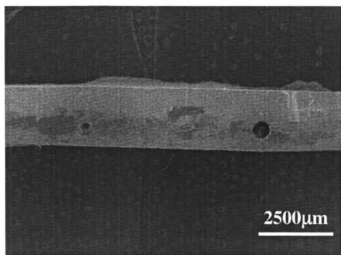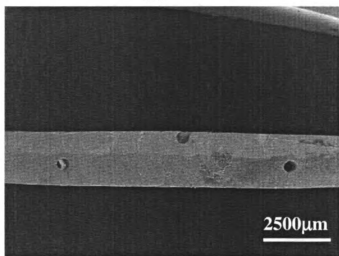
Figure IV-1 Pre-sintered at 900 ^{o}C for four hours and sintered at 1430 ^{o}C for four hours in air in a conventional furnace.(a) with 700 micron diameter pencil lead as fugitive phase, (b) with 500 micron diameter pencil lead as fugitive phase. Materials were shown in configuration respectively.
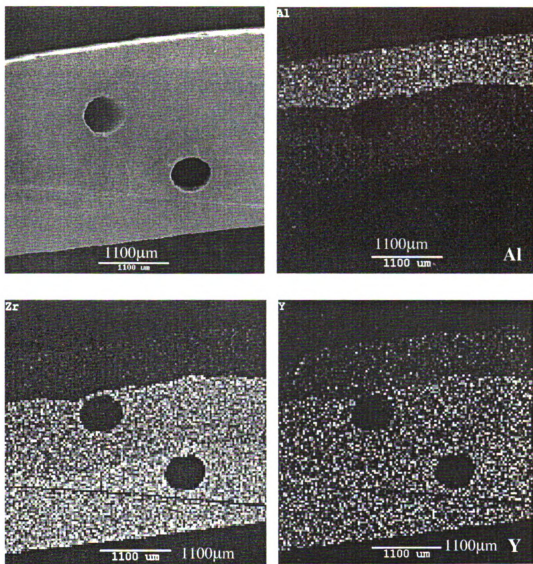
FOUR LAYERED SPECIMENS
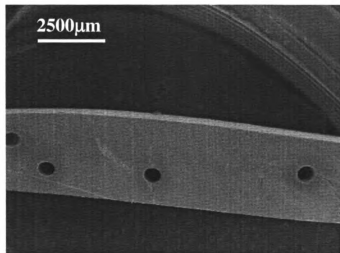
65 %TZ3YS / 35%CERAC
70 %TZ3YS / 30%CERAC
30%TMDAR / 70%(70%T/30%C)
TMDAR

(a)
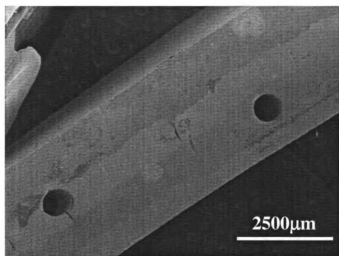
65 %TZ3YS / 35%CERAC
70 %TZ3YS / 30%CERAC
70%TMDAR / 30%(70%T/30%C)
TMDAR

(b)

Figure IV-2 Pre-sintered at 900 °C for four hours and sintered at 1430 °C for four hours in air in a conventional furnace.(a) with 700 micron diameter pencil lead as fugitive phase, (b) with 700 micron diameter pencil lead as fugitive phase. Materials were shown in configuration respectively

11 LAYERED SPECIMENS

(a)
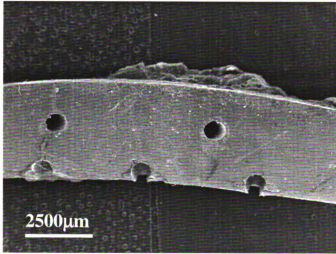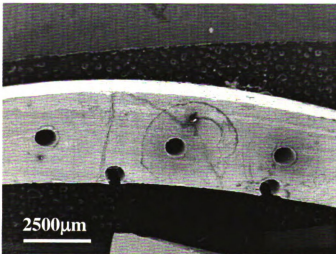
1,TMDAR
2,90%TMDAR+10%TZ3YS
3,80%TMDAR+20%TZ3YS
4,70%TMDAR+30%TZ3YS
5,60%TMDAR+40%TZ3YS
6,50%TMDAR+50%TZ3YS
7,40%TMDAR+60%TZ3YS
8,30%TMDAR+70%TZ3YS
9,20%TMDAR+80%TZ3YS
10,10%TMDAR+90%TZ3YS
11,TZ3YS

(b)

Figure IV-3 Pre-sintered at 900 °C for four hours and sintered at 1430 °C for four hours in air in a conventional furnace.(a) with 900 micron diameter pencil leads, (b) with 900 micron diameter pencil leads. Materials were shown in configuration respectively

APPENDIX V

Element Mapping of Functionally Gradient Materials

| 65% TZ3YS/35% CERAC |
| 70% TZ3YS/30% CERAC |
| 30%TMDAR/ 70% (70%T/30%C) |
| TMDAR |

Figure V-1. Element mapping based on energy dispersive spectroscopy (EDS) of the SEM sample. X-ray beams characteristic of aluminum, yttrium and zirconium are collected from the sample surface and the signal is magnified proportionally as brightness. The different colors are arbitrarily chosen.
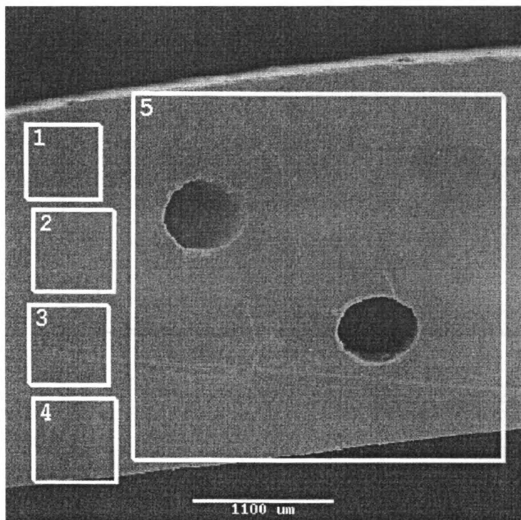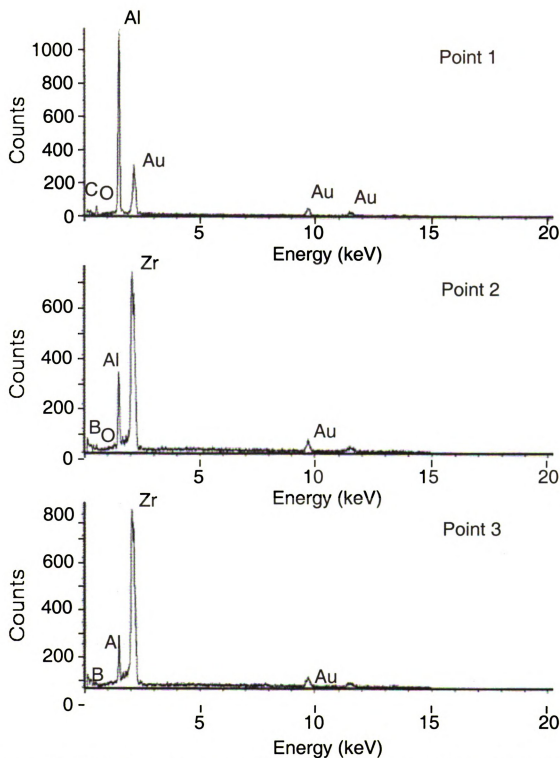
Figure V-2 Square region (for the figure V-3) of the sample surface

Figure V-3. EDS elemental scan over the indicated, square region (figure V-2) of the sample surface. X-ray beams (created by shining an imaging, electron beam on the target) of different energies are detected are correlated to x-ray signatures of different elements. The JEOL 6400 microscope is capable of detecting all elements from boron to uranium.
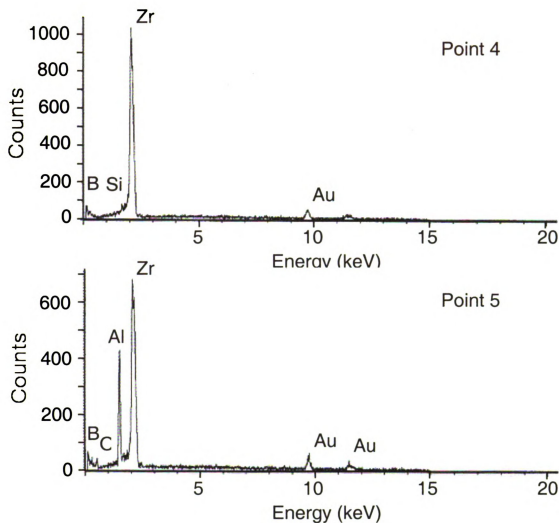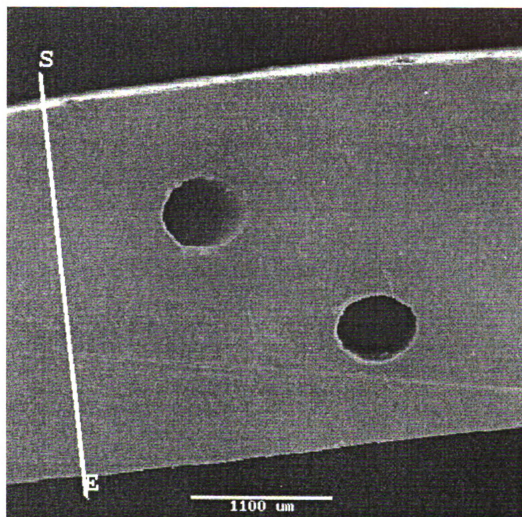
Figure V-4. EDS elemental scan over the indicated, square region (figure V-2) of the sample surface. X-ray beams (created by shining an imaging, electron beam on the target) of different energies are detected are correlated to x-ray signatures of different elements. The JEOL 6400 microscope is capable of detecting all elements from boron to uranium.

Figure V-5. Line across the samples for line scan of the x-ray count based on energy dispersive spectroscopy(For figure V-6.)
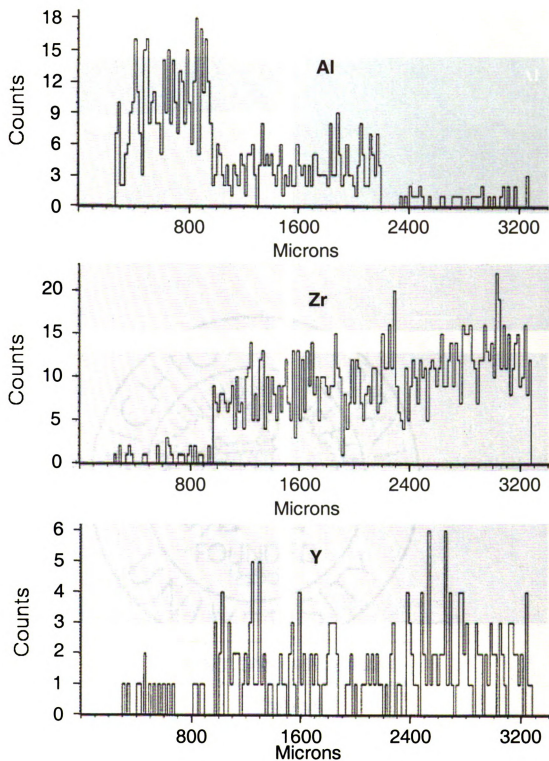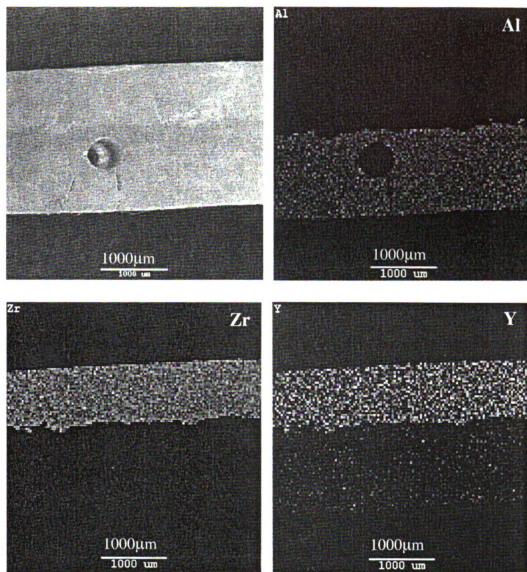
Figure V-6. Line scan of the x-ray count based on energy dispersive spectroscopy. The amount of an element (Al, Zr, or Y) along the line(figure V-5) is shown by the number of x-ray particles detected over a dwell time of 100 milliseconds. Element mapping and EDS element scan shown in figure V-1,figureV-3,4.

| 55%TZ3YS / 45 %CERAC |
| TMDAR |

Figure V-7. Element mapping based on energy dispersive spectroscopy (EDS) of the SEM sample. X-ray beams characteristic of aluminum, yttrium and zirconium are collected from the sample surface and the signal is magnified proportionally as brightness. The different colors are arbitrarily chosen.
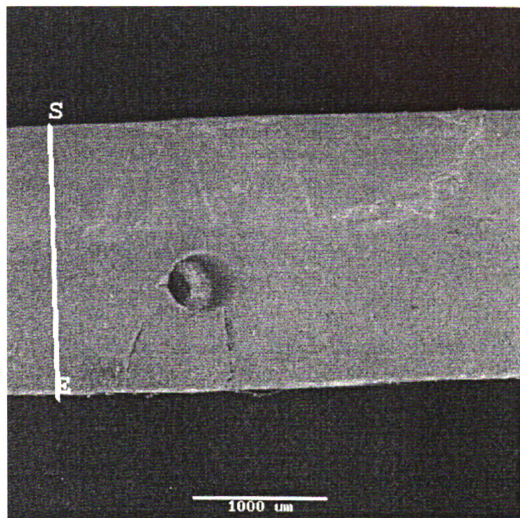
Figure V-8. Line across the samples for line scan of the x-ray count based on energy dispersive spectroscopy(For figure V-9.)
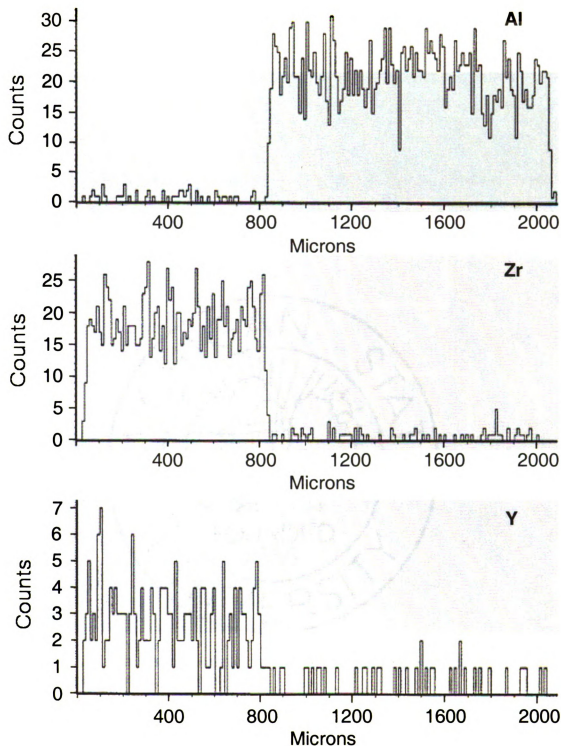
Figure V-9. Line scan of the x-ray count based on energy dispersive spectroscopy. The amount of an element (Al, Zr, or Y) along the line (figure V-8) is shown by the number of x-ray particles detected over a dwell time of 100 milliseconds. Element mapping and EDS element scan shown in figure V-7, figure V-11
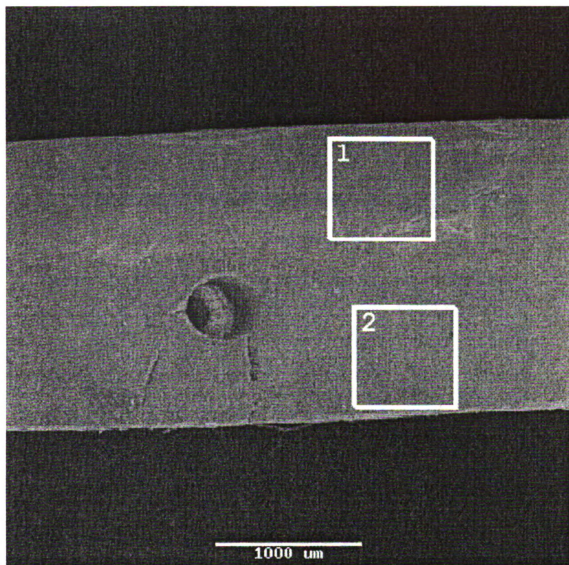
Figure V-10. Line across the samples for line scan of the x-ray count based on energy dispersive spectroscopy(For figure V-11.)
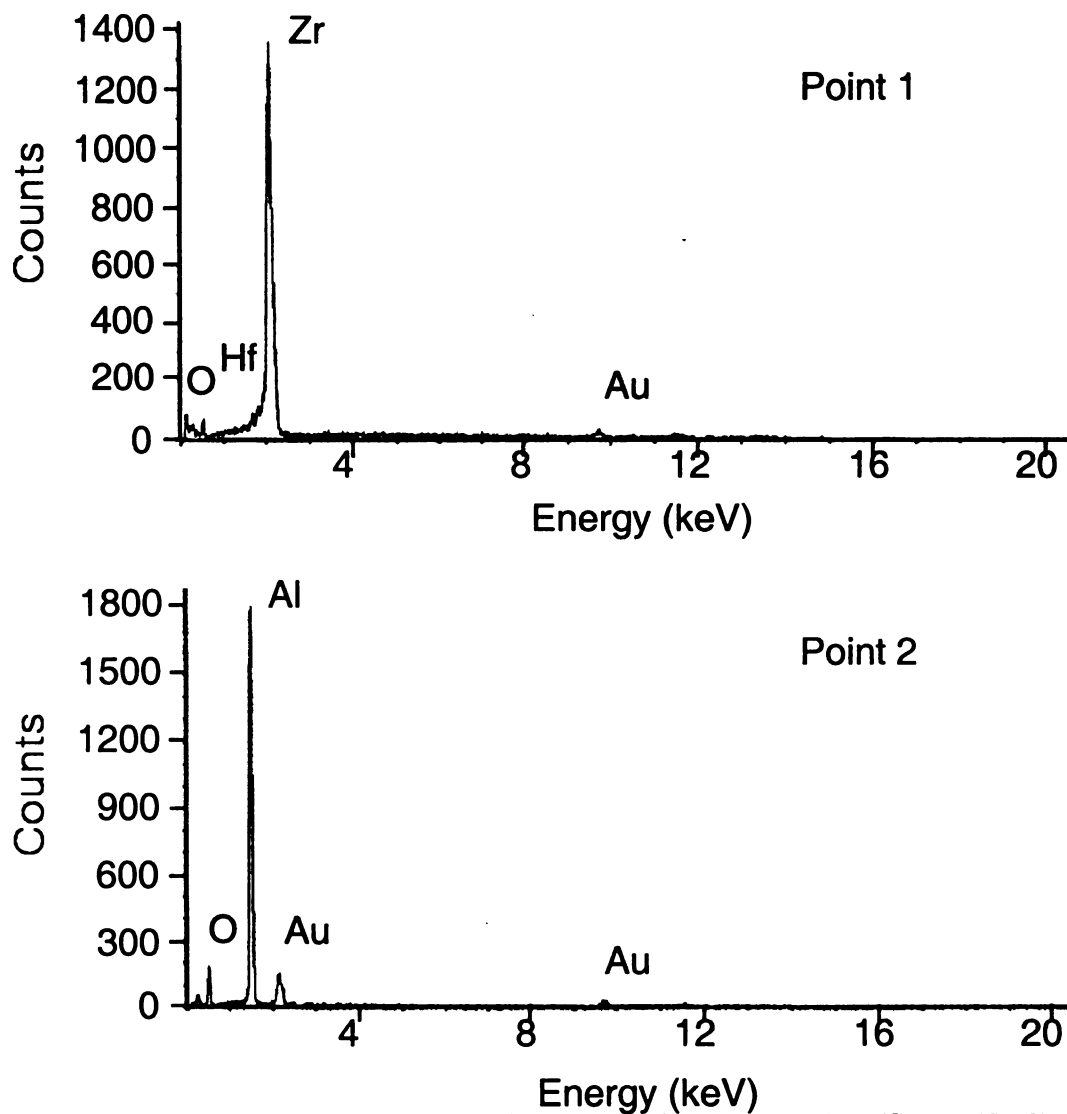
Figure V-11. EDS elemental scan over the indicated, square region (figure V-10) of the sample surface. X-ray beams (created by shining an imaging, electron beam on the target) of different energies are detected are correlated to x-ray signatures of different elements. The JEOL 6400 microscope is capable of detecting all elements from boron to uranium.